

AN ABSTRACT OF THE DISSERTATION OF

Amber L. Kramer for the degree of Doctor of Philosophy in Chemistry
presented on December 9, 2019.

Title: Polycyclic Aromatic Hydrocarbons in Atmospheric Fine Particulate
Matter: Beyond the Priority Pollutant List

Abstract approved:

Staci L. Massey Simonich

Atmospheric fine particulate matter (PM_{2.5}) has been linked to the death of 7 million people per year around the planet. The organic portion of PM_{2.5} is responsible for increases in oxidative stress, inflammation, mutation and carcinogenesis. Anthropogenic activity releases more organic material into the atmosphere, and has increased the amount of PM_{2.5} which contains organic aerosol including polycyclic aromatic hydrocarbons (PAHs) in the atmosphere. PAHs are ubiquitous environmental contaminants emitted to the atmosphere through incomplete combustion, which traverse the planet in PM_{2.5}. Protected in PM_{2.5} by glassy organic aerosol coatings, PAHs undergo long-range atmospheric transport.

Recent studies have shown that PAHs increase the viscosity and atmospheric lifetimes of secondary organic aerosol (SOA) particles formed naturally in the atmosphere, but have not shown the chemical speciation responsible for these trends. This dissertation measured PAH oxidation

products formed during SOA formation in the presence of PAH vapor. These SOA particles grew larger, resulting in up to a 600% mass loading increase over SOA formed without PAH vapor present, and had longer atmospheric lifetimes. This indicated that the presences of PAHs during particle growth increases the formation less-volatile organic compounds, which remain condensed in the atmosphere. High-resolution time-of-flight aerosol mass spectrometry (HR-ToF-AMS) showed that SOA particles formed in the presence of PAH vapor had increased signals of mass to charge ratios (m/z) at higher m/z . Other studies have demonstrated a large number of oligomers in SOA which could have the m/z signals measured here, suggesting a synergistic effect on SOA non-volatile compound formation.

In the second part of this dissertation, ambient $PM_{2.5}$ samples (collected in collaboration with the Swinomish Indian Tribal Community of the Northwest coast of the US State of Washington) were found to contain the same PAH oxidation products measured in our SOA experiments. The presence of these compounds in ambient samples proved the real world application of the experimental data collected in the first part of this dissertation. Along with these oxidation products, measured concentrations of ~130 PAHs in the ambient $PM_{2.5}$ analyzed in this dissertation were used to assess the air quality of the Swinomish Reservation during different atmospheric conditions. Significant differences in PAH concentrations were found during changes in wind direction, the presence of regional wildfires, and during atmospheric inversions. Excess Lifetime Cancer risk assessment was

performed on PM_{2.5} samples to demonstrate that during inversions, the inhalation cancer risk rises to levels above WHO safety guidelines.

The oxidative potential (OP) of atmospheric fine particulate matter (PM_{2.5}) has been linked to the organic content of PM_{2.5}, including polycyclic aromatic hydrocarbons (PAHs). Using the results from individual PAHs in the assay, computational modeling was performed to calculate the free energy of reaction (ΔG_{rxn}) for each PAH in the consumption assay. Significant correlations were found between the DTT₅₀ and the ΔG_{rxn} of subclasses of PAHs, the molecular weight (AMU) of PAHs, the assay response (linear slope), and various physical structural components of the PAHs. While mixtures of the 16 PAHs currently found on the US EPA Priority Pollutant List tested in this study appeared to show an additive mixture effect in the DTT assay, whole mixtures of PAHs prepared to match ambient PM_{2.5} PAH measurements did not. The compounds in the mixtures appear to either have antagonistic effects, or a non-linear relationship in oxidative potential at the low concentrations measured in PM_{2.5} samples. Extract measurements were significantly less

This dissertation used advanced aerosol instrumentation, analytical characterization, and chemical assays to demonstrate ways to improve our understanding of PAH fate and transport in the atmosphere, as well as potential impact on human health. The results of this research illustrate both the presence of a large number of PAHs in ambient PM_{2.5} and their implications on atmospheric lifetimes and PM_{2.5} exposure induced oxidative stress.

©Copyright by Amber L. Kramer
December 9, 2019
All Rights Reserved

Polycyclic Aromatic Hydrocarbons in Atmospheric Fine Particulate Matter:
Beyond the Primary Pollutant List

by
Amber L. Kramer

A DISSERTATION

submitted to

Oregon State University

in partial fulfillment of
the requirements for the
degree of

Doctor of Philosophy

Presented December 9, 2019
Commencement June 2020

Doctor of Philosophy dissertation of Amber L. Kramer presented on
December 9, 2019

APPROVED:

Major Professor, Representing Chemistry

Head of the Department of Chemistry

Dean of the Graduate School

I understand that my dissertation will become part of the permanent collection of Oregon State University libraries. My signature below authorizes release of my dissertation to any reader upon request.

Amber L. Kramer, Author

ACKNOWLEDGEMENTS

I would like to express my appreciation to my advisor, Staci L. Massey Simonich, for her guidance and support throughout my graduate studies at Oregon State University. When self-doubt arose, Staci was quick to point out my accomplishments and remind me of my worth. Her emphasis on a work-life balance and equity for all have shaped my approach to life and will forever be part of my guiding principles. I would also like to acknowledge the members of my committee: Jennifer Field, Claudia Meier, Mark Dolan, Alla Zelenyuk, and Stephen Giovannoni for their patience and guidance through my studies.

I would like to thank my fellow Simonich lab-mates. I am not always a ray of light, but they accepted me regardless. Working with people you can trust and lean on is invaluable, and I am forever grateful to each of them.

I would like to acknowledge Dr. Molly Kile for her unofficial mentorship throughout my studies. Though I was not in her lab, she always had time to discuss my progress both on our collaborative work, as well as in my professional development. Working with Molly reminded me of the impact that research can have, and I will always strive to keep that lens on my work.

I would like to thank my collaborators at Pacific Northwest National Laboratory for allowing me to join them in their lab space and take part in their research. The lessons learned from them are invaluable.

And I would like to thank my friends and family, who may have questioned my decision to pursue a PhD at 35, but supported me anyways. I know that no matter where my next journey lands me, I have a wealth of love in all of you, and you have my love in return.

TABLE OF CONTENTS

	<u>Page</u>
Dissertation Art.....	1
Chapter 1	
1.0 Introduction.....	2
1.1 Polycyclic Aromatic Hydrocarbons (PAHs).....	3
1.1.1 Toxicity of PAHs.....	5
1.1.2 PAH Environmental Contamination.....	7
1.2 Atmospheric Particulate Matter and PAHs.....	8
1.2.1 Gas-particle PAH Partitioning.....	8
1.2.2 Fine Particulate Matter.....	9
1.2.3 Secondary Organic Aerosols.....	11
1.2.4 Long-Range Atmospheric Transport.....	12
1.3 Exposure to PM _{2.5}	13
1.3.1 Oxidative Stress from PM _{2.5} Exposure.....	13
1.3.2 Risk Assessment for PM _{2.5} Exposure.....	15
1.4 Environmental Justice.....	16
1.4.1 Exposure inequities.....	17
1.4.2 Native American Communities.....	17
1.5 Dissertation Objectives.....	18
Chapter 2. Formation of Polycyclic Aromatic Hydrocarbon Oxidation Products in a-pinene Secondary Organic Aerosol Particles Formed Through Ozonolysis.....	20

TABLE OF CONTENTS (Continued)

	<u>Page</u>
2.1 Abstract.....	22
2.2 Introduction.....	23
2.3 Methods and Materials.....	26
2.3.1 Materials.....	26
2.3.2 Experimental Design.....	26
2.3.3 QFF Extraction.....	31
2.3.4 Chemical Analysis.....	32
2.3.5 Statistical Analysis.....	33
2.4 Results and Discussion.....	34
2.4.1 Phenanthrene.....	34
2.4.2 Dibenzothiophene.....	40
2.4.3 Pyrene.....	41
2.4.4 Benz(a)anthracene.....	43
2.4.5 Implications.....	44
2.5 Associated Content.....	46
2.5.1 Supplemental information.....	46
2.5.2 Author information	46
2.5.3 Notes	46
2.6 Acknowledgements	47
Chapter 3: Impact of Local and Regional Sources of PAHs on Tribal Reservation Air Quality in the U.S. Pacific Northwest	48

TABLE OF CONTENTS (Continued)

	<u>Page</u>
3.1 Abstract	50
3.1.1 Keywords	50
3.1.2 Highlights	50
3.2 Introduction	51
3.3 Methods and Materials.....	54
3.3.1 Materials.....	54
3.3.2 Sample collection.....	55
3.3.3 PM _{2.5} extraction.....	56
3.3.4 PAH characterization.....	57
3.3.5 Meteorological data.....	58
3.3.6 Human Health Implications	59
3.3.7 Statistical analysis	61
3.3.8 Source apportionment	61
3.4 Results	62
3.4.1 Analysis of wind speed and direction during normal atmospheric conditions	62
3.4.2 Sampling location comparison	66
3.4.3 Atmospheric reactant analysis	66
3.4.4 Fire and inversion events	68
3.4.5 Excess Lifetime Cancer Risk Assessment	69
3.4.6 Source Apportionment	71

TABLE OF CONTENTS (Continued)

	<u>Page</u>
3.5 Discussion	73
3.5.1 Source regions in wind directions	73
3.5.2 Local sources of PAHs	74
3.5.3 UPAH transformation products	75
3.6 Conclusions	78
3.7 Acknowledgements	80
3.7.1 Funding	80
3.7.2 Supplemental information	80
Chapter 4: Oxidative Potential of PAHs in Ambient Atmospheric PM _{2.5} using Dithiolthreitol (DTT) Consumption Assay	81
4.1 Abstract	83
4.2 Introduction	83
4.3 Materials and Methods	85
4.3.1 Materials	85
4.3.2 DTT Assay	86
4.3.3 PM _{2.5} Samples	87
4.3.4 Statistical Analysis	88
4.3.5 Computational Analysis	89
4.4 Results and Discussion	90
4.4.1 DTT ₅₀ Results	90
4.4.2 Response Factor	92

TABLE OF CONTENTS (Continued)

	<u>Page</u>
4.4.3 ΔG_{rxn} of DTT Reaction	93
4.4.4 Mixtures Results.....	94
4.5 Associated Content	96
4.5.1 Supplemental Information	96
4.5.2 Corresponding Author Information	96
4.5.3 Notes	96
4.6 Acknowledgements	96
Chapter 5: Conclusions and Future Directions	98
Chapter 6: References	104

LIST OF FIGURES

<u>Figure</u>	<u>Page</u>
1 Dissertation Art	1
2.0 Table of Contents Art for Chapter 2	20
2.1 SOA Experimental Design Diagram	28
2.2 Phenanthrene SOA results graphs (A, B, C)	36
2.3 HR-ToF-AMS Chromatographs (A, B, C, D).....	37
3.0 Graphical Abstract for Chapter 3	48
3.1 Map of Sampling Region provided by the Swinomish Indian Tribal Community	55
3.2 Results graphs of Wind Direction Analysis (A1, A2, B1, B2, C1, C2).....	64
3.3 Figure of Fire and Inversion Event Analysis	68
3.4 BaP _{EQ} Results by PAH Class Graph	70
3.5 Diagnostic Ratios Results Graphs	72
3.6 Excess Lifetime Cancer Risk Assessment Results Graphs	77
4.0 Table of Contents Art for Chapter 4	81
4.1 ΔG_{rxn} by PAH Class Results Graph	93
4.2 Results Graph of Mixtures Analysis	96

LIST OF TABLES

<u>Table</u>	<u>Page</u>
2.1 Results of SOA chemical analysis	35
4.1 Statistically Significant Correlations	91

LIST OF APPENDICES

<u>Appendix</u>	<u>Page</u>
Appendix 1: Chapter 2 Supporting Information	115
A1.1 Detailed Methodology	123
A1.1.1 GC/MS Parameters	123
A1.1.2 Real-Time In-Situ Characterization	125
A1.1.3 Sample Aliquots	126
A1.1.4 Phenanthrene Standard Purity Testing	126
A1.1.5 Sonication Extraction Efficiency	127
A1.2 Gas-partitioning	130
A1.2.1 Vapor-phase PAH Concentration Calculations	130
Appendix 2: Chapter 3 Supporting Information	132
A.2.1 Detailed GC/MS Parameters	137
A.2.2 Derivatization of OHPAHs	141
Appendix 3: Chapter 4 Supporting Information	158

LIST OF APPENDIX FIGURES

<u>Figure</u>	<u>Page</u>
A1.F1 Mean weight percent of PAHs in freshly formed SOA	118
A1.F2 Phenanthrene oxidation products graph	128
A1.F3 Normalized HR-ToF-AMS chromatographs	131
A2.F1 Retene analysis results graph	155
A2.F2 Seasonal variations in BaP _{EQ}	157
A3.F1 Diagram of DTT reactions in Assay	163
A3.F2 Diagram of structural properties used for analysis.....	169

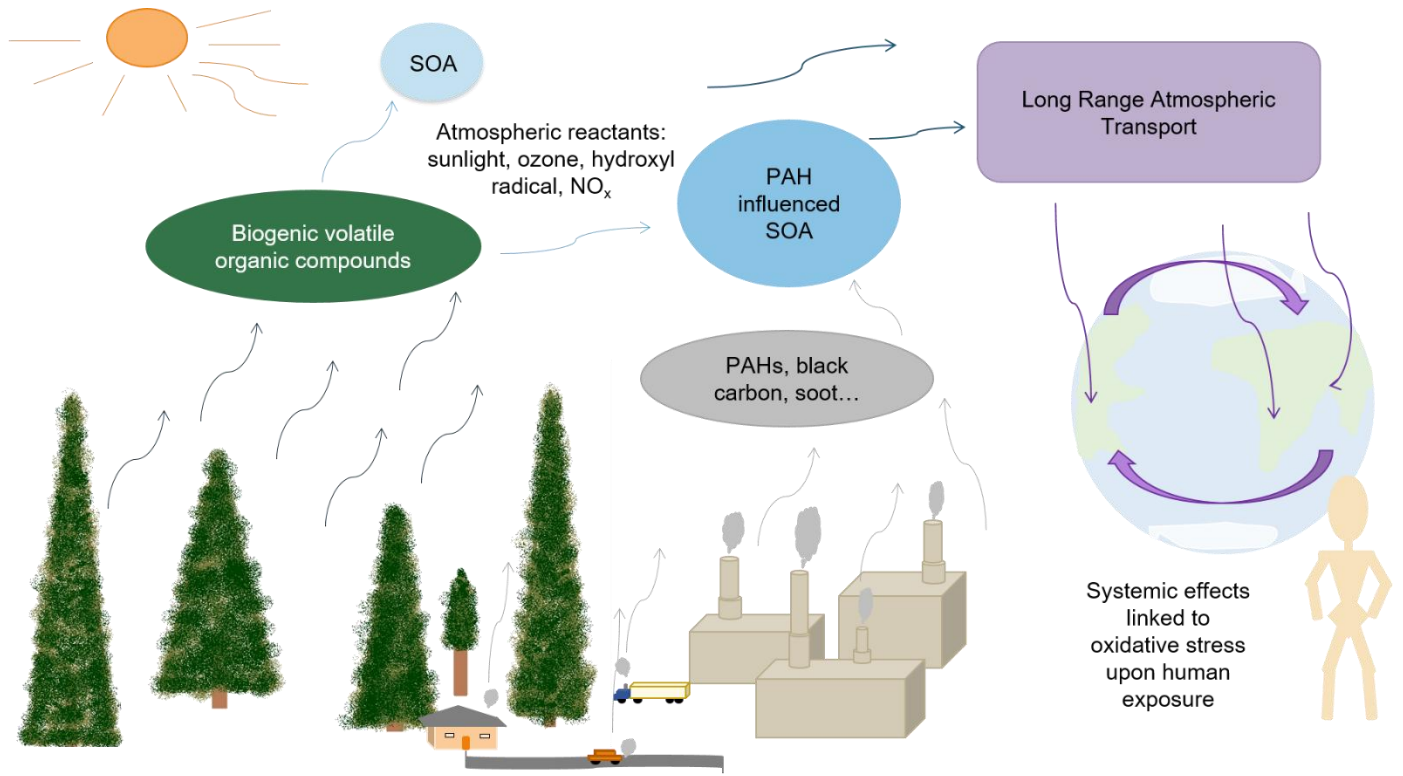
LIST OF APPENDIX TABLES

<u>Table</u>	<u>Page</u>
A1.T1 SOA Analytes information table.....	116
A1.T2 Ozone exposure table	120
A1.T3 Table of isotope labeled compounds	121
A1.T4 Sonication extraction efficiency table	122
A1.T5 Calculated PAH partitioning parameters	129
A1.T6 Calculated PAH vapor pressures in Teflon bags	130
A2.T1 Full Analytes list with properties	134
A2.T2 Results of PAH Significant changes with wind direction increases ...	142
A2.T3 PAH Correlation results table	146
A2.T4 PAH correlations with atmospheric reactants	148
A2.T5 Relative Potency Factors	149
A2.T6 PAH measurements Results.....	150
A2.T7 BaP _{EQ} averages and medians per wind direction	156
A3.T1 Analytical standards used	159
A3.T2 Full DTT assay results	164
A3.T3 Mixtures results table	170

DEDICATION

I would like to dedicate my dissertation to my mother, Dawn E. Kramer, whose life and death continue to guide my path towards becoming the best person I can be. I love you mom!

Dissertation Art



Chapter 1: Introduction

1.0 Background. Around the world, over seven million people die every year due to exposure to atmospheric particulate matter (PM).¹ The complex, and changing nature of PM inhibits vital risk assessment and exposure prevention.² This complexity impairs the determination of which constituents of the PM are driving toxicity to humans.³ Human activity since the industrial revolution has greatly increased the amount of PM in the atmosphere, and continues to change the complex chemical composition of particles.^{2 4 5 6} The largest contribution is the result of combustion processes used for industry, energy, transportation, and cooking.^{7 8} The continuing use of combustion to drive economic needs only continues to exacerbate the problem.^{8 6}

Polycyclic aromatic hydrocarbons (PAHs), which are transported through atmospheric PM, continue to be a major human health concern, decades after being classified as known toxins and/or carcinogenic compounds.^{9 10} PAHs are measured in all environmental compartments, but primarily transported through the atmosphere.^{9 11} Atmospheric emission of PAHs leads to PAH incorporation in PM, increases in PM mass in the atmosphere, and long-range transport of PAHs away from their emission sources.^{12 13 14 15 16} The mechanisms by which PAHs are transported away from their emission sources in PM is beginning to be understood.^{13 12}

However there is a large gap in PM transport data regarding PAH transformation products.¹⁷

When PAHs become oxidized during atmospheric reactions, they transform into compounds with different physical and chemical properties, different bioavailability pathways, and different toxicity profiles.^{18 19 20} These transformation products are not currently included in screenings via regulatory action, modeled for fate and transport, or considered during human risk assessments. This dissertation combines laboratory experiments, field sampling, and chemical assays to assess the oxidation products of PAHs in atmospheric PM transport, and provides data for inclusion of these compounds in long-range atmospheric transport (LRAT) modeling and risk assessment.

1.1 Polycyclic Aromatic Hydrocarbons (PAHs)

Polycyclic aromatic hydrocarbons (PAHs) are a class of organic compounds naturally found in fossil fuels, emitted during the combustion of organic material, or are the product (or byproduct) of industrial processes.²¹
²² PAHs range in size from two to seven aromatic rings. Aromaticity is determined by the conjugation of double bonds around the 5 or 6 atom hydrocarbon rings. Rings are fused together along a bonded side. This results in hydrocarbon ring chains that are straight, bent, or clustered in structure. The number of rings, along with the structure of those rings, determines the individual PAH chemical and physical properties. For the purpose of this dissertation, the abbreviation PAH will be used to refer to the

entire largely defined class of compounds consisting of aromatic hydrocarbon rings, UPAH will be used when referring to the unsubstituted, or 'parent' PAHs. As a class, PAHs are considered semi-volatile, with individual compound volatility related to molecular weight and structure.

While many environmental analyses focus on UPAHs, PAHs contain more subclasses than UPAHs. High molecular weight PAHs (HMWs) are a subclass of PAHs, classified as having a mass larger than 302 AMU, usually 6 or more aromatic rings. Although these are generally also unsubstituted, their high molecular mass changes their chemical and physical properties enough to classify them differently from UPAHs. Particularly because they are less volatile, and highly hydrophobic. While considered a separate subclass of PAHs, HMWs should undergo the same fate and transportation as UPAHs in the environment. HMWs are produced through the same mechanisms that produce UPAHs, and can be found alongside them in nature and emission sources.²³

Subclasses are also identified by substitutions within UPAHs. These substitutions change the chemical and physical properties of the molecules. Substitutions within the ring structures, usually by nitrogen, oxygen or sulfur, result in heterocyclic PAHs (HPAHs). These molecules have different reactivity due to the properties of the heterocyclic atom which is present.²⁴ HPAHs are naturally occurring along with UPAHs in crude fossil fuels, and can be released along with UPAHs into the environment.^{23 25}

Substitutions outside the ring structure also change the properties of the compounds. Common substituents found on PAHs are carboxyl, nitrate, and alcohol groups, resulting in oxy-PAHs (OPAHs), nitro-PAHs (NPAHs), and hydroxy-PAHs (OHPAHs), respectively. These substituents can be found singularly on PAHs or in any number of combinations between them. While some OPAHs and NPAHs can be found in crude fossil fuels, they are, along with OHPAHs, created through chemical transformations in the environment.⁹

²⁶ ²³ Substitutions of UPAHs increase mobility in the environment by adding polarity to the structure of the compounds, changing the way they can interact with the environment.²⁷ ²⁰

1.1.1 Toxicity of PAHs

PAHs, as a class, are considered toxic, with many having mutagenic, and/or carcinogenic properties⁹. There are currently 16 UPAHs on regulation watch lists such as the United States Environmental Protection Agency (USEPA) Priority Pollutant List²⁸. Actual toxicity is not class specific, but rather is compound specific. Each individual PAH has different modes of action in the human body that result in different adverse health effects. Some compounds can be toxic and mutagenic or carcinogenic, while others can have certain toxic effects, but no mutagenic or carcinogenic capacity.

The first compound to be identified as carcinogenic was the five ringed PAH benzo(a)pyrene (BaP). Due to being the first compound found to cause cancer, and the thought at the time that it was the most toxic, BaP has been used as a benchmark cancer-causing agent in many studies. There are now

several other known PAHs that have been shown to have higher carcinogenicity than BaP. To account for this, BaP relative potency factors (RPFs) have been assigned to nineteen other PAHs²⁹. Thirteen of these compounds are UPAHs, and six are HMWs. This equivalency is one way in which remediation technologies measure their success, by comparing the contaminated BaP equivalency with the post-remediation BaP equivalency.

The means by which a compound, or mixture of compounds, can cause harm to humans greatly depends on the route of exposure. PAHs found in groundwater and/or soil are either ingested or absorbed through dermal contact for humans to be exposed. Atmospheric PAHs on the other hand, are in the air we breathe both indoors and outdoors. Data on the modes of toxicity exists only for a small subset of the detectable PAHs. Watch lists do not generally include HPAHs, OPAHs, OHPAHs, NPAHs, or HMWs, and there continues to be little literature on the different routes of toxicity each compound in these classes represent. Many studies choose only a few compounds to assess toxicity. While this is resourceful, important differences may be missed when drawing conclusions on the toxicity of an entire classes of compounds based on only a few model compounds.

The largely unknown human health effects of substituted and HMW PAHs have negative consequences on human risk assessment. Without validated toxicity data about the HPAHs, OPAHs, NPAHs, OHPAHs, and HMWs regulatory agencies cannot perform accurate risk assessments that are needed to protect communities near industrial locations and downstream

of emission plumes^{9 30}. Such risk assessments require not only the toxicity information on compounds in the environment, but are also beholden to the knowledge of what those compounds are and how they are transformed in the environment.

1.1.2 PAH Environmental Contamination

PAHs are formed during geological processes that result in fossil fuel production deep in the Earth, known as petrogenesis, UPAHs and HPAHs are released during extraction, transport, refinement, and use of fossil fuels for energy and industrial resources^{31 23}. During anthropogenic use, UPAHs and HPAHs can contaminate nearby groundwater, soil, and air. PAH contamination is common in soil and groundwater samples near heavily industrial sites, petrochemical storage and/or refinement sites, as well as industrial spill and landfill locations^{9 6 32 11}. Most prevalently, UPAHs and HPAHs are emitted in both gas and particle phase to the atmosphere from exposed crude petrochemical stores.

The most common form of atmospheric emission is through incomplete combustion of organic materials^{5 9 6}. PAHs are released from organic materials they naturally occur in, such as crude fossil fuels, or they can be formed through high-temperature reactions of hydrocarbons produced during combustion processes. Depending on the temperature of the combustion, PAHs are emitted as either gas, or bound to liquid or solid particulate matter, such as soot or organic aerosol particles. Gas-phase PAHs can either, remain in vapor state, or depending on their individual vapor pressures, they

can condense if the temperature in the atmosphere is not amenable to their vapor state, or they can sorb to nearby organic material^{21 33}.

1.2 Atmospheric Particulate Matter and PAHs

Once emitted there is a rapid cooling of the vapor leaving a combustion source, which is commonly visualized as steam released from industrial smokestacks. Depending on the individual PAH, at atmospheric conditions the compound may not condense to liquid phase. If there are organic based molecules nearby, this condensation can lead to liquid aerosol production. While this is possible, a more common occurrence is UPAH sorption to existing organic particles, either liquid or solid. The process of vapor moving to liquid or solid state is known as partitioning.

1.2.1 Gas-particle PAH Partitioning

Under normal atmospheric conditions, (temperature and pressure), compounds with high vapor pressures will naturally transition into the gas-phase, while compounds with lower vapor pressures will remain in the condensed phase. Vapor pressure can be useful in predicting the phase a compound may be found in, but a more relevant estimation comes from assessing how an individual compound could react when surrounded by environmental conditions. Vapor in the atmosphere is surrounded by liquid or solid water-based particles, solid black carbon particles, liquid organic particles, ionic salt-based particles, and a number of reactive gas species.³⁴ All of these components can alter the phase-state a compound will be found in.

The method used to estimate gas partitioning in the atmosphere involves the use of octanol as a surrogate for liquid phase organic particulate matter. From this assumption, a partitioning coefficient for the amount of a compound found in octanol versus in air can be estimated. This method has been around for years and is thoroughly described in “Environmental Organic Chemistry” by Rene P. Schwarzenbach et al.³⁴ The estimation for partitioning takes into account the physio-chemical properties of each molecule, the temperature, pressure, ionic strength, fugacity, and the total pressure of all gaseous molecules in the air. Using computer software, such as the EPISuite 4.1 software available from the US EPA, the partitioning coefficient (K_{OA}) for PAHs in the atmosphere can be estimated.

Estimated K_{OA} values for UPAHs results in a range of values ranging from 1×10^6 to 6×10^{10} . [EPISuite 4.1]. These estimated values indicate that UPAHs will be found in the particle phase. This has led to the monitoring of UPAHs on pollution watch lists through PM sampling and modeling. Many UPAHs, however, are frequently measured in higher concentrations in vapor phase, which directly negates these K_{OA} values.^{15 21} This represents a large disparity in attempts to predict and track UPAHs around the planet.

1.2.2 Fine Particulate Matter

Atmospheric particulate matter (PM) exists with a range of different properties. PM is the solid or liquid portion of the atmosphere, usually found suspended in air. Depending on current conditions, PM can be visible, such as ashes near a fire, or microscopic. When considering long-range

atmospheric transport (LRAT) and human health concerns, fine particulate matter is of the utmost concern.³⁵ Fine PM is classified as PM with an aerodynamic diameter of 2.5 micrometers or less, and is commonly referred to as PM_{2.5}. Larger particles, coarse PM, are filtered by human defense mechanisms upon inhalation.⁴ However, PM_{2.5} has the ability to pass through lung tissue and enter the blood stream. Once in the bloodstream, the chemical contents of PM_{2.5} can desorb from the particles and interact with biological systems.

Exposure to outdoor PM_{2.5} has been linked to over 3 million human deaths per year¹. High PM_{2.5} exposure occurs most frequently in developing nations where emission regulations are less stringent. Chronic PM_{2.5} exposure often leads to the early development of asthma, where acute exposure has been linked to numerous respiratory infections.^{36 37 38} Many of the components of PM_{2.5} have the ability to alter cellular redox homeostasis through the production of reactive oxygen species (ROS). Lung and heart tissue exhibit an increase in ROS after exposure to atmospheric PM_{2.5}.^{39 40 41} ROS are responsible for the depletion of electrolytes, which maintain cellular homeostasis with naturally occurring ROS, leading to oxidative stress in the affected tissues.³⁹ ROS caused oxidative stress has been linked to chronic inflammation, alterations to cell membrane transport lipids, proteins and DNA, cardiovascular and respiratory disease, cardiopulmonary morbidity and mortality disease, diabetes mellitus, neurodegenerative disorders, atherosclerosis, and many forms of cancer.^{42 43}

PM_{2.5} is the main source of atmospheric PAH transport. Gas-phase PAHs sorb to nearby organic particles after emission.⁹ [Walgreave 2010]^{20 44} Solid carbon based particles can sorb UPAHs, as well as organic liquid particles that naturally form on the surface of solid particles as well as on their own through condensation mechanisms. The largest fraction of atmospheric PM_{2.5} is organic aerosol particles.²

1.2.3 Secondary Organic Aerosols

Biogenic processes lead to the natural release of many volatile organic compounds (VOCs). Under natural conditions, these molecules have the ability to oxidize through reactions with naturally occurring reactive species in the atmosphere. These newly oxidized compounds are less volatile, and so condense and coalesce, forming liquid phase particles.^{45 46} Liquid phase oxidized compounds often contain reactive oxygen species (ROS) and highly oxidized organic molecules (HOMs) both of which are short lived, but have the ability to react with and sorb nearby organic molecules.^{45 47} This process results in secondary organic aerosol (SOA) particles forming. SOA particles do not remain liquid upon formation, the compounds within them continue to react forming long-chain hydrocarbon oligomers which result in highly viscous, semi-solid particles.^{48 49 50}

Studies show that SOA particles sorb nearby VOCs and semi-volatile organic compounds.^{51 52} Once sorbed to the SOA, these compounds, such as PAHs, become part of the semi-solid particles, and are therein thought to be shielded from oxidative degradation during atmospheric transport.^{52 50 53}

Recent works suggest that PAH transformation products are also contained inside SOA particles.^{54 13 13} This shielding is thought to be one of the main factors in the LRAT of UPAHs on PM_{2.5}.^{44 17} Once incorporated into SOA particles, the UPAHs become trapped from re-evaporating or being oxidized by the highly viscous SOA.¹³

There remains a large amount of ambiguity in the chemical composition of SOA, primarily because it is highly dependent on the geographic region it is formed in. Increasing the urgency to get a better understanding of the processes dominating SOA production and transport, is the increase in anthropogenic VOCs and SVOCs in the atmosphere.²

Recent studies have shown that, while SOA continues to make up a large and growing portion of atmospheric PM_{2.5}, continued anthropogenic emissions are creating an even larger mass of SOA in the atmosphere.²

1.2.4 Long-Range Atmospheric Transport

Atmospheric emissions are not contained to specific areas. Conditions such as temperature, relative humidity, irradiance, and wind. The complexity by which compounds are transported after emission continues to provide difficulty in predicting where the emitted compounds will end up. Chemical properties such as phase partitioning, as mentioned previously, can dictate what compartment of the atmosphere that compound will end up in.^{30 11} As discussed previously, SOA can form from emitted VOCs, and can sorb and entrap nearby compounds. PM_{2.5} has a known ability to translocate globally, carrying with it any number of compounds that have sorbed to the particles

throughout the journey, along with any transformation products that may be formed along the way. Understanding the chemistry of PM_{2.5} is necessary in reducing global deaths from exposure to PM_{2.5}.

Modeling the transport of emissions throughout the atmosphere requires accurate input of the chemistry involved in the transport. VOCs from different ecosystems present different chemistry in SOA formation and PAH sorption.^{48 49 13 51} Atmospheric conditions, such as temperature and relative humidity affect the way particles form, and the viscosity of them over time.⁴⁸
^{55 47} Improving the accuracy of the models to predict the movement of compounds through the atmosphere is essential for protecting communities from exposure. To do this, accurate chemical composition of PM_{2.5} is needed.
17

1.3 Exposure to PM_{2.5}

Inflammation, asthma, cardiovascular disease, neurological disorders, and increases in cancer have all been linked to PM_{2.5} exposure.^{36 37 35 4}
Exposure to PM_{2.5} disproportionately effects minority, impoverished, and traditional indigenous communities around the world.^{1 36 56} These communities are more likely to have higher indoor exposures to PM_{2.5} than industrialized communities, and symptoms of chronic exposure to PM_{2.5}.^{1 56}
Protecting communities from exposure requires accurate prediction of transport, as well as comprehensive toxicological data about the vast suite of compounds transported in PM_{2.5}.^{17 57}

1.3.1 Oxidative Stress from PM_{2.5} exposure

Inhalation of PM_{2.5} results in oxidative stress in both lung and heart tissue.^{58 59 60 43} Oxidative stress results when ROS are introduced to cells. ROS are also referred to as free radicals, as many are compounds containing radical oxygen.^{61 62} Cellular response to ROS is the deployment of anti-oxidants to counter the free radical species. Depletion of anti-oxidants results in stress on the cell resulting in an array of damage culminating in DNA or RNA damage and apoptosis.^{63 64} SOA and PAHs have also been linked to oxidative stress in humans.^{65 66 67 68 69}

To examine if a sample will cause oxidative stress upon exposure, its oxidative potential can be measured.^{42 39 60} Biological assays which measure the amount of 8-hydroxy deoxyguanosine, malondialdehyde, and F₂-isoprostanes have been used to show direct biological responses to oxidative stress inducing samples.^{42 70 39} Many biological assays require a different extraction process than are required for full analytical chemical analysis.⁷¹ For environmental chemists, a common practice is to split samples for both chemical analysis and toxicological assays. This can result in a lower mass of chemicals in analytical methods due to smaller samples sizes, and may result in a higher number of non-detects.^{72 25 73}

A common way to measure for oxidative potential of samples is the Dithiothreitol (DTT) assay. In this assay DTT reacts with samples to create reactive oxygen species (ROS) the same way cellular assays do.^{74 43 75} The DTT assay has become a vital tool employed by environmental chemists to assess PM_{2.5} oxidative potential, as indicators of toxicity, without the need for

biological assays.⁶⁰ The reaction of DTT with samples to create ROS is commonly used to measure peroxide production in a number of settings.⁷⁶ Recent works have shown that using a DTT consumption assay replicates oxidative stress biological assays, and reduces false negatives due to ROS presence in SOA particles.^{76 74}

The individual components of PM_{2.5} responsible for causing oxidative stress remain unknown, while recent research has demonstrated that the organic portion of PM_{2.5} is responsible for more oxidative stress than the inorganic portion.^{63 77} Smaller particles and particles containing more oxidized organic compounds have been linked to higher levels of oxidative stress.^{78 79 58 77 66} The link between chemical constituents and oxidative stress cannot be described without knowing the chemicals in PM_{2.5} that are responsible, and their modes of producing oxidative stress in exposed tissues.^{75 80 60}

1.3.2 Risk Assessment for PM_{2.5} exposure

Protecting communities from the harmful effects of PM_{2.5} requires both the ability to accurately predict atmospheric transport, and complete understanding of the compounds in the PM_{2.5}. The development of relative potency factors (RPFs) values by the US EPA, allows for excess lifetime cancer risk assessment for PAHs using the equivalent carcinogenic potency of BaP.²⁹ Such assessments utilize population averages of body mass, exposure rates and durations, as well as age of individuals (i.e. child or adult). For inhalation risk assessments, these values include the average inhalation

rate per day, average exposure time per day, and duration of exposure in years. The equation used to estimate cancer risk for inhalation is:

$$\text{Cancer Risk} = \sum_{i=1}^{\infty} (\text{CPAH}_i \times \text{RPF}_i) \times \text{UR}_{\text{BaP}}$$

Where CPAH_i is the measured concentration of individual PAH_i , RPF_i is the relative potency factor of PAH_i , and UR_{BaP} is the unit risk for BaP concentration (ng/m^3 air). The California State Environmental Protection Agency has determined the UR_{BaP} to be 1.1×10^{-6} , based on toxicological testing on mice. The WHO has set this value at 8.7×10^{-5} , based on epidemiological studies of the urine of coke oven workers.⁸¹ As this demonstrates, these values are set by different agencies around the world, and can vary by orders of magnitude. Different UR_{BaP} are established for different portions of the populations, such as children, adults, and the elderly. The value used must be dependent on the population of interest in a study. Cancer Risk calculations are used to calculate the risk of developing cancer due to a lifetime of exposure to the measured concentrations, assuming a 70 year lifetime.^{29 10}

1.4 Environmental Justice

Environmental justice has been a topic of research for many years. Broadly, the concept behind environmental justice encompasses both science into environmental contamination, and social sciences addressing inequalities of certain communities to access scientific information⁸². Researching environmental justice includes community concerns, translating scientific

research for the consumption and use of affected communities, and addressing the concerns of affected communities all in the research design⁸².

1.4.1 Exposure inequities.

Minority and low-income communities around the planet are disproportionately exposed to PM_{2.5}.¹ Many of these communities are not only exposed to PM_{2.5} in outdoor air, but also to higher incidence of indoor PM_{2.5} and higher rates of outdoor PM_{2.5} intrusion into their living spaces.^{1 83}
⁵⁶ Due to lower rates of accessibility to clean air technologies, low-income communities are regularly exposed to larger quantities of PM_{2.5}.^{1 56} Many such communities also still rely on open burning stoves to cook and heat their homes, creating more indoor PM_{2.5} containing combustion byproducts, such as PAHs.¹

1.4.2 Native American Communities.

The 1855 Treaty of Point Elliot designated Native American Communities to own land known as Reservations recognized by the US Federal Government.^{83 84} Many Reservation lands are small subsets of the land historically inhabited by the tribal communities, and are situated near industrial complexes.⁸⁴ Native Americans, along with indigenous people around the globe, are disproportionately affected by the adverse health outcomes associated with PM_{2.5} exposure, and are less equipped to address concerns.⁵⁶

1.5 Dissertation Objectives

The goal of this dissertation is to assess what types of PAHs are present in $PM_{2.5}$. Most $PM_{2.5}$ monitoring studies focus their measurements on the UPAHs with known toxicity profiles, and which appear on chemical exposure warning lists such as the PPL. Advances in analytical methods have expanded the list of PAHs which can be quantified beyond the PPL 16 PAHs. Due to their lower volatility, HMW, HPAH, NPAH, OPAH and OHPAHs have been measured in other environmental compartments. This dissertation examines the presence of these subclasses of PAHs in $PM_{2.5}$.

Using advanced aerosol technology, the effect that PAH vapor has on the formation of SOA particles was assessed in collaboration with scientists at Pacific Northwest National Laboratory (PNNL). Changes in SOA particle size, number, and density due to the presence of four individual vapor phase PAHs, were measured at PNNL. Filters of SOA particles formed with and without PAH vapor were collected on quartz fiber filters, extracted, and analyzed for PAH and PAH transformation products composition using gas chromatography mass spectrometry, at OSU.

To determine if the chemistry observed in the SOA study was applicable to atmospheric $PM_{2.5}$, field studies were performed in collaboration with the Swinomish Indian Tribal Community (SITC) of the northern portion of the Puget Sound in the US state of Washington. Two high-volume air samplers were deployed on the SITC Reservation alongside meteorological instrumentation to collect $PM_{2.5}$ from the Reservation. Paired filters were

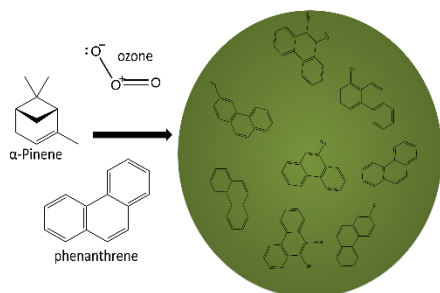
collected over a two-year period, and stored in a freezer (-20°C). Extraction of the filters was performed using accelerated solvent extraction, and analyzes were performed using gas chromatography mass spectrometry to quantify six sub-classes of PAHs from the PM_{2.5}.

The DTT consumption assay was used to assess the oxidative potential of PAHs measured in the PM_{2.5} from the SITC Reservation. Individual PAHs, mixtures of PPL PAHs, PM_{2.5} extracts, and mixtures of PAHs measured in PM_{2.5} were analyzed using a high efficiency microscale (96 well plate) DTT assay. Matching PAH concentrations to measured PM_{2.5} concentrations allowed us to examine what portion of the PM_{2.5} oxidative potential was due to the measured PAH concentrations, and established a calculation to predict oxidative stress of the PM_{2.5} using the measured concentrations of PAHs.

Chapter 2

Formation of Polycyclic Aromatic Hydrocarbon Oxidation Products in α -Pinene Secondary Organic Aerosol Particles Formed Through Ozonolysis

Produced α -pinene SOA in the presence of phenanthrene vapor



Quantified phenanthrene and phenanthrene oxidation products in collected SOA

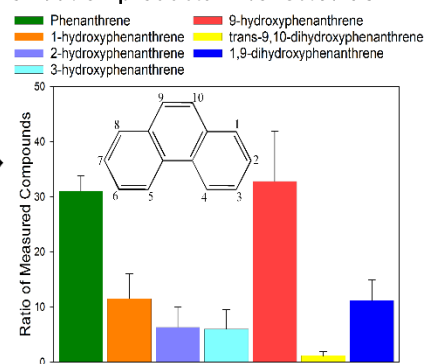


Figure 2.0

Chapter 2:

Formation of polycyclic aromatic hydrocarbon oxidation products in α -pinene secondary organic aerosol particles formed through ozonolysis

Amber L. Kramer[†], Kaitlyn J. Suski[‡], David M. Bell[‡], Alla Zelenyuk[‡], Staci L. Massey Simonich^{†*}

[†] Department of Chemistry, [‡] Department of Environmental and Molecular Toxicology, Oregon State University, Corvallis Oregon 97331, United States

[‡] Atmospheric Sciences and Global Change, Pacific Northwest National Laboratory, Richland Washington 99354, United States

Contributions – Prepared by Amber L. Kramer with editorial comments provided by Kaitlyn J. Suski, David M. Bell, Alla Zelenyuk and Staci L. Massey Simonich. Amber Kramer assisted in SOA production and characterization at PNNL, collected SOA on filters, extracted and performed chemical analysis of SOA extracts at OSU.

Published – *Environmental Science & Technology* 53.12 (2019): 6669-6677

Copyright © 2019 American Chemical Society

*Corresponding Authors: staci.simonich@oregonstate.edu & Alla.Zelenyuk-Imre@pnnl.gov

2.1 ABSTRACT

Accurate long-range atmospheric transport (LRAT) modeling of polycyclic aromatic hydrocarbons (PAHs) and PAH oxidation products (PAH-OPs) in secondary organic aerosol (SOA) particles relies on the known chemical composition of the particles. Four PAHs, phenanthrene (PHE), dibenzothiophene (DBT), pyrene (PYR), and benz(a)anthracene (BaA), were studied individually to identify and quantify PAH-OPs produced and incorporated into SOA particles formed by ozonolysis of α -pinene in the presence of PAH vapor. SOA particles were characterized using real-time in-situ instrumentation, HR-ToF-AMS, and collected on quartz fiber filters for offline analysis of PAHs and PAH-OPs. PAH-OPs were measured in all PAH experiments at equal or greater concentrations than the individual PAHs they were produced from. The total mass of PAH and PAH-OPs, relative to the total SOA mass, varied for different experiments on individual parent PAHs: PHE and 6 quantified PHE-OPs (3.0%), DBT and dibenzothiophene sulfone (4.9%), PYR and 3 quantified PYR-OPs (3.1%), and BaA and benz(a)anthracene-7,12-dione (0.26%). Further exposure of PAH-SOA to ozone generally increased the concentration ratio of PAH-OPs to PAH, suggesting longer atmospheric lifetimes for PAH-OPs, relative to PAHs. These data indicate that PAH-OPs are formed during SOA particle formation and growth.

2.2 INTRODUCTION

Polycyclic aromatic hydrocarbons (PAHs) are toxic and ubiquitous environmental pollutants and have been shown to undergo long-range atmospheric transport (LRAT) bound to fine particulate matter (PM_{2.5})^{85 15}. Several PAHs have been demonstrated to have adverse human health effects, which has led to the global monitoring of 16, primarily parent, unsubstituted PAHs^{85 86}. PAHs are found naturally in crude fossil fuels and are emitted into the environment through anthropogenic extraction, transportation, refinement, and use of these fuels⁸⁵. Additionally, incomplete combustion of organic material represents the largest source of PAH emissions to the environment^{87 88}. The complex mixture of compounds in natural organic matter results in a wide range of PAH emission profiles when combusted, and the varying chemical and physical properties of PAHs emitted during combustion results in differing degrees of absorption and adsorption to atmospheric PM_{2.5}, defined as particulate matter having an aerodynamic diameter of 2.5 microns or less^{15 31 9}.

PM_{2.5} is a growing public health concern which has been linked to respiratory, cardiovascular, and neurological adverse health effects^{89 36}. Human exposure to PM_{2.5} leads to increases in reactive oxygen species in heart and lung tissue, and has been linked to over 3 million deaths per year around the world^{89 1}. In addition, atmospheric PAH transport has largely been predicted to occur as a result of sorption, or incorporation into, secondary organic aerosol (SOA). SOA, formed from atmospheric

reactions of biogenic and/or anthropogenic volatile organic compounds (VOCs) with reactive atmospheric species (such as ozone, hydroxyl radical, and NO_x), accounts for an increasing proportion of global PM_{2.5} mass in the atmosphere (50% - 80%)^{90 91 20 92 19 93}.

The presence of PAHs during SOA formation can significantly affect SOA formation and particle properties, including particle or chemical composition, volatility, and viscosity, leading to their longer atmospheric lifetimes and higher loadings than predicted by models^{44 13 94}. Gas-phase PAHs adsorb on the surfaces of SOA particles during their formation and growth, where they react with gas-phase atmospheric reactants and become entrapped and highly dispersed throughout highly viscous, semi-solid SOA particles^{13 53}. The limited diffusion of the entrapped PAHs shields them from evaporation and oxidation, which enables their LRAT^{53 95}. Since gas-phase ozonolysis of PAHs occurs at a much slower rate than particle sorption, PAH sorption into SOA particles is considered to be the dominant fate of PAHs in the atmosphere^{90 96}. In addition, SOA particles, formed by ozonolysis in the presence of the PAH vapor, contain not only parent PAHs, but also products of surface reactions between PAHs with ozone^{13 94 97}.

Due to their ranges in toxicity, modeling PAH transport in atmospheric PM_{2.5} is essential for human risk assessment, especially in developing countries¹. However, many models assume relatively short PAH atmospheric lifetimes and short volatile and semi-volatile organic

compound retention times of VOCs in SOA particles¹⁷. This may partially explain under-predictions (30-70%) of PAH atmospheric concentrations as compared to those measured in field campaigns^{17 20 87}. Moreover, current atmospheric models take only a limited number of unsubstituted PAHs into account. These models neglect PAH-OPs that may form during atmospheric transport and are less volatile, and may be more toxic than, their parent PAHs^{17 20 94 18}. Including oxidized compounds, such as PAH-OPs, into the SOA models may more accurately predict the atmospheric lifetimes of PAHs and bring modeled PAH concentrations closer to measured PAH concentrations from field campaigns¹⁷. There is currently a lack of data describing the speciation of organic pollutants, such as PAHs, in both laboratory and ambient SOA^{17 13}.

To gain a better understanding of the synergistic relationship between SOA formation and PAH incorporation in SOA, this study was designed to quantify PAHs and PAH-OPs produced during the formation of α -pinene (α -P) SOA through ozonolysis, and in the presence of PAHs. After the cessation of particle formation, these particles were then exposed to additional ozone to assess if further oxidation of PAHs occurs during atmospheric transport. α -P SOA particles were produced in the presence of PAH standards (PAH-SOA), characterized using real-time in-situ instrumentation, a high resolution time-of-flight aerosol mass spectrometer, collected on quartz fiber filters, and extracted and analyzed for PAHs and PAH-OPs. Phenanthrene (PHE), dibenzothiophene (DBT),

pyrene (PYR), and benz(a)anthracene (BaA) were chosen for this study because of their ubiquitous presence in the atmosphere and their range of vapor pressures ($2.8 \times 10^{-5} - 2.73 \times 10^{-2}$ Pa at 25°C) (Table S1)^{87 88}. To our knowledge, this study is the first to show the formation of PAH-OPs in SOA and their subsequent aging.

2.3 MATERIALS AND METHODS

2.3.1 Materials. A list of all compounds, abbreviations, chemical characteristics, and manufactures can be found in the supplementary information (Table A1.T1). Analytical standards were used for extraction efficiency testing and the production of calibration curves for quantitative purposes. Standards were stored in the dark at -20°C. To quantify hydroxylated compounds, derivatization was performed using N-tert-butyltrimethylsilyl-N-methyl-trifluoroacetamide (MTBSTFA) for mono-hydroxy PAHs, and N,O-bis(trimethylsilyl)trifluoroacetamide (BSTFA) for poly-hydroxy PAHs, as previously described⁹⁸. Quartz fiber filters (QFFs) were purchased as 8" x 11" sheets, (G.E. Whatman (Buckinghamshire, UK)), and were cut to fit an inline filter trap. Before use, QFFs were placed in a ventilated oven and held at a temperature over 350°C for 12 hours to remove any organic contaminants and were then sealed in aluminum foil packets and placed inside plastic zip-seal bags.

2.3.2 Experimental Design.

SOA Formation. Figure 2.1 illustrates the generation of PAH-SOA, as previously described^{44 13}. Briefly, to ensure PAH vapor was at or near

saturation vapor pressure, in triplicate experiments, ~0.5 g of individual PAH solid was placed into ~70 L Teflon bags filled with zero air and allowed to equilibrate for 48 hours ahead of SOA production. Estimates of PAH vapor phase mixing ratios can be found in the supplemental information (S14-S15). As detailed elsewhere^{44 13}, PAH-SOA formation was initiated by introducing 100 ppm cyclohexane (used as a hydroxyl radical scavenger), 600-800 ppb ozone (produced using Jelight Company (Irving, CA) model 600 ozone generator), and 400 ppb α -P (used as model system for biogenic SOA precursors) into Teflon bags^{99 52}. Ozone was measured using a Thermo Scientific (Waltham, MA) model 49i Ozone Monitor. The SOA was allowed to grow for ~1 hour. Size distributions and mass loadings of PAH-SOA particles were measured in-situ in real time (RTIS) using a Scanning Mobility Particle Sizer (SMPS), which was comprised of a TSI (Shoreview, MN) Differential Mobility Analyzer (DMA) model 3080 and a TSI ultrafine condensation particle counter (CPC) model 3786, using the documented α -P SOA density of 1.18 g/cm³ as a reference^{44 100}. Particle characteristics, such as vacuum aerodynamic diameter, shape, density, and mass spectra were measured using a single particle mass spectrometer, miniSPLAT, as described in detail elsewhere.⁴⁴ Additionally, an Aerodyne high resolution time-of-flight aerosol mass spectrometer (HR-ToF-AMS) was used to obtain average mass spectra of polydisperse SOA particles¹⁰¹.

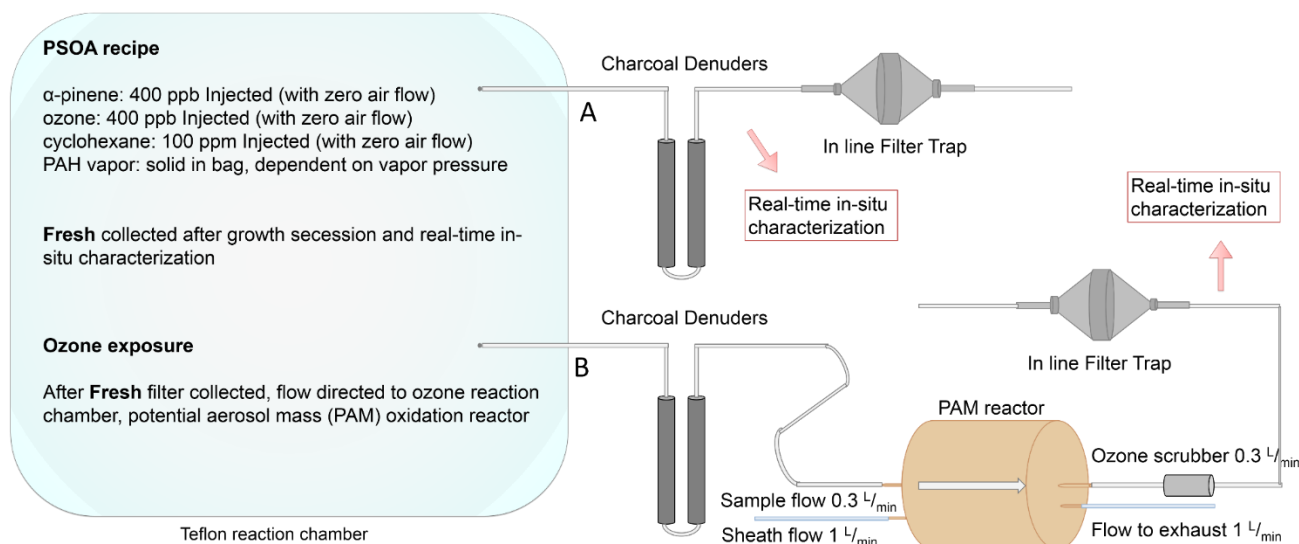


Figure 2.1. Experimental setup: SOA was produced by injecting 400 ppb α -pinene, 600-800 ppb ozone, and 100 ppm cyclohexane (to act as OH radical scrubber) into a \sim 100 L Teflon reaction chamber filled with zero air equilibrated with PAH vapor from solids. Particle growth was monitored using SMPS. When particle growth stopped (\sim 1 hour), the *fresh* filter (A) was collected by directing a flow of the sample through charcoal denuders, to remove gas phase organic molecules, and onto a QFF in an inline filter trap, after real-time in-situ particle characterization was performed using single particle mass spectrometer (miniSPLAT). After *fresh* SOA collection was complete, the sample flow was directed into an oxidation flow tube reactor (PAM), for ozone exposure samples (B), allowed to mix, and again analyzed using miniSPLAT and collected using the inline filter trap.

To assess the volatility of the SOA particles, particles were size-selected with a DMA, passed through two activated charcoal denuders, and loaded into a stainless steel evaporation chamber that contained a layer of activated charcoal as detailed elsewhere⁹⁹. Particle vacuum aerodynamic diameter was periodically measured as a function of time to quantify particle evaporation kinetics^{99 102}. Triplicate controls of pure α -P SOA were also collected in each experimental setup and analyzed along with each PAH-SOA experiment. No PAH or PAH-OPs were detected in the pure α -P SOA controls (Figure A1.F1). All experiments presented were conducted at low (\leq 5%) relative humidity (RH). Given that previous works

have shown that increased RH decreases SOA viscosity and diminishes the ability of SOA to shield PAHs from oxidation¹⁷, future studies will include experiments conducted at different RHs.

Fresh PAH-SOA. After particle growth had ceased in each individual Teflon bag, the total SOA mass loading ($\mu\text{g}/\text{m}^3$) was measured for each batch of α -P SOA or PAH-SOA using SMPS. Using Teflon tubing, air from the Teflon bag was pulled through two charcoal denuders (in series), to remove gas-phase organic molecules (including PAHs), and then through a QFF fitted into a 4.7 cm inline filter trap. This was done until at least 15 μg of PAH-SOA (or α -P SOA) mass was collected (based on mass loading calculations). Due to the low vapor pressure of BaA, and preliminary experimental results that showed no BaA concentration above the detection limits in the QFF extracts, ~ 150 μg of BaA-SOA (from two individual bags) was collected on a single QFF to ensure the BaA concentration were above the detection limit. QFFs were removed from the inline trap, sealed in pre-baked aluminum foil packets, stored at -20°C to reduce volatilization loss, and transported on dry ice, until extraction.

Ozone-exposed PAH-SOA. In order to test if PAHs and PAH-OPs incorporated in freshly formed highly viscous PAH-SOA particles can undergo heterogeneous oxidation reactions during atmospheric transport, a 13.3 L potential aerosol mass oxidation flow reactor (PAM, an Aerodyne (Billerica, MA)) was used to expose particles to high concentrations (6-10 ppm) of ozone¹⁰³. Dry zero air was used as the sheath flow at 1 L/min

and the sample flow rate was 0.3 L/min (Figure 2.1). To ensure particles were well-mixed with ozone in the PAM reactor, QFF collection began after the individual PAH-SOA or α -P SOA was flowed through the PAM reactor for 10-15 minutes. The high concentration of ozone in the PAM reactor, and the residence time of \sim 10 min for particles in the PAM reactor, resulted in a particle exposure to ozone equivalent to that experienced by PM_{2.5} during LRAT¹³. The flow from the PAM reactor was passed through a Perma Pure ozone scrubber (Toms River, NJ) to strip away gas phase ozone from the sample stream before QFF collection. An average \sim 20-fold decrease in mass loading was measured through all experiments after ozone exposure in the PAM reactor. This was primarily due to dilution, wall losses, and evaporation in the PAM reactor and transfer lines.

The PAH-SOA ozone exposure experiments were conducted in triplicate with the activated charcoal denuders before the PAM reactor to remove the gas-phase organic compounds (PAHs, PAH-OPs, α -P, and PAH-SOA). To assess if gas-phase organic compounds changed the measured chemical composition of the PAH-SOA particles, triplicate ozone exposure experiments were performed with and without the charcoal denuders placed in line before the PAM reactor. In addition to QFF collection, particles underwent real-time in-situ characterization in all experiments. Due to variability in particle losses during PAH-SOA exposure in the PAM reactor, and the significantly lower mass of collected

particles on the QFF, ozone exposure data had higher uncertainty and higher standard error than fresh SOA data. No statistical difference was measured in the compounds detected between PAH-SOA ozone exposures with or without gas phase organic compounds present (Table A1.T2).

To clean the experimental system between PAH-SOA experiments, nitrogen gas was flushed through the entire system (with PAM reactor lights turned on) until the CPC no longer detected particles. System blanks were collected on QFFs by flowing zero air (2 L/min for 5 to 10 minutes) through the entire experimental system. System blanks were analyzed along with all samples, and no PAHs or PAH-OPs were detected above lab blank concentrations. This indicates that the cleaning procedure removed any lingering PAH-SOA from the experimental system.

2.3.3 QFF extraction. The QFFs were removed from their cold-stored sealed foil envelopes, and immediately folded in half, tightly rolled and inserted into 4 mL amber glass vials. Isotope labeled surrogate standards (Table A1.T3) were spiked on QFFs and used to account for extraction losses.

Due to the volatility of some parent PAHs and PAH-OPs, many extraction methods resulted in significant analyte loss during solvent evaporation¹⁰⁴. To reduce losses, sonication of the QFF was chosen to reduce extraction steps. Dichloromethane, ethyl acetate, and acetone

were tested for the highest analyte recovery, and while the dichloromethane and ethyl acetate had high recovery for the nonpolar PAHs (~50% for each), acetone provided the highest recovery for the more polar PAH-OPs (~80%) while slightly lower for the PAHs (~43%). Sonication was therein performed with 2 mL acetone solvent for 60 min at room temperature as the QFF extraction method. This procedure did not require solvent evaporation or exchanges, and provided an average of ~68% extraction recovery for spiked analytes (details for efficiency testing are in the SI, and on Table A1.T4).

The extract was transferred into 2 mL amber vials with pre-baked Pasteur pipettes. The QFF extract volume average was between 1000 and 1200 μ L. To ensure accurate dilution calculations, all extracts were brought to a final volume of 1500 μ L with acetone. Aliquots of the extract were then used for chemical analysis as described in the SI.

To account for any laboratory PAH or PAH-OP contamination, clean lab blank QFF filters were extracted and analyzed alongside experimental QFF. Low concentrations of DBTS, PHE, PYR, BaA and 1,9-OHPHE were measured in lab blank and were subtracted from sample measurements.

2.3.4 Chemical analysis. Prior to analysis, isotopically labeled internal standards (Table A1.T3) were added to QFF extract aliquots. Identification and quantification was performed using an Agilent J&W 30 m X 0.25 mm i.d. (0.25 μ m film thickness) DB-5 capillary column on an

Agilent 5977A Gas Chromatograph, coupled to a quadrupole Mass Spectrometry (GC-MS) operated in 70 Volt electron impact ionization mode. Detailed GC-MS methods can be found in supplementary information (SI). Extracts were analyzed using both selected ion monitoring (SIM) mode, to look for and quantify PAHs and PAH-OPs with available analytical standards, and full scan mode (with and without derivatization) to identify unknown peaks that might be associated with other PAH-OPs without available analytical standards. To measure hydroxy substituted PAHs (OHPAHs), derivatization using MTBSTFA for mono-hydroxylated OHPAHs, and BSTFA for poly-hydroxylated OHPAHs, was performed. This process required incubation at 65°C for 25 minutes (MTBSTFA) or 70°C for 45 minutes (BSTFA) and is described in the SI. Mass spectra of GC-MS fragmentation were interpreted using Mass Hunter software. Lab blank PAH or PAH-OP concentrations were subtracted from their measured concentrations, and divided by the total SOA mass collected, to give the weight percent (wt%) of PAH or PAH-OP. We report the mean weight percent \pm one standard error (SE).

2.3.5 Statistical analysis. For each experiment, PAH-SOA were produced in triplicate reaction chambers and fresh and ozone-exposed QFFs were collected from each reaction chamber experiment for statistical analysis. Statistical analysis was performed using R and R-studio software. A two sample Students T-test was used to test for significance,

with p -value ≤ 0.05 . Due to its low vapor pressure, only one BaA experiment was conducted and no statistical analysis was performed.

2.4 RESULTS AND DISCUSSION

The measurements of PAH and corresponding PAH-OPs for all the experiments in this study are presented in Table 2.1, Figure 2.2A, and Figure A1.F2. The results are reported as the mean weight percent (wt%) of PAHs and PAH-OPs relative to the total collected mass of PAH-SOA on the QFF (\pm one standard error). The PAH-OP concentrations are also reported as a ratio relative to the parent PAH concentration in Table 2.1.

2.4.1 Phenanthrene. PHE, with a vapor pressure of 1.61×10^{-2} Pa, was measured at 0.91% (± 0.28) of the *fresh* PHE-SOA mass (Figure 2.2A) and had the largest number of different PAH-OPs identified of all the PAHs tested. A total of six individual PHE-OPs (including 1-,2-,3-, & 9-OHPHE, *trans*-9,10-OHPHE, and 1,9-OHPHE) were identified and quantified in the PHE-SOA QFF extracts. The sum of PHE-OP masses measured within the *fresh* PHE-SOA extracts was 2.75 times the mass of the PHE measured in the same extracts (Table 2.1). The percent of individual PHE-OPs measured in the *fresh* PHE-SOA extracts, was: 9-OHPHE 0.84% (± 0.09), 1,9-OHPHE 0.53% (± 0.16), 2-OHPHE 0.52% (± 0.08), 3-OHPHE 0.49% (± 0.08), 1-OHPHE 0.48% (± 0.04), and *trans*-9,10-OHPHE 0.04% (± 0.02).

PAH in Teflon Bag Oxidation Product	Abbrev.	Fresh PAH-SOA		Ozone-exposed PAH-SOA	
		wt % (\pm SE) of PAH-SOA	Ratio to Parent PAH (OP/PAH)	wt % (\pm SE) of PAH-SOA	Ratio to Parent PAH (OP/PAH)
Phenanthrene (n=4)	PHE	0.91% (0.28)		0.53% (0.22)	
1-hydroxyphenanthrene	1-OHPHE	0.48% (0.05)	0.56	ND	
2-hydroxyphenanthrene	2-OHPHE	0.52% (0.08)	0.34	ND	
3-hydroxyphenanthrene	3-OHPHE	0.49% (0.08)	0.33	ND	
4-hydroxyphenanthrene	4-OHPHE	ND	ND	ND	
9-hydroxyphenanthrene	9-OHPHE	0.84% (0.09)	0.91	6.27% (2.63)	12.11
<i>cis</i> -9,10-dihydroxyphenanthrene	<i>cis</i> -9,10-OHPHE	ND	ND	ND	
<i>trans</i> -9,10-dihydroxyphenanthrene	<i>trans</i> -9,10-OHPHE	0.04% (0.02)	0.02	0.09% (0.02)	0.15
1,9-dihydroxyphenanthrene	1,9-OHPHE	0.53% (0.55)	0.59	12.33% (5.75)	9.74
phenanthren-1,4-dione	1,4-PHE-dione	ND	ND	ND	
9,10-phenanthrenequinone	9,10-PHEQ	ND	ND	ND	
2'-formyl[1,1'-biphenyl]-2-carboxylate	2'F(1-1'BP)2C	ND	ND	ND	
Dibenzothiophene (n=3)	DBT	2.45% (0.61)		6.86% (1.85)	
Dibenzothiophene sulfone	DBTS	2.46% (0.76)	1.01	2.29% (0.49)	0.33
Diphenyl Sulfoxide	DPS	ND	ND	ND	
Pyrene (n=3)	PYR	1.79% (0.62)		6.32% (3.42)	
1-hydroxypyrene	1-OHPYR	1.25% (0.31)	0.70	5.91% (2.24)	0.94
4H-cyclopenta[cd]phenanthren-4-one	4H-CPP	0.07%	0.01	ND	ND
6H-benzo(cd)pyrene-6-one	6H-BcdP	0.04% (0.02)	0.02	0.70% (0.22)	0.11
4-carboxy-5-phenanthrenecarboxylate	4C5PC	ND	ND	ND	
Benz(a)anthracene (n=1)	BaA	0.08%			N/A
3-hydroxybenz(a)anthracene	3-OHBaA	ND	ND		
benz(a)anthracene-7,12-dione	7-12-BaA-dione	0.19%	2.5		

Table 2.1. Measured PAH and PAH-OP in PAH-SOA. Reported values represent the mean wt% of the compound in the PAH-SOA with 1 standard error (\pm SE) reported. Ratio to Parent PAH was determined by dividing the detected mass of PAH-OP into the detected mass of the Parent PAH. n indicates the number of individual SOA experiments performed in separate reaction chambers using each PAH. ND indicates not detected and N/A indicates not applicable.

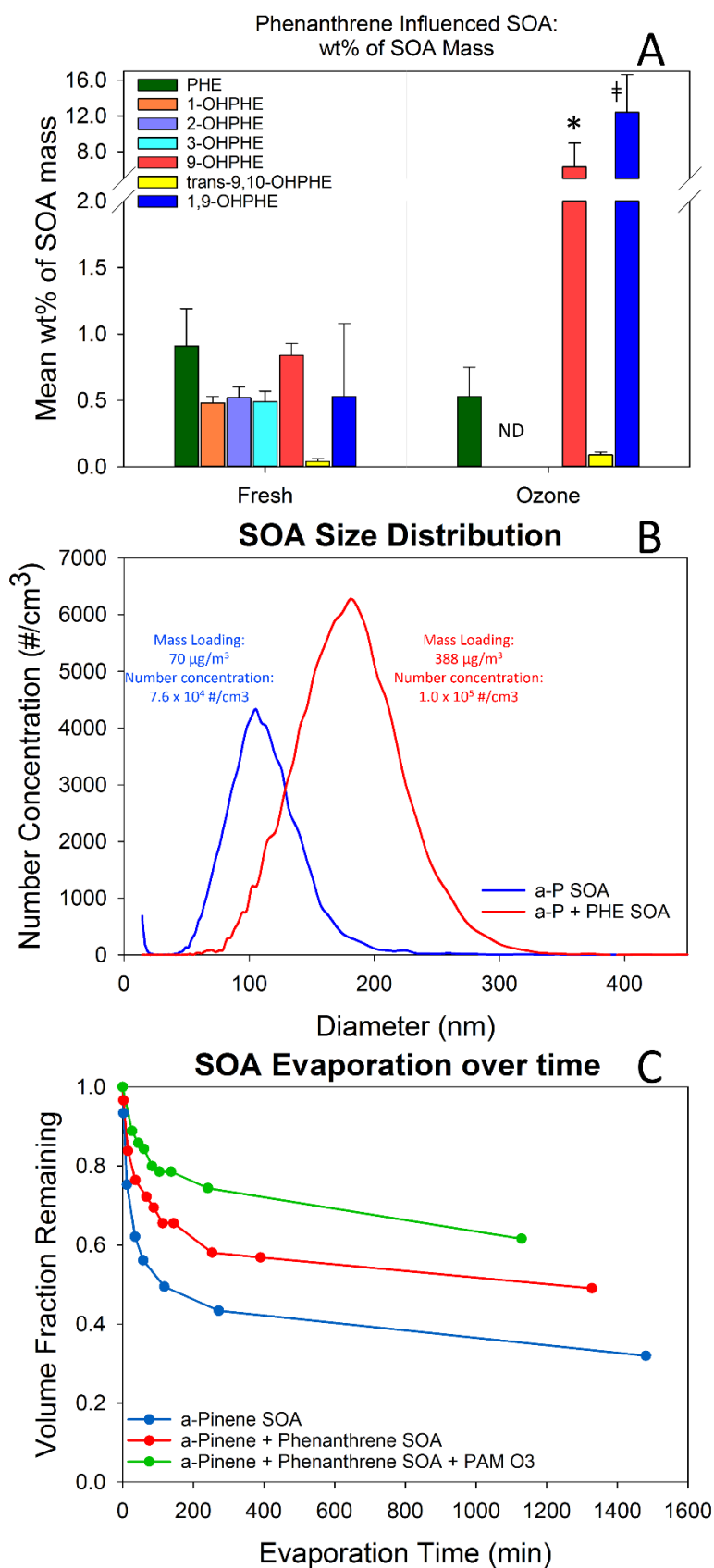
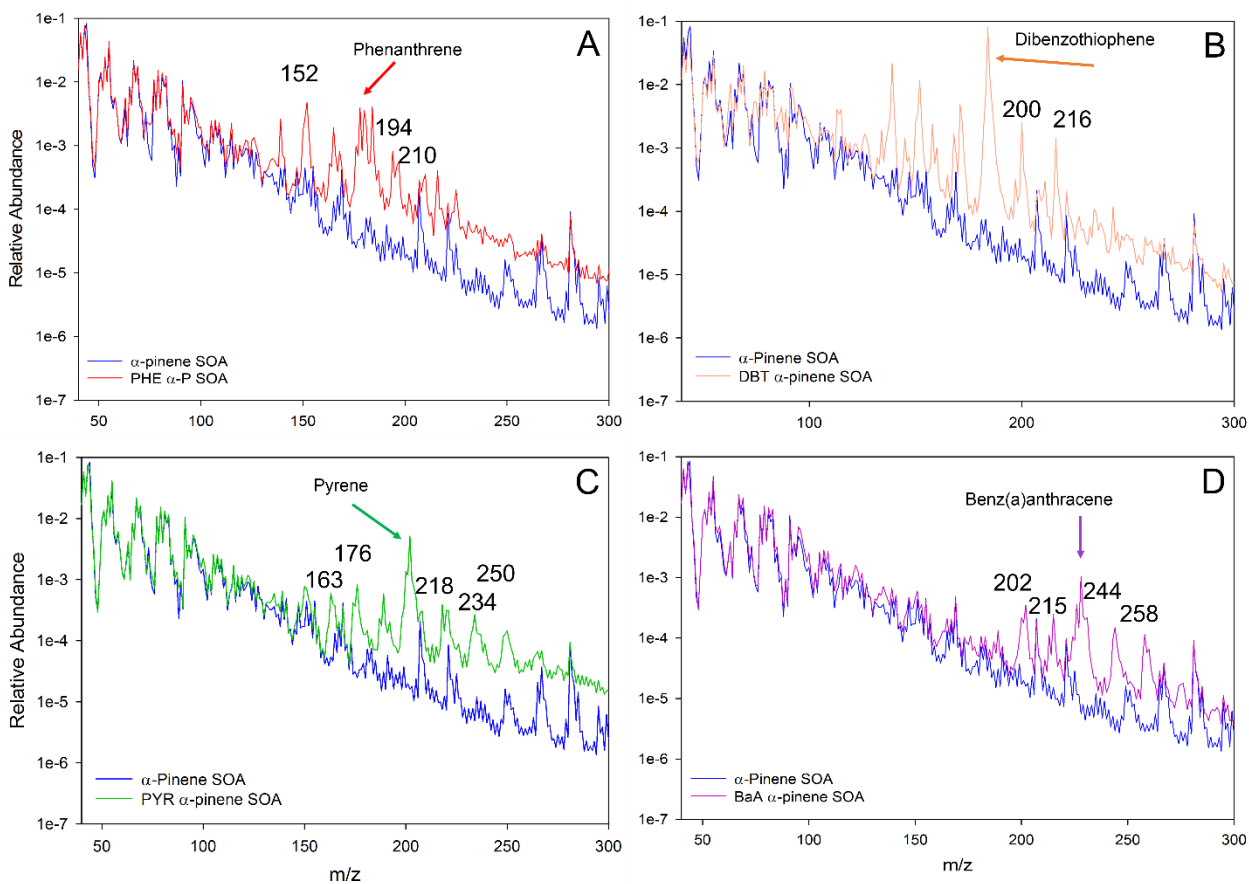


Figure 2.2. A) Mean wt% (± 1 standard error) of compounds measured in collected freshly formed and ozone-exposed PHE-SOA, measured using GC/MS. * indicates a statistically convincing evidence of a difference (p -value < 0.10) in the measured concentration (wt%) from fresh to ozone-exposed. ‡ indicates a statistically significant difference in measured concentration of PHE-OP than the PHE in ozone exposed PHE-SOA. B) Mobility size distributions of pure α -P SOA particles (blue) and PHE-SOA particles formed by ozonolysis of α -pinene in the presence of gas-phase PHE (red). C) Evaporation kinetics of α -P SOA (blue), PHE-SOA (red), and PHE-SOA exposed to additional ozone (green) measured as the volume fraction of particles remaining over time in minutes, measured with single particle mass spectrometer (miniSPLAT).

The HR-ToF-AMS mass spectrum of the PHE-SOA particles in Figure 2.3A shows an increase in the number of higher m/z peaks associated with PHE-SOA particles, relative to SOA particles. This suggests that additional non-volatile compounds (including PHE-OPs) were present in the PHE-SOA

HR-ToF-AMS



particles than were detected by GC/MS (with and without derivatization).

Figure 2.3. HR-ToF-AMS data for the four PAHs tested in this study. Each plot shows the relative abundance of the peaks plotted in log scale as a function of the m/z measured. Each plot has α -pinene SOA (blue) with the PAH tested; A = phenanthrene, B = dibenzothiophene, C = pyrene, D = benz(a)anthracene. Each plot has an arrow pointing to the experimental PAH peak, and m/z peaks which may be associated with PAH-OPs based on previous works ^{105 106 107}.

These additional non-volatile compounds may include long-lived reactive oxygen intermediates (ROIs), which can play an important role in heterogeneous ozonolysis of PAHs^{108 102}. It has been suggested that the weakly bound physio-sorbed O₃ molecules can undergo dissociation to form molecular oxygen and a ROI, such as chemisorbed O atom bound to the delocalized π-electrons of PAH aromatic surfaces¹⁰⁸. These long-lived ROIs may then form PAH-OPs or react with other chemical species, including those formed during oxidation of α-P SOA precursor. The surface interactions of long-lived ROIs were suggested to lead to the formation of oligomers, with high molecular weight and low vapor pressure, which can lead to the nucleation and growth of new particles¹⁰⁹.

The potential effects of PHE vapor on the formation of SOA particles were measured using real-time in-situ characterization¹³. SMPS measurements showed an increase in mean particle size, as well as number concentrations of SOA particles, leading to a larger SOA mass forming when PHE vapor was present (Figure 2.2B). The presence of PHE vapor in the Teflon bag increased the SOA mass loading by ~450%, compared to pure α-P SOA created under the same conditions. This increase in SOA particle mass loading cannot be explained by the small fraction of PHE and PHE-OP mass present in the particles (~2%). This suggests that while the presence of PHE enhances SOA formation, it is not the cause of the increase in mass loading. A comparison of the

normalized mass spectra of pure α -P-SOA and PHE-SOA, with significantly higher mass loadings, points to their similarities at lower m/z (Figure 2.3A & A1.F3A), indicating that the additional PHE-SOA mass is dominated by α -P oxidation products. A similar trend is observed for all other PAHs used in the present study and for other PAHs and SOA precursors.¹³ Given the surprisingly large magnitude of the effect of PAHs on SOA formation, it requires further understanding of the processes involved, which is a focus of ongoing and future studies.

The measured PHE concentration after PHE-SOA ozone exposure appeared to change from the *fresh* PHE-SOA concentration (from 0.91% (± 0.28) to 0.53% (± 0.22) of the total PHE-SOA mass), but was not statistically significantly different (Figure 2.2A). The sum of PHE-OP masses measured within the ozone-exposed PHE-SOA extracts was approximately 12 times the mass of the PHE measured in the same extracts (Table 2.1). After PHE-SOA exposure to ozone, the 1-, 2-, and 3-OHPHEs concentrations were below the detection limit. The 9-OHPHE (6.27% (± 2.63)), trans-9,10-OHPHE (0.09% (± 0.02)), and 1,9-OHPHE (12.33% (± 5.75)) concentrations increased from fresh PHE-SOA to the ozone-exposed PHE-SOA (Table 2.1). As mentioned above, given the variability in particle losses during sample exposure in the PAM reactor and significantly lower mass of the collected samples, the absolute values of PHE and PHE-OPs concentrations after ozone exposure present higher uncertainty, compared to fresh PHE-SOA. The data suggest that, during

transports through the PAM reactor, PHE-SOA particles underwent additional heterogeneous reactions with ozone and/or evaporation of more volatile PHE-SOA components occurred. Whichever occurred, the processes resulted in slower particle evaporation kinetics (Figure 2.2C). The retention of PHE and PHE-OPs in PHE-SOA particles exposed to high ozone concentrations suggests that, while some of the volatile components in the PHE-SOA particles were evaporated during high ozone concentration exposure, the less volatile OPs remained in the particles.

Ozonolysis of aromatic compounds can lead to different substitutions on the PAH rings^{105 108}. Thermodynamic calculations suggest that an OH adduction is favorable over carbonyl adductions due to the highly unstable epoxide intermediates, both resulting in low-volatility products¹¹⁰. PHE ozonolysis has previously been measured to form 2'-formyl[1,1'-biphenyl]-2-carboxylate (2'F(1-1'BP)2C) in laboratory studies of PHE bound to the surface of silica particles⁹⁶. However, this compound was not detected in the QFF extracts of PHE-SOA. In addition, non-targeted screening of the PHE-SOA extracts, using electron impact ionization in full scan mode (with and without derivatization), showed the same three unidentified chromatographic peaks in both PHE-SOA and α -P SOA QFF extracts (Figure A1.F1), suggesting that additional peaks observed in the HR-ToF-AMS mass spectra (Figure 3a) were non-volatile compounds.

2.4.2 Dibenzothiophene. DBT has the highest vapor pressure (2.73×10^{-2} Pa) of the PAHs tested in this study (Table A1.T1), and comprised

the largest mass percent of the *fresh* PAH-SOA mass collected on the QFFs (2.46% (\pm 0.60)) (Figure A1.F2). The only quantifiable DBT-OP detected in the *fresh* and *ozone* reacted DBT-SOA was dibenzothiophene sulfone (DBTS). DBTS (2.46% (\pm 0.76)) accounted for an equal average mass percent as DBT in the *fresh* DBT-SOA. The sum of DBT and DBTS measured in the DBT-SOA was 4.91% (\pm 1.31) of the DBT-SOA mass collected. HR-ToF-AMS data shows a large number of peaks in the DBT-SOA extract that were not present in the α -P SOA extract and were not detected using GC/MS (Figure 3B). This suggests that these unidentified compounds were non-volatile. Similarly to PHE, the presence of DBT vapor during SOA formation resulted in ~600% increase in mass loading of DBT-SOA particles.

Upon additional exposure of DBT-SOA to *ozone*, DBT appeared to represent a somewhat larger wt% of the DBT-SOA (6.86 % (\pm 1.85)) while DBTS remained at 2.29% (\pm 0.49) wt% of the DBT-SOA total mass, but was not statistically significantly different (Table 2.1). This suggests that DBT and DBTS were shielded from evaporation during the ozone exposure.

2.4.3 Pyrene. In *fresh* PYR-SOA, PYR (vapor pressure 6.0×10^{-4} Pa) was measured at 1.79% (\pm 0.62) of the total PYR-SOA mass, and the combined mass of PYR and all measured PYR-OPs was 3.10% (\pm 0.88) of the total PYR-SOA mass collected. The sum of PYR and PYR-OPs in these particles is in good agreement with previously reported values

(~5%) of the PYR-SOA mass estimated from real-time in-situ mass spectrometric analysis of PYR-SOA particles¹³. Three individual PYR-OPs were measured in the fresh PYR-SOA, with the main product being 1-OHPYR at 1.25% (± 0.31), and two minor products, 6H-benzo(cd)pyren-6-one (6H-BcdP) at 0.04% (± 0.02) and 4H-cyclopenta(def)phenanthren-4-one (4H-CPP) at 0.07% (Table 2.1 and Figure A1.F2). 6H-BcdP was measured near the detection limits on 2 of the 3 *fresh* filters, while 4H-CPP was only measured above the detection limit on one of the 3 *fresh* PYR-SOA samples. HR-ToF-AMS data, as with the other PAHs, shows a larger abundance of higher m/z peaks in PYR-SOA in comparison to pure α -P SOA (Figure 2.3C). The presence of PYR vapor during SOA formation resulted in ~320% increase in mass loading of SOA particles. The observed similarities between the normalized mass spectra of pure α -P-SOA and PYR-SOA at lower m/z (Figure 2.3C), indicate that, as it was a case for other PAHs, the additional mass is dominated by α -P oxidation products.

After PYR-SOA exposure to additional *ozone*, the PYR concentration was measured to increase, though not statistically significant, from 1.79% (± 0.62) to 6.32% (± 3.42) of the total PYR-SOA mass (Table 2.1). The 1-OHPYR concentration also appeared to represent a larger wt% of the PYR-SOA (5.91% (± 2.24)) of the total SOA mass, and the 6H-CPP concentration increased from 0.04% (± 0.02) to 0.70% (± 0.22) of the total SOA mass, but was not statistically significantly different. 4H-CdeP was

not detected in the ozone-exposed PYR-SOA samples. The lack of statistical difference in the fresh and ozone exposed PYR-SOA is suggestive of the variability in the particle losses during the exposure through the PAM reactor, and supports previous studies showing the retention of PAHs and PAH-OPs in SOA particles, even as more volatile components may leave during atmospheric aging and transport^{13 17}. The ratio of PYR-OPs to PYR concentrations remained relatively unchanged; 0.73 in the *fresh* PYR-SOA, and 1.05 in the *ozone-exposed* PYR-SOA. Normalized PYR-OPs to PYR wt% showed no statistically significant difference before and after ozone exposure, indicating that both PYR and the PYR-OPs were shielded from volatilization and oxidation during the high ozone concentration exposure. In addition to 1-OHPYR, a previous laboratory study detected 4-carboxy-5-phenanthrenecarboxylate (4C5PC) as the main PYR-OP during heterogeneous reactions of PYR bound to azelaic acid particles and ozone¹⁰⁵. However, 4C5PC was not detected in the QFF extracts of PYR-SOA.

2.4.4 Benz(a)anthracene. BaA was not detected on the QFF after collection of 15 µg of BaA-SOA from a single Teflon bag, suggesting less incorporation into BaA-SOA than the other PAHs examined in this study, due to the low vapor pressure of BaA (2.8×10^{-5} Pa, Table A1.T1). To overcome this and identify BaA-OPs, 147 µg of BaA-SOA was collected from two individual Teflon bags onto a single QFF (n=1). Only BaA (0.08%) and benz(a)anthracene-7,12-dione (7,12-BaAone) (0.19%) were

quantifiable in the QFF extract from the BaA-SOA (Table 2.1, Figure S2). HR-ToF-AMS data shows a large number of peaks in the BaA-SOA extract that were not present in the α -P SOA extract and were not detected using GC/MS (Figure 2.3D). This suggests that these unidentified compounds were non-volatile. The presence of BaA vapor during SOA formation resulted in ~140% increase in mass loading of SOA particles. The BaA-SOA was not exposed to additional ozone due to the low concentration of BaA and 7,12-BaAone in the fresh BaA-SOA experiment.

2.4.5 Implications. While the 16 priority PAHs currently monitored on global pollution lists have well defined toxicity profiles, many PAH-OPs have incomplete or no known toxicity profile^{72 18 111 25}. The PHE-OPs measured in this study have been shown to have different toxic effects than PHE^{18 111}. DBT has been described as a cytochrome P450 A1 inhibitor, and DBTS has been described as having comparable toxicity to DBT in tissue alteration studies^{18 112}. While 1-OHPYR has been described as having comparable toxicity to PYR, 6H-BcdP and 4H-CPP have been measured to possess different toxicity profiles^{18 86}. The US Environmental Protection Agency lists BaA as a human carcinogenic compound¹¹³, while 7,12-BaAone has been evaluated for and found to possess developmental toxicity¹⁸. There is currently no available data on the mutagenicity or carcinogenicity of this 7,12-BaAone^{18 113}.

This study provides evidence that PAHs are partially oxidized as they become incorporated into SOA particles during particle formation and growth in the presence of PAH vapor. This study, for the first time, quantifies PAHs with a range of vapor pressures, and their PAH-OPs incorporated into SOA particles. Individual PAHs show different reactivity and incorporation into the SOA, partially, but not completely, explained by their respective vapor pressures. The presence of both PAHs and PAH-OPs (which are generally less volatile than PAHs (Table A1.T1)) within SOA supports the proposed mechanism of LRAT of both of these classes of compounds in SOA particles. The semi-solid nature of the SOA particles, at least partially, protects PAHs and PAH-OPs from evaporation or further chemical reactions during atmospheric transport^{44 13 17 50}. The higher mass loadings of SOA produced in the presence of PAH vapor observed in this study, suggest that they contain low-volatility and non-volatile compounds, including oligomers and some PAH-OPs that were not measurable using GC/MS. The increased oligomer signature on HR-ToF-AMS data cannot be attributed to α -pinene or PAH vapor without full analysis of oligomer composition. Along with the observed retention of PAHs and PAH-OPs in particles exposed to ozone in this study, the slower evaporation kinetics observed here, and elsewhere¹³, suggest that shielding occurs in SOA particles which protects entrapped compounds during LRAT.

The synergy between PAH vapors and SOA formation, highlighted in this work, requires further studies aimed to develop an understanding of the processes involved and their atmospheric implications. Similarly, the relationship between the composition of PAH-SOA particles generated in this study and atmospheric samples is not direct, and needs to be further probed to assess the LRAT of PAHs and PAH-OPs under various atmospheric conditions. While this study evaluated the more volatile PAH-OPs of the PAHs studied here, future studies need to include analysis of low-volatility and non-volatile PAH-SOA constituents. LRAT models of atmospheric SOA particles influenced by anthropogenic activity will continue to be incomplete in their predictions until a better understanding of the chemical composition is known.

To improve LRAT models for more accurate human risk assessment, this area of research requires more comprehensive studies of the underlying processes, the quantification of the many trapped chemical species in SOA particles, such as PAHs and PAH-OPs, and the effects on the global climate and human health these synergistic relationships might have.

2.5 ASSOCIATED CONTENT

2.5.1 Supporting Information

Supplemental information for this chapter can be found in Appendix 1.

2.5.2 AUTHOR INFORMATION

Corresponding Author

*Tel: (541) 737-9194. Fax: (542) 737 0497. E-mail:

staci.simonich@oregonstate.edu

2.5.3 Notes

The authors declare no conflicts of interest.

2.6 ACKNOWLEDGEMENTS

This publication was made possible in part by Grant Numbers AGS-1411214 from the National Science Foundation (NSF), and P42-ES016465 and P30-ES00210, from National Institute of Environmental Health Sciences (NIEHS), National Institute of Health (NIH). Its contents are the sole responsibility of the authors and do not represent the official view of the NIEHS or NIH. Additional support was provided by the U.S. Department of Energy (DOE) Atmospheric Systems Research (ASR) program (K.S., D.B., A.Z.). (A portion of) The research was performed using EMSL (Ringgold ID 130367), a DOE Office of Science User Facility sponsored by the Office of Biological and Environmental Research and located at Pacific Northwest National Laboratory.

Chapter 3:

Impact of Local and Regional Sources of PAHs on Tribal
Reservation Air Quality in the U.S. Pacific Northwest

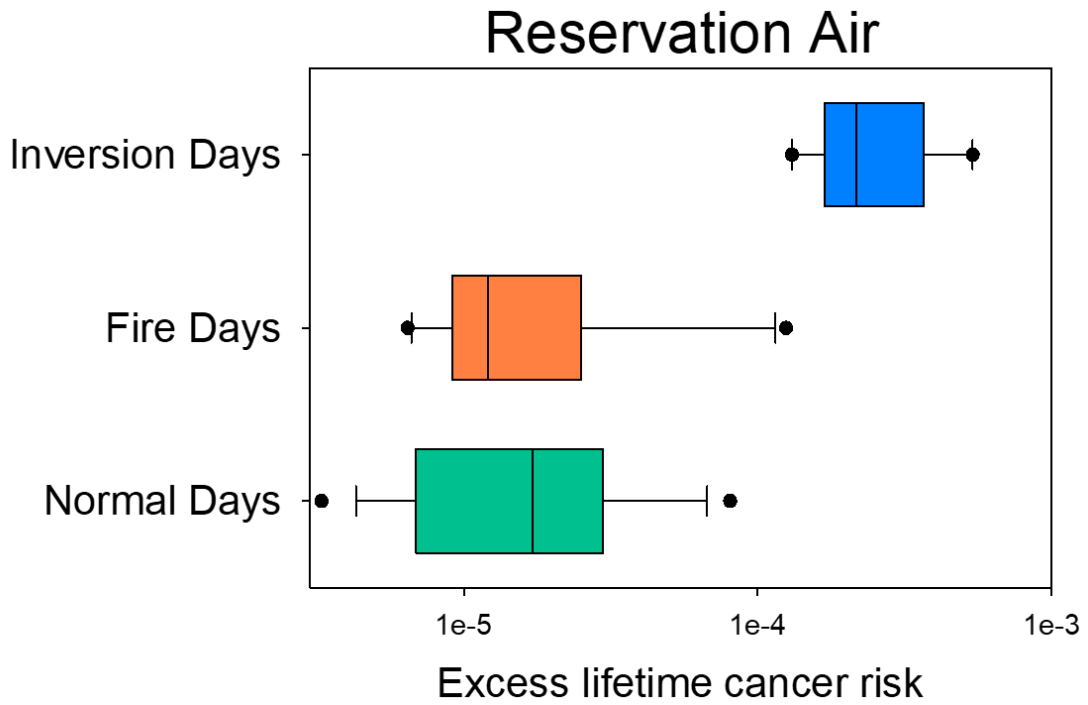


Figure 3.0

Impact of Local and Regional Sources of PAHs on Tribal Reservation Air Quality in the U.S. Pacific Northwest

Amber L. Kramer_{a,b}, Larry Campbell_c, Jamie Donatuto_c, Myk Heidt_c, Molly
Kile_d, Staci L. Massey Simonich_{a,b}¹

a – Oregon State University Department of Chemistry, Corvallis OR

b – Oregon State University Department of Environmental and Molecular Toxicology,
Corvallis OR

c – Swinomish Indian Tribal Community, La Conner WA

d - Oregon State University School of Biological and Population Health Sciences, Corvallis
OR

Contributions – Prepared by Amber L. Kramer with editorial comments provided by Larry Campbell, Jamie Donatuto, Myk Heidt, Molly Kile and Staci L. Massey Simonich. Amber Kramer installed high volume air samplers, trained Tribal Community employees (supervised by Myk Heidt and Jamie Donatuto) to collect PM_{2.5} samples, performed extraction and chemical analysis on all samples.

Written and submitted for publication – *Science of the Total Environment*

Resubmitted 11 December 2019

*Corresponding Author: staci.simonich@oregonstate.edu

3.1 ABSTRACT

Atmospheric fine particulate matter (PM_{2.5}) transports polycyclic aromatic hydrocarbons (PAHs) regionally and globally, influencing the air quality of communities around the planet. Concentrations of 130 PAHs extracted from PM_{2.5}, collected on a Native American Tribal Reservation in the Northern Puget Sound region of the American Pacific Northwest, were used to assess the air quality impacts of regional and local PAH sources, atmospheric transport, and human health implications. Wind coming from the southeast of the sampling locations increased the overall PAH concentration of the PM_{2.5}, while winds from the southwest decreased the PAH concentration. Concentrations of PAH subclasses increased or decreased independently at the two sampling locations with different changes in wind patterns, changing the excess lifetime cancer risk significantly. No long-range transport was measured, but emissions from local and regional PAH sources were measured. Samples collected during regional wildfires showed increased PAH concentrations. Samples collected during predicted weather inversions resulted in the highest PAH concentrations, and up to a ten-fold increase in excess lifetime cancer risk over the normal days.

3.1.1 Keywords

- Polycyclic Aromatic Hydrocarbons (PAHs)
- Atmospheric Fine Particulate Matter (PM_{2.5})
- Tribal reservation air quality

3.1.2 Highlights

- Paired PM_{2.5} samples were collected over a Native American Reservation
- Extracted PM_{2.5} samples were analyzed using GC-MS for 131 PAHs
- PAH concentrations were compared to local weather patterns and analyzed for correlations
- Weather inversions and regional wildfires increased PAH concentrations on the Reservation

3.2 INTRODUCTION

Atmospheric fine particulate matter (PM_{2.5}) exposure is responsible for an array of respiratory and cardiovascular diseases³⁵. As of 2017, PM_{2.5} exposure has been directly linked to around 7 million deaths around the world each year¹. The search to understand the mechanisms for PM_{2.5} toxicity has shown that organic components in PM_{2.5} are responsible for detrimental health effects^{65, 66}. Anthropogenic activity has increased the mass of organic compounds traversing the global atmosphere in PM_{2.5}^{1, 2}.

Polycyclic aromatic hydrocarbons (PAHs) are ubiquitous environmental contaminants found naturally in petrochemicals, and released as byproducts of incomplete combustion.^{85 16 81} Atmospheric emissions, mainly attributed to incomplete combustion, and can undergo long-range atmospheric transport bound up in PM_{2.5}^{85, 16, 81}. Some unsubstituted PAHs (UPAHs) have been well characterized in terms of toxicity, which has led to the inclusion of 16 of these compounds on the US Environmental Protection Agency's (US EPA) Priority Pollution List (PPL). PAHs exist in many subclasses other than

UPAHs: heterocyclic (HPAHs) contain a non-carbon atom in the ring structure, -NO₂ substituted (NPAHs), and carbonyl substituted (OPAHs), and high molecular weight (HMWs), characterized by having an atomic mass of more than 302 Da. These subclasses can all be directly emitted from various sources to the atmosphere along with UPAHs, and have been characterized in PM_{2.5}^{20, 31, 114}. Substitutions can occur through atmospheric reactions of UPAHs with an array of atmospheric reactants, specifically, nitrogen oxide compounds (NO_x), ozone (O₃), and hydroxyl (OH[•]) radicals. These reactions can lead to NPAHs, OPAHs, and hydroxy (OHPAHs) substitutions to a hydrogen on the UPAH rings^{20, 12}. While UPAH exposure has been linked to inflammation, cardiopulmonary and respiratory diseases, and cancer, the human health implications of the other subclasses of PAHs remains highly unclassified^{80, 115, 68, 18}.

Native Americans have strong cultural, spiritual, and physical relationships with the natural environment they evolved to inhabit⁸³. Due to colonization and relocation by the Federal government, Native American reservations comprise a fraction of the lands each Tribe previously inhabited⁸⁴. This constriction of land for Native American societies, results in increased sensitivity to changes to the environment^{84, 56}. Globally, indigenous peoples are disproportionately susceptible to and affected by PM_{2.5} adverse health outcomes⁵⁶. One example is the Swinomish Indian Tribal Community whose reservation was recognized in 1855 by the Treaty of Point Elliot. In 1955 and 1958, two oil refineries were built on March Point, which is within the Treaty

Reservation. These oil refineries have contributed to local PAH pollution in the marine environment ¹¹⁶. Unplanned air toxic releases have also impacted the Swinomish reservation ¹¹⁷.

When air masses move over emissions sources, PM_{2.5} is transported downwind of the source, sometimes resulting in PM_{2.5} transport thousands of miles from sources ^{85, 16, 81, 20}. Events such as wildfires greatly increase the amount of PAH containing PM_{2.5} entering and transporting throughout the atmosphere ¹¹⁸. When atmospheric inversions occur, warm air masses move over cold air masses, trapping the cold air nearer the surface. Such atmospheric pressure systems result in lessened vertical air movement, which results in enhanced PM_{2.5}, ozone and NO_x concentrations during the inversion events ^{119, 120}. Changes in weather patterns, wind directions, and atmospheric conditions can result in significantly different air quality concerns at any one location.

The objective of this study was to assess local and regional source contributions to PAH concentrations on a tribal reservation in the Pacific Northwest, and their impact on inhalation health risks. In partnership with the Swinomish Indian Tribal Community (SITC), located near the San Juan Islands of the upper Pacific Northwest (USA), an extensive air quality study measured UPAHs, as well as NPAHs, OPAHs, HPAHs, OHPAHs, and HMWs, on PM_{2.5} from two air samplers on the SITC Reservation. PM_{2.5} samples were collected at the same two locations as meteorological measurements for the assessment of the impact of local and/or regional

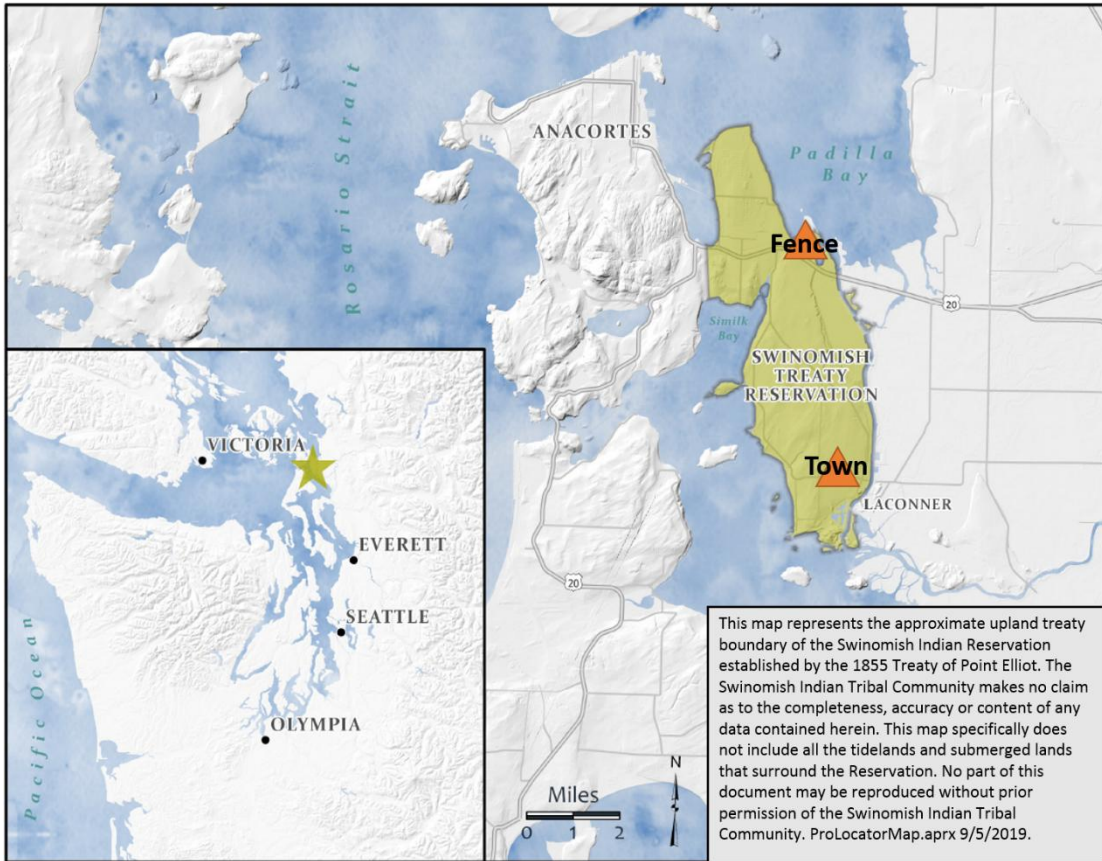
emission sources and weather patterns on the air quality of the SITC Reservation. Well established diagnostic ratio analysis of PAHs, and positive matrix factorization was used to assess if sources of PAHs could be attributed.

3.3 MATERIALS AND METHODS

3.3.1 *Materials.* Compound names, abbreviations, manufacturers, main emission sources, and estimated detection limits can be found on Table A2.T1 of the appendix. Derivatization of hydroxylated PAHs (OHPAH) occurred using N-tertbutyldimethylsilyl-N-methyl-trifluoroacetamide (MTBSTFA)⁹⁸. Quartz fiber filters (QFFs) were purchased from G. E. Whatman (Buckinghamshire, UK) in 8 x 11 inch sheets (PM_{2.5}), and in 4 x 5.5 inch slotted sheets (larger PM). QFFs were prepared by placing individually into aluminum packets and baked at >350°C for 12 hours to remove organic contaminants and sealed in the aluminum packets, and then in plastic bags. After PM collection, all filters were resealed in their packets, and then stored and transported on ice to reduce vaporization losses during transport.

3.3.2 *Sample collection.* Two Tisch Environmental (Village of Clevel Ohio, USA) High Volume Cascade Impact air samplers were installed 7 km apart from each other on the Swinomish Reservation on the Northwest coast of the US State of Washington (Figure 3.1). Sampling locations were chosen to coordinate with meteorological stations owned and operated by the Swinomish Indian Tribal Community. The first location was situated on a hill, 48 meters (asl) above the main business district of the Swinomish Village

(Town). (Town: 48.397789 (latitude), -122.504971 (longitude)). The second location was on the Reservation, situated near a Tribal owned and operated casino, and about 1 km off the fence-line (Fence) of two oil refineries that are located within the Reservation recognized by the 1855 Treaty (Fence:



48.459928 (latitude), -122.520388(longitude), 1.5 m asl). Paired samples

Figure 3.1. Local and Regional map of the Swinomish Indian Tribal Community Reservation.

Map represents the 1855 Treaty of Point Elliot boundaries of the Swinomish Indian Tribal Reservation.

Triangles mark the two sampling locations (Fence and Town).

were collected during the same 24 hour periods between April 2016 and September 2018. A total of 56 pairs of filters were analyzed for this study. Of the 56 pairs, 48 were used for wind pattern analysis, 5 pairs were collected

during periods of predicted impact from nearby wildfires (Fires), and 3 pairs were collected during weather inversion events (Inversions) predicted by weather forecasts. Days with more than 3 hours of ≥ 0.01 inch of precipitation were used for this study. Data from Fires and Inversions were analyzed separately from the rest of the data (Normal).

3.3.3 *PM_{2.5} extraction.* Collected sample filters were sealed in prebaked aluminum packets and sealed plastic bags, and stored at -20°C until extraction. Filters were extracted using ThermoFisher (USA) Dionex ASE 350 – Accelerated Solvent Extractor. Two cycles of dichloromethane and two cycles of a 2:1 mixture of ethyl acetate: acetone were used in 100% volume (66 mL ASE cells) with oven temperature set to 100°C, to extract both non-polar PAHs as well as more polar PAH transformation products. ASE extracts were cleaned using Agilent Technologies (Santa Clara California, USA) 500 mg silica solid phase extraction (SPE) cartridges, and concentrated to a final volume of 1000 μ L in ethyl acetate. Filters were extracted without the additional isotope labeled surrogate compounds to ensure extracts could be used for future toxicological studies. Isotope labeled standards were added before GC/MS analysis for quantification purposes. Final extraction efficiency was evaluated by spiking analytes onto clean QFF and extracting along with filters. Extraction efficiency was measured at: UPAH = 81%, HMW = 86%, NPAH = 124%, OPAH = 127%, HPAH = 76%, and OHPAH 54%. To monitor extraction efficiency throughout extraction processes, standard reference material (NIST SRM 1648A) was weighed onto clean filters, and

extracted alongside sample filters. SRM 1648A has certified concentrations for only some of the analytes measured in this study. For certified concentrations in the SRM, the relative standard deviation of the measured compounds ranged from 1% - 26%, suggesting the extraction was consistent throughout the study.

3.3.4 PAH characterization. SPE extracts were characterized for UPAH, HPAH, OPAH, and OHPAH using Agilent 7890 Gas Chromatograph (GC), while HMWs were characterized on an Agilent 6890N GC, each partnered to a quadrupole mass spectrometer run in electron impact mode at 70 electron volt. NPAH characterization occurred using Agilent 6890 GC partnered to a quadrupole mass spectrometer run in chemical ionization mode. Identification and quantification for UPAH, NPAH, OPAH, OHPAH, and HPAH was performed using an Agilent J&W DB-50Mg 30 m X 0.25 mm i.d. (0.25 μ m film thickness) DB-5 capillary column, and HMW were analyzed using an Agilent J&W DB-17Mg 60 m X 0.25 mm i.d. Detailed GC-MS methods can be found in supplementary information (Appendix section A2.1). Extracts were analyzed using selected ion monitoring (SIM) mode, to look for and quantify PAHs and PAH-OPs with available analytical standards. Calibration curves, with linear ranges from 1-1000 pg/m³ ($r^2 > 0.995$) were used for quantification of each class of PAH. To measure hydroxy substituted PAHs (OHPAHs), derivatization using MTBSTFA for was performed. This process is described in the Appendix (A2.2). Mass spectra of GC-MS fragmentation were interpreted using Mass Hunter (UPAH, OPAH, HPAH,

OHPAH) or ChemStation (NPAH and HMW) software. To account for non-sample contamination, clean QFF were extracted alongside sample filters as lab blanks. Lab blank measured concentrations of all analytes were subtracted from their measured concentrations. Calibration on the High Volume motors, air samplers allowed for all measured concentrations to be calculated back to the mass of analyte per cubic meter of sampled air, and is presented as pg/m^3 air.

3.3.5 Meteorological data. Meteorological data such as wind speed, wind direction, relative humidity, precipitation, barometric pressure, etc., were collected hourly at the two sampling locations using R.M. Young Company model 05305 (Traverse City Michigan, USA). Using trigonometric sine and cosine functions, wind speed (mph) and direction (degrees) for each sample were transformed to (X,Y) coordinates for wind ratio analysis. Nitric oxide (NO), nitrogen dioxide (NO₂) were collected, at the Fence location, using Teledyne API T200 (Caringbah New South Wales, Australia), and ozone (O₃) readings were collected, at the Town location, using a Thermo 49i (Franklin Massachusetts, USA). To assess if local emissions were being transformed, versus transported from regional or global sources, NO_x and O₃ data were correlated with wind and compound measurements. Temperature and barometric pressure were monitored using Campbell Scientific Inc., (Logan Utah, USA) model Viasala HMP45C (temperature and relative humidity), and Vaisala PTB101B (barometric pressure). Meteorological instrumentation is owned and operated by the Swinomish Indian Tribal Community, and data

was shared with us when available. Temperature and pressure were used to calibrate the High Volume air sample motors and calculate air mass sampled each day at each location.

To assess if air masses were influenced from trans-Pacific long-range atmospheric transport, HySplit back trajectories were calculated using the NOAA Air Resource Library (ARL) publically available on the www.noaa.gov website. Analysis of HySplit data for 7-day back trajectories for the sampling days did not indicate significant trans-Pacific long-range atmospheric transport.

3.3.6 Human Health Implications. Benzo(a)pyrene (BaP) has long been held as the standard for assessing PAH toxicity in the environment. With well documented toxicity and carcinogenic properties, BaP concentrations are often used as a representation of all PAHs present in samples. Worldwide, there are exposure limits to BaP concentrations set under the context of expected lifetime cancer risk. In their 2010 report, The World Health Organization (WHO), documents that exposure to a BaP concentration of 1200 pg/m^3 air, increases the risk of developing cancer to 1 in 10,000^{10, 121}. Due to this, a recommended BaP concentration limit of 1000 pg/m^3 air has been set in the European Union to diminish the increased risk of developing cancer due to BaP inhalation exposure¹²¹.

To better encompass the breadth of PAHs present in $\text{PM}_{2.5}$, relative potency factors (RPFs), established by the US Environmental Protection Agency, are used to calculate BaP equivalent (BaP_{EQ}) concentrations of

samples²⁹. These RPF values act to transfer a measured PAH concentration to a relative BaP concentration, using established carcinogenic potency factors, which can then be used to perform risk assessments. BaP_{EQ} concentrations, (calculated using equation 3.1), derived from available RPF values were used in this study to perform inhalation risk assessment.²⁹

$$\text{Equation 3.1: } BaP_{EQ} = \sum_{i=0}^n (CPAHi \times RPFi)$$

This assessment is based on known toxicity, assumes average inhalation rates, body mass, and exposure lengths over an adult lifetime (70 years). Together these assumed values are used to create unit risk factors (UR_{BaP}) which are set by various governmental and/or regulatory agencies. This risk assessment (equation 3.2) estimates the excess risk of developing cancer due to inhalation exposure of measured compounds.

$$\text{Equation 3.2: } Cancer\ Risk = BaP_{EQ} \times UR_{BaP}$$

Due to the fact that many Native American Tribal lands encompass both sides of the US / Canadian border, the WHO inhalation UR_{BaP} (of 8.7×10^{-5} per ng/m^3 of measured BaP) was used to calculate inhalation excess lifetime cancer risk for this study.^{83 10 20} Substituting the European Union regulatory limit of $1000\ pg/m^3$ air BaP in this equation results in an extra 87 out of 1 million (excess cancer risk of 8.7×10^{-5}) cases of cancer expected due to a lifetime of exposure to the measured concentration.

3.3.7 Statistical analysis. PAH concentrations were censored for statistical modeling. Non-detect measurements were censored by using half of the method detection limits (MDL), and measurements that fell between the

MDL and limit of quantification were assigned the MDL value for each compound^{122, 123}. MDLs, calculated using US EPA methods, for all compounds can be found in Appendix Table A2.T1¹²⁴. Pearson matrix correlations, and Student's t-tests were performed using R statistical software, on the R-Studio user platform, on censored measurements for each day and location. Compounds measured in less than 60% of the samples were excluded from statistical analysis. Statistical significance is reported as significant if $p\text{-value} \leq 0.05$. In reported data, the number of samples is indicated with 'n = x'. Error bars on graphs, and ($\pm x$) values represent the standard error.

3.3.8 Source apportionment. PAH Diagnostic ratios found in Yunker et al. 2002, were used to identify possible source contributions. To assess if crude petroleum from the nearby oil refineries was affecting the air quality over the Reservation, the ratio of PAHs with an atomic mass of 202, (FLN / FLN + PYR) was used. The ratio of PAHs with an atomic mass of 276, (IcdP / IcdP + BghiP), was used to distinguish between different types of combustion. Retene, which has been linked to biomass combustion, was analyzed along with UPAHs, and considered for evidence of biomass burning.¹²⁵

Positive matrix factorization (PMF) was performed using the EPA PMF 5.0 software package. Possible sources in the region include wood/biomass burning, crude oil, automobile emissions, ship emissions, and industrial emissions. PMF parameters included 6 factors, 20 runs, bootstrap of 100 times with a minimum correlation value of 0.7.

3.4 RESULTS

3.4.1 *Analysis of wind speed and direction during normal atmospheric conditions.* To determine the effect of wind direction and wind speed on PAH concentrations at the two sampling locations, the plotted hourly polar coordinates of wind speed and wind direction, (for each 24-h sample and sampling location), were binned into one of four quadrants: Northwest (NW), Northeast (NE), Southeast (SE) and Southwest (SW). The number of hours the resulting coordinate was in one of the four quadrants was used to calculate the percentage of time the wind came from that wind direction. For comparative purposes, samples were grouped based on differences in wind direction during the sampling timeframe. A cutoff of < 20% of the wind coming from one wind direction was compared to when >80% of the wind was coming from same wind direction. For the NW wind direction, > 70% was used to keep the number of samples at or above three for statistical purposes. No days at the Fence location had winds from the NE that were more than 30% during the sampling period, while no days at the Town location had winds from the NE that were more than 50% during the sampling period. Correlations of individual compound concentrations with winds coming from both SE and SW directions indicated a significant air quality impact over the sampling locations (Table A2.T3). Wind coming from the NW and NE had some correlation with individual PAH concentrations, but very few were statistically significant. Due to the low prevalence of winds from the NE, and low compound concentrations correlations with NE winds, the NE

wind direction was considered to not be influential on air quality during these sampling days, and is therefore not included in the detailed results.

Comparison of PAH concentrations in $PM_{2.5}$ collected when there was <20% to >80% of SE winds during the sample collection, had significantly lower (p-value < 0.05) $\Sigma OPAH$ concentrations at both sampling locations (Figure 3.2C). At the Fence sampling location, comparison of <20% of the wind coming from the SE (n=23) to >80% of the wind coming from the SE (n=9) resulted in a significant decrease in the sum of $\Sigma OHPAH$ concentrations. While the sum of the other classes of PAHs did not significantly change with the increase in SE wind during sampling, a number of quinone-, dione-, and hydroxy PAH concentrations decreased by more than 65% when there was more SE wind during the sample collection (Table A2.T2).

Comparison of PAH concentrations in $PM_{2.5}$ collected when there was <20% to >80% of SW winds during the sampling collection, had significantly lower $\Sigma UPAH$, $\Sigma NPAH$ and ΣHMW concentrations at both sampling locations (Figure 3.2B). While $\Sigma OPAHs$ and $\Sigma OHPAH$ concentrations did not significantly change, with the increase in SW wind during sampling, 1,4-anthraquinone, 9,10-phenanthrenequinone, and 2-hydroxyfluorene concentrations significantly increased at the Town sampling location when the SW wind increased from <20% (n=22) to >80% (n=6) of the sample collection.

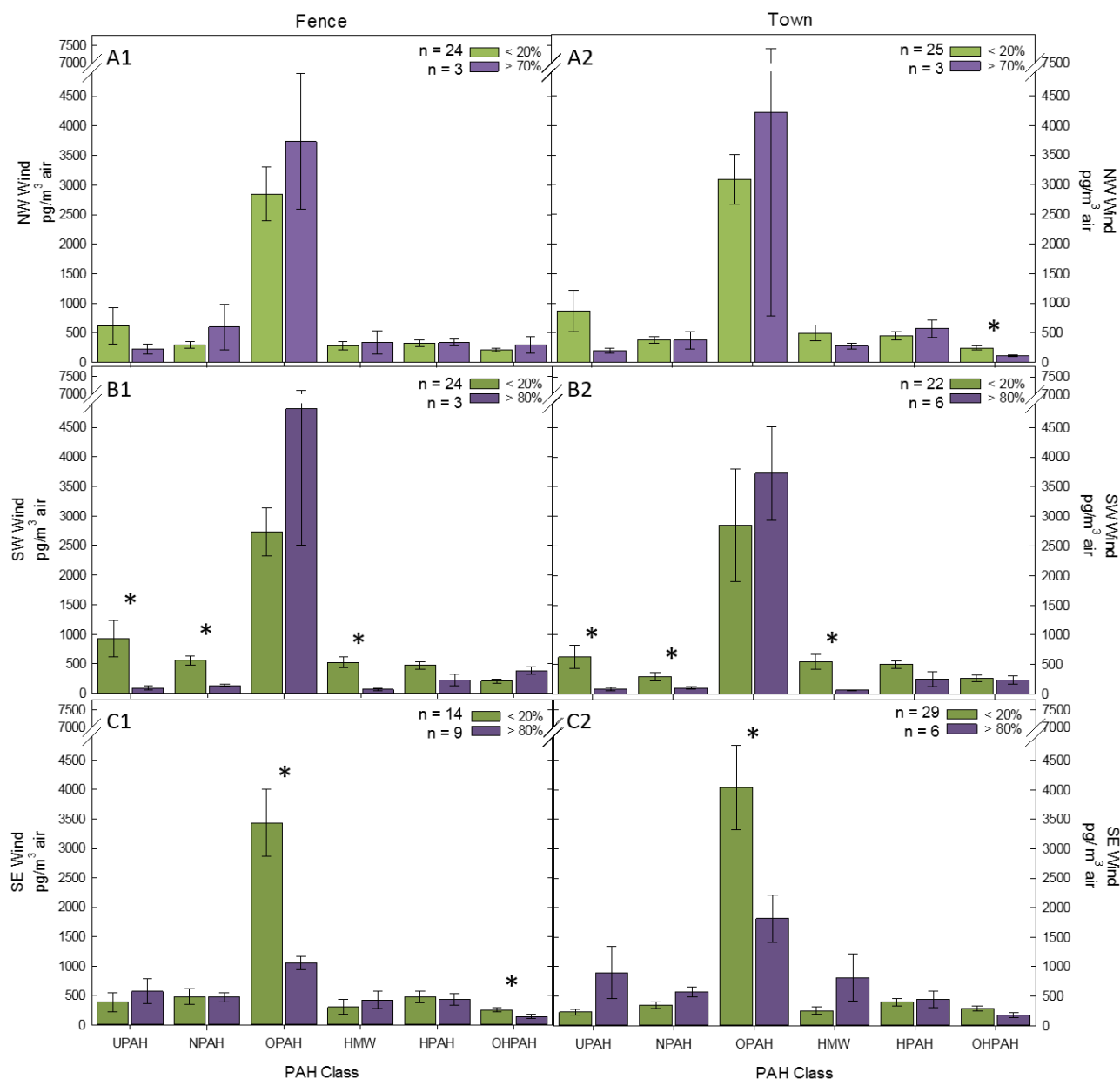


Figure 3.2. ΣPAH class graphs for each location and wind direction. Figure 3.2 shows the average sum of concentrations for each PAH class (\pm SE) for each wind direction (A = NW, B = SW, C = SE wind), for each location (1 & 2). In each panel, green bars represent data for days with < 20% wind coming from the indicated direction, and purple bars represent days with > 70% for NW, and > 80% for SW and SE wind coming from each direction. “n” indicates the number of samples that matched that particular wind direction criteria. * indicates a significant change (Student’s t-test $p < 0.05$) in the sum concentration of each class between low to high wind conditions.

Chromone concentrations significantly increased at the Fence sample location with the increase of SW wind from <20% (n=24) to >80% (n=3) during sample collection (Table AA2.T2). Many individual PAH concentrations decreased significantly with the increase of SW wind at both sampling locations (Table A2.T2).

When the wind coming from the NW directional quadrant increased from < 20% (n=25) to > 70% (n=3), a significant decrease in the Σ OHPAH concentration was measured at the Town location (Figure 3.2, Table A2.T2), while both 2,6-dihydroxynaphthalene and 3-hydroxybenz(a)anthracene concentrations both increased significantly (Table A2.T2). No significant changes were measured in the sum of any of the PAH class concentrations at the Fence sampling location with the increase of wind coming from the NW (< 20% = 24 samples, > 70% = 3 samples). Several individual PAHs were measured in significantly lower concentrations in the Town sampling location collected when > 70% of the wind was coming from the NW during the sampling timeframe (Table A2.T2).

3.4.2 Sampling Location Comparison. The PAH concentrations at the two sampling locations were compared to identify local emissions sources unique to each sampling location. The PAH concentrations and profiles were not statistically significantly different between the Fence and Town sampling locations (Figure 3.2). While there were differences in which PAHs changed with increased winds from each direction, between the two sampling

locations, no pattern was found in the data to provide evidence of specific sources or their contributions in each direction of the sampling locations.

Compound concentration correlations with wind ratios for each wind direction gave more information on local sources. For example, the concentration of chrysene & triphenylene (Cr/Tr) was positively correlated (p-value = 0.028) with the SE winds at the Town sampling location and negatively correlated (p-value = 0.047) with the SW wind at the Fence sampling location. This indicates that there is a source of Cr/Tr nearby the two sampling locations that gets enhanced at the Town sampling location with increasing SE winds, but also gets diluted at the Fence sampling location when the SW winds increase. A full list of correlations appears in the Appendix (Table A2.T3). Correlation data provided clues, but no definitive local sources were identified based on compound correlation data.

3.4.3 Atmospheric reactant analysis. To distinguish between local emissions and transformation products, atmospheric reactants responsible for PAH transformations were monitored and correlated with PAH concentrations. NO and NO₂ concentrations (ppm) were both negatively correlated with SE wind at the Town sampling location (Table A2.T3). O₃ concentrations (ppm) were positively correlated with SE wind at the Fence sampling location, and negatively correlated with NW wind at both sampling locations. Due to the relatively short atmospheric lifetime of NO_x species (2-8 hours), the presence of NO_x, and any influence NO_x species may have on the PM-bound PAHs, was thought to be distinguishable through correlations of

NO_x with PAHs or classes of PAHs. The O₃ atmospheric lifetime is much longer than NO_x (~22 days), and therefore has more time to react with PM-bound compounds during transport. High correlations of individual OPAH or OHPAH concentrations with O₃ concentrations could indicate the transport of these compounds from sources far from the sampling locations.

Several individual PAH concentrations were correlated with individual atmospheric reactants, such as 1-hydroxy-9-fluorenone negatively correlated with O₃ concentrations, and 12-hydroxybenzo(a)pyrene positively correlated with NO₂ concentration at the Town sampling location, (Table A2.T4). While, compound concentrations were positively correlated with NO_x concentrations and negatively correlated with O₃ concentrations, no clear pattern of PAH concentration correlation was observed at either location, resulting in no conclusion about the influence NO_x and O₃, on the PM_{2.5}-bound PAHs in the Reservation air-shed.

3.4.4 Fire and inversion events. Data from PM_{2.5} samples collected during regional wildfires (n=5), and during a weather inversions (n=3), were interpreted separately from the rest of the samples. In general, both the fire and inversions days had higher PAH concentrations than the rest of the sampling days (normal days) (Figure 3.3).

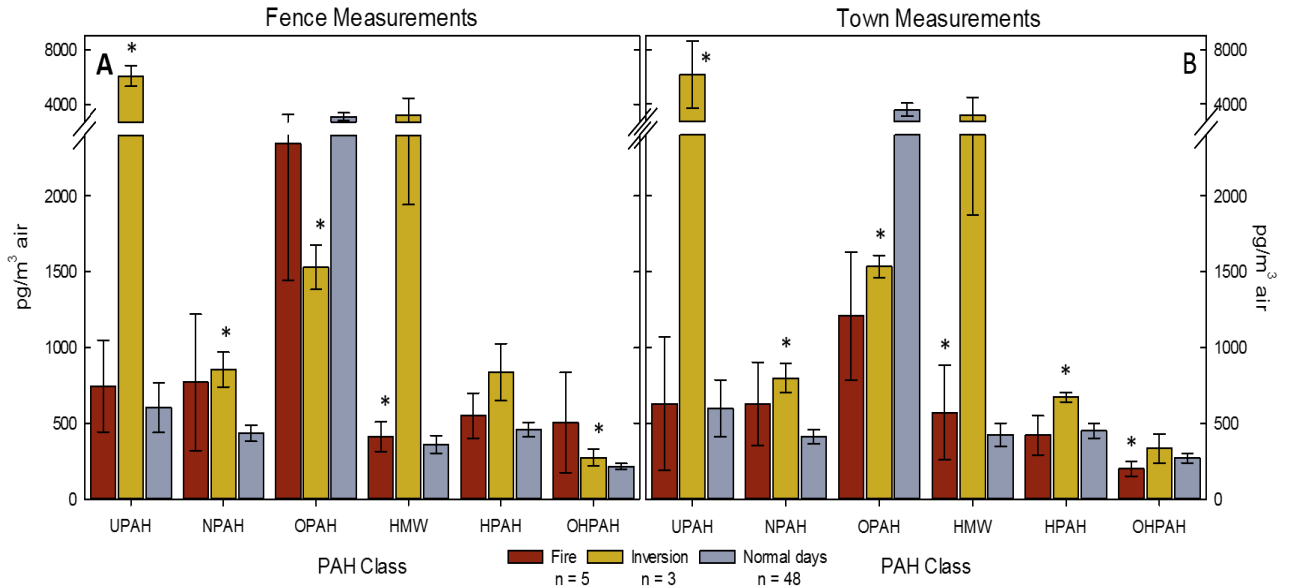


Figure 3.3. Atmospheric Condition Comparison. The average concentration of the sum of each PAH class during Normal Days (gray bars), compared to events of wildfires (red bars), or weather inversions (yellow bars) influencing the sampling area for both sampling locations; Fence (A) and Town (B) locations. * indicates a statistically significant (p -value < 0.05) difference from the Normal Days measurements. There were five sampling events during incidence of wildfire influence ($n = 5$) on the region, and three during inversions ($n=3$), and 48 days when neither of these atmospheric conditions were noted.

Data from samples collected during regional wildfires had significantly increased concentrations of Σ HMWs over data from Normal Days, at both sampling locations, suggesting that HMW PAHs may be emitted from wildfires. There was also a significant decrease in Σ OHPAH concentrations at the Town location during wildfire collections.

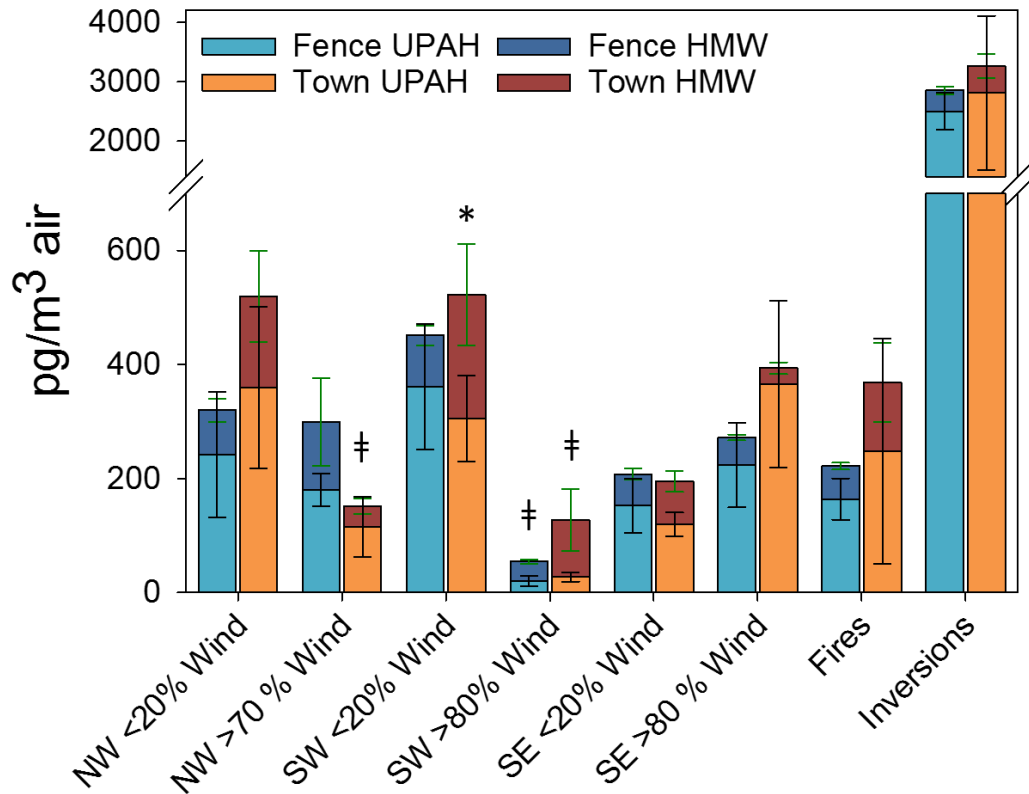
Σ UPAH and Σ NPAH concentrations were significantly higher during inversions at both sampling locations, while Σ OPAH concentrations were significantly lower during the inversions. Σ OHPAH concentrations were

higher at the Fence location, and Σ HPAHs were higher at the Town location during inversion events.

3.4.5 Excess Lifetime Cancer Risk assessment. RPF values currently only exist for 19 PAHs (Table A2.T5), 13 UPAHs and 6 HMWs. BaP_{EQ} concentrations were calculated for samples in this study for both UPAHs and HMWs with these RPF values (Figure 3.4 & Table A2.T7). The data shows decreased Σ UPAH and Σ HMW concentrations when SW winds increase from < 20% to > 80%, and have a significant effect on the BaP_{EQ} concentrations at both sampling locations. There was also a significant change to the BaP_{EQ} concentration when adding HMWs BaP_{EQ} to the UPAH BaP_{EQ} at the Town sampling location during times of <20% SE wind (Figure 3.5). UPAHs represented 68% or 63% of the overall BaP_{EQ} concentration at the Fence and Town sampling locations, respectively.

While no BaP concentrations were measured above the 1000 pg/m³ air EU regulatory limit at either sampling location (Figure A3), during Inversion

Benzo(a)pyrene Equivalent Concentrations



events BaP_{EQ} concentrations exceeded the EU BaP guideline by a factor of 3 (Figure 3.4). There currently is no regulatory limit on BaP_{EQ}, which we are aware of, but the significant changes in BaP_{EQ} with wind directions and inversion events demonstrate a need for updated regulatory information. During Inversion events, the BaP_{EQ} concentration averaged 2855 (± 376) pg/m³ air and 3267 (± 1479) pg/m³ air at the Fence and Town sampling locations respectively (Figure 3.4). The median BaP_{EQ} concentration for normal days was ~200 pg/m³ air at both sampling locations.

Figure 3.4. Benzo(a)pyrene Equivalent Concentrations. Calculated benzo(a)pyrene (BaP) equivalent concentrations. * indicates a significant (p -value < 0.05) difference between BaP_{EQ} concentrations using RPFs for UPAHs (13 compounds) and all available (19 total compounds) (available on www.epa.gov) at the Town sample location. † indicates a significant decrease in BaP_{EQ} when winds increase from $<20\%$ to > 70 or 80% (as indicated). Shades of blue/teal are Fence concentrations and orange/red colors are Town concentrations for indicated wind direction or atmospheric condition (x-axis).

3.4.6 Source apportionment. Diagnostic ratios of PAHs, with a molecular weight of 202 AMU, have been shown to indicate the presence of crude petroleum contamination. Specific ratios of PAHs, with a mass of 276, can give clues about specific combustion sources⁷. These diagnostic ratios were applied to data from this study to assess if local PAH sources could be identified. While figure 3.5 indicates that the PM_{2.5} in the samples, heavily influenced by SE winds, primarily contained PAHs produced during liquid fuel and biomass combustion processes, there was no significant correlation with specific source PAH emissions⁷. The same diagnostic ratios indicate that mainly liquid fuel combustion (~ 66%) was the source of the PAHs measured in the PM_{2.5} samples when $> 70\%$ of the wind came from the NW and SW (Figure 3.5). This indicates that gasoline, liquid natural gas, and diesel combustion is the dominant source of PAHs in the SITC Reservation air shed. The diagnostic ratios from the inversion days suggest that both diesel and biomass combustion are important local sources of PAHs in PM_{2.5} on the reservation.

PMF results indicated no clear pattern of PAH concentrations that could identify specific sources when there was no prevalent wind direction,

nor when specific wind directions prevailed during the sampling period at either sampling location.

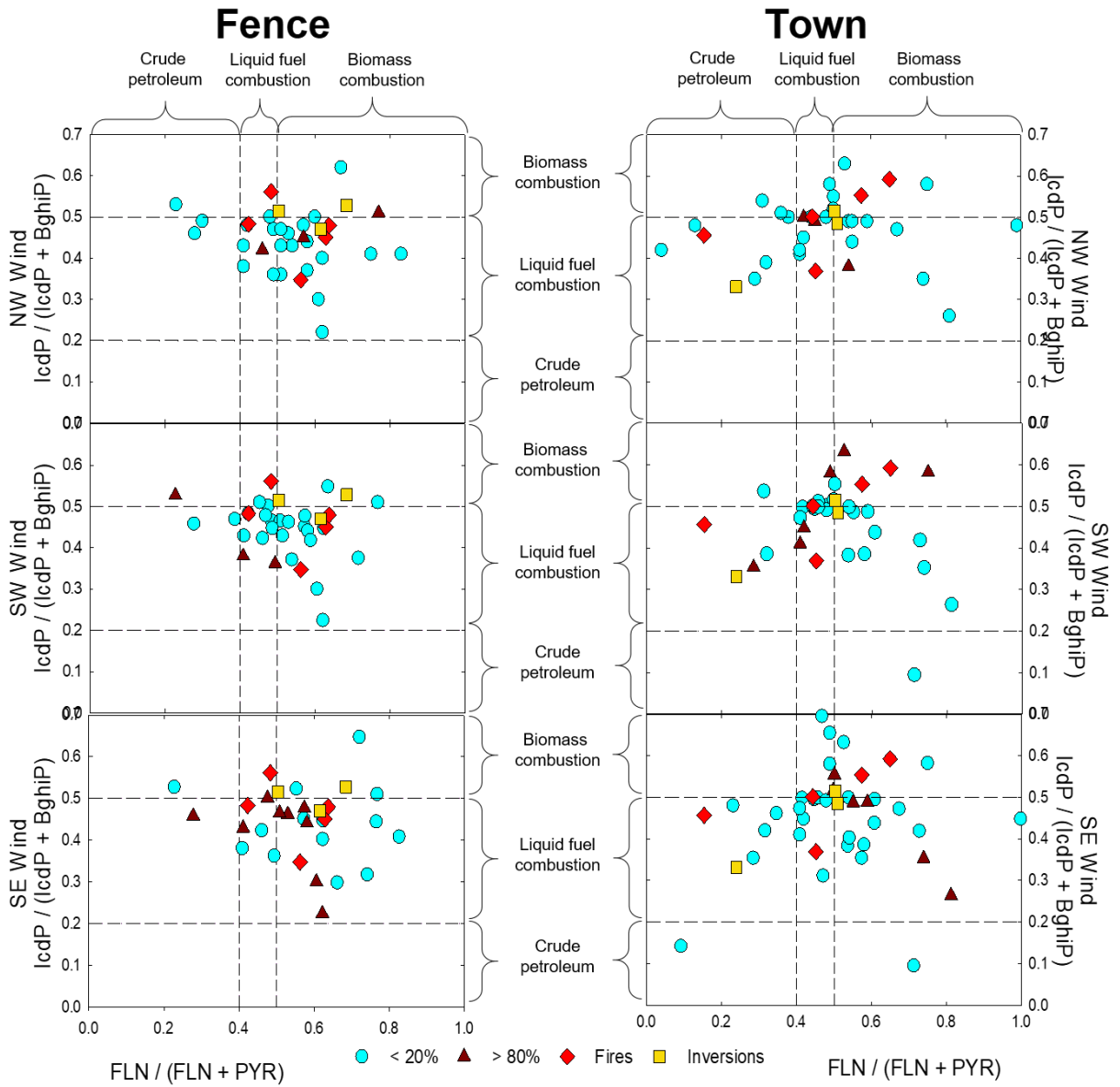


Figure 3.5. Diagnostic Ratio Analysis. Scatter plots of data for diagnostic ratios of PAHs. PAH₂₀₂ (FLN/FLN+PYR), used to assess if crude petroleum is a contributing source, and PAH 276 (IcdP/IcdP+BghiP), used to distinguish between types of combustion (Yunker 2002). Circles (teal)

indicate low wind in quadrant direction, while triangles (burgundy) indicate high winds coming from specified direction at the two locations for the three impactful wind directions. Diamonds (red) show ratios for samples collected during regional wildfires, and squares (yellow) are ratios during weather inversions.

3.5 DISCUSSION

3.5.1 *Source regions in wind directions.* At the Fence and Town sampling locations, the SW and SE winds resulted in the greatest change in PAH concentrations (Figure 3.2). At both sampling locations, when SW winds were >80%, the concentrations of multiple PAH classes and individual PAHs significantly decreased, relative to when SW winds were <20% (Table A2.T2). This suggests that higher winds from the SW diluted PAH concentrations in air at both sampling locations, which is reinforced by correlation data (Table A2.T3). In addition, at both sampling locations, SE winds >80% resulted in increased PAH concentrations, relative to when SE winds were <20%. The Seattle/Tacoma metropolitan area is located 100 km SE of the reservation and contains many industrial centers, transportation media, and energy sectors that may be contributing to the PAHs concentrations in the PM_{2.5} at the sampling locations when winds are from the SE.

In contrast, NW winds did not significantly impact the PAH concentrations at the sampling locations (Figure 3.2), even though there are a number of shipping lanes for major Canadian ports, including the city of Vancouver, BC, and minor US ports, as well as a number of oil refineries NW of the sampling locations. While shipping lanes are an important source of

PM, and many ocean-going vessels use diesel fuel, leading to complex PM chemistry around shipping lanes, there was no evidence in our data to confirm shipping lane influence on the PAH concentrations¹²⁶.

3.5.2 Local sources of PAHs. Increased PAH concentrations, at both sampling locations, during inversion events indicated that there are a number of local PAH sources, including traffic, home heating, local industries, and marinas. There is a lack in the current data to suggest which, if any, of these sources are contributing specific portions of the measured PAH concentrations to the PM_{2.5}. Future studies in the area should focus on identifying which local sources are responsible for local PAH contamination in Reservation air-shed PM_{2.5}. The data from this study, added to previous studies, which have shown that weather inversions during winter months increase the amount of PM_{2.5} measured in different locations, provides information about air quality during inversion events¹¹⁹.

While diagnostic ratios give clues to possible sources, the variation in individual source PAH profiles, along with the number of possible PAH sources within the local/regional air-shed of the sampling locations makes their use alone ambiguous¹²⁷. Retene was analyzed for changes with wind direction influence as well as during predicted wildfire influence and weather inversions. While no statistical difference was measured between the two locations, or between normal days and Fire events, retene was found to be statistically higher at both locations during inversions (Figure A2.F1). Retene inclusion in PMF did not resolve source fingerprints.

The SITC Reservation is surrounded on the East side by a large number of agricultural fields. These fields may result in PAH emissions from farming equipment and resuspension of dust particles during tilling and harvest that may contribute to increased PAH concentrations during SE winds. Interstate (I5) is located 19 km east of the Reservation. There are railroads, local wood mills, and local marinas located on Reservation lands. The northern peninsula of the Reservation, March Point, contains several industries including oil refineries. Diesel trains transporting materials to and from the oil refineries cross the reservation daily and have over 100 train cars.

The oil refining process was thought to be a significant source of PAHs in the PM_{2.5} over the Reservation, but our analysis shows mixed emission sources nearby and subsequently was unable to prove or disprove this theory. The number of different crude oils that may be coming into the two independent refineries, as well as the number of possible refined products that are leaving the area, make distinguishing a specific molecular marker for the refineries difficult. Our efforts to identify a PAH fingerprint coming from the refineries was unsuccessful, in part due to a lack of replicate sampling events when emissions of these sources would be directly affecting the sampling locations.

3.5.3 UPAH Transformation Products. At both sampling locations, during inversion events the Σ OPAH concentrations decreased, while the Σ OHPAH and Σ NPAH concentrations increased, relative to non-inversion days (Figure 3.3). This suggests that during inversion events, atmospheric

conditions favor the transformation of UPAHs to either NPAHs or OHPAHs on PM_{2.5}. Laboratory experiments using O₃ to form secondary organic aerosol (SOA) particles with UPAHs present have shown that OHPAHs are the most prevalent transformation products formed during the process of SOA formation¹². Studies have shown that PM-bound UPAHs can react with NO_x to form NPAHs²⁰. During inversions, the suppressed vertical movement of air traps atmospheric reactants along with volatile emissions and PM¹²⁸. An increase in atmospheric reactants during inversion events explains an increase in both ΣNPAHs and ΣOHPAHs during these conditions. The decrease in ΣOPAHs however does not fit, unless transformations into OPAHs are occurring through a different mechanism. This discrepancy illustrates a greater need to study the reaction pathways of UPAHs in PM_{2.5}.

The Inhalation Cancer Risk Assessment over the reservation indicated that, when NW winds increase (from < 20% to > 70% of the sampling time) the cancer risk at the Town sampling location significantly decreases, while at the Fence sampling location it remains unchanged (Figure 3.6). Increasing SW winds significantly decrease the cancer risk at both sampling locations, and SE winds do not significantly change the risk.

During normal atmospheric conditions, both sampling locations had similar excess lifetime cancer risk of 23 (± 5) people in a million at the Fence sampling location and 28 (± 6) people in a million at the Town sampling location. During Fire events, the Town sampling location had a higher Inhalation cancer risk (~32 people in a million) than the Fence sampling

location (~19 people in a million). During Inversion events, both sampling locations had a significant increase in the excess lifetime cancer risk, with 248 (± 33) people and 284 (± 129) people per million at the Fence and Town locations, respectively.

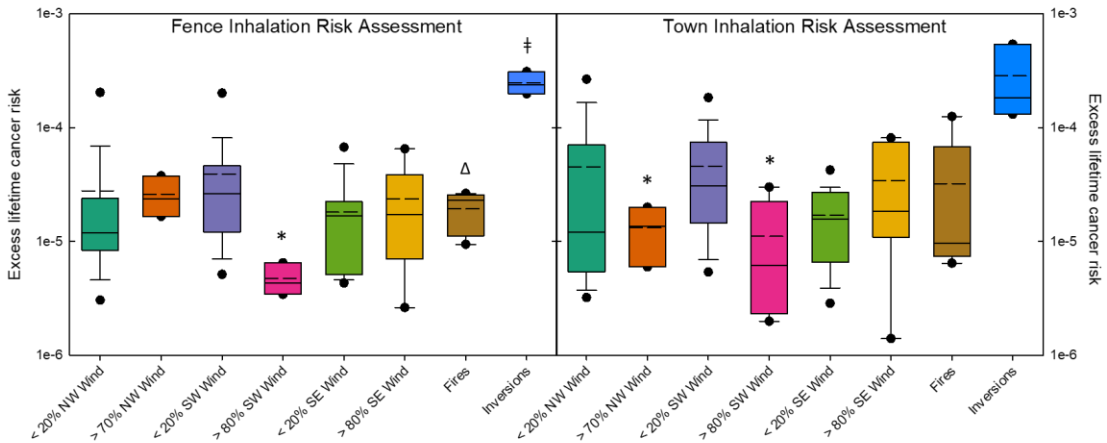


Figure 3.6. Estimated Lifetime Cancer risk assessment using World Health Organization (WHO) unit risk (8.7×10^{-5} per ng/m^3 BaP) for BaP (UR_{BaP}) as a proxy for the mixture of PAHs measured in $\text{PM}_{2.5}$. Boxes represent the top and bottom 25% of estimates for each weather condition (x-axis) with the solid lines representing the average value for excess cancer risk. Whiskers represent Standard Deviation, the 5th and 95th percentiles are represented by the dots, and dashed lines represent the geometric mean estimate. * indicate a significant difference between low (<20% wind) and high (> 70 or 80% wind) from one direction, † indicates a significant difference in inversion Lifetime Cancer Risk over all other data in this study, Δ indicates significantly higher excess lifetime cancer risk during fire events than during periods of >80% SW winds at the Fence site location

As demonstrated by the BaP_{EQ} concentrations of this study, the RPF values available for 19 PAHs, are helpful in distinguishing possible toxicity of $\text{PM}_{2.5}$ samples, but a broader list of RPFs is needed to better understand the complexity of $\text{PM}_{2.5}$ toxicity. The HMW BaP_{EQ} concentrations represented

between 10-40% of the overall BaP_{EQ} concentrations, suggesting that studies using only the UPAHs on the PPL could result in the under-prediction of risk.

The order of magnitude increase in inhalation cancer risk during predicted periods of weather inversions, observed in this study, illustrate the gaps in the available data surrounding such events and the best way to protect the health of people during them. The differences in transformation products measured during the inversion events illustrates a gap in available knowledge about the reaction pathways for PAH transformation products. While other studies have shown increases in atmospheric reactants and PM during inversions, more toxic compound analysis is needed to fully understand the health risks of such events ^{128, 119}.

3.6 CONCLUSIONS

The number of PAHs measured in PM_{2.5} in this study, illustrates the need to expand upon the US EPA's PPL. The 16 PAHs included on the PPL, are all UPAHs and are commonly measured in PM_{2.5} around the globe. This study shows the relevance of the other subclasses of PAHs. While the toxicity of many UPAHs have been well studied, the human health effects of NPAH, OPAH, HPAH, HMW and OHPAHs in PM_{2.5} remains highly unknown. PM_{2.5} exposure has been linked to over 7 million deaths per year ¹. However, the components of the PM_{2.5} responsible for these deaths are still not known. Expanding the current screening lists to include the subclasses of PAHs measured in PM_{2.5} in this study will help global scientists better understand the nature of PM_{2.5} exposure. Toxicological studies of the impact of the

compounds measured here is needed to fully understand the contribution to $PM_{2.5}$ toxicity linked to PAHs.

Data presented here illustrates the negative impact of regional PAH sources on the air quality of the SITC Reservation. When winds increased from the SE, the reservation air quality was impacted by increased PAH concentration in the $PM_{2.5}$ over the reservation. While SW winds diluted PAHs in the $PM_{2.5}$ from local sources, inversion events trapped local emissions and greatly increased the harmful $PM_{2.5}$ components in the Reservation air.

Indigenous communities are less equipped to measure and address environmental health concerns⁵⁶. The SITC sought scientific help in understanding the environment in which they live. The air quality over the SITC Reservation is directly impacted by different anthropogenic sources of PAH contaminated $PM_{2.5}$ from nearby local and regional sources. Data from this study demonstrates the need to be vigilant of atmospheric conditions in efforts to protect the health of the SITC peoples. The highest risk of adverse health effects occurred during Inversion events, which coincide with winter months in the US. Pacific Northwest¹²⁹. During these months, communities are heating their homes and businesses, often using wood burning stoves and fireplaces. The data in this study suggest there are different air quality concerns on different parts of the Reservation at any given time. General steps to reduce exposure may not have the same efficacy across all parts of

the Reservation. To more fully understand the local PAH sources on the SITC Reservation, more detailed studies are needed.

As global climate change continues to change weather patterns across the planet, the Pacific Northwest will experience increases land and sea temperatures, which will change the local weather patterns ^{129, 130}.

Communities, such as SITC, need to be take measures to ensure the safety of their people, from the local, regional, and global sources of air pollution moving into their air-shed. Increased wildfires and changing inversion patterns will continue to raise PM_{2.5} concentrations across impacted areas, increasing the concentration of toxic compounds, such as PAHs ^{119, 131}.

3.7 ACKNOWLEDGMENTS

3.7.1 Funding. This publication was made possible in part by Grants AGS-1411214 from the National Science Foundation (NSF), and P42-ES016465 and P30-ES00210 from National Institute of Environmental Health Sciences (NIEHS), National Institute of Health (NIH). Its contents are the sole responsibility of the authors and do not represent the official view of the NIEHS or NIH.

3.8 Supplementary data

Supplemental information for this chapter can be found in Appendix 2.

Chapter 4:
**Oxidative Potential of PAHs in Ambient PM_{2.5} using Dithiolthreitol (DTT)
Consumption Assay**

Linking Chemical Data to Toxicological Outcomes

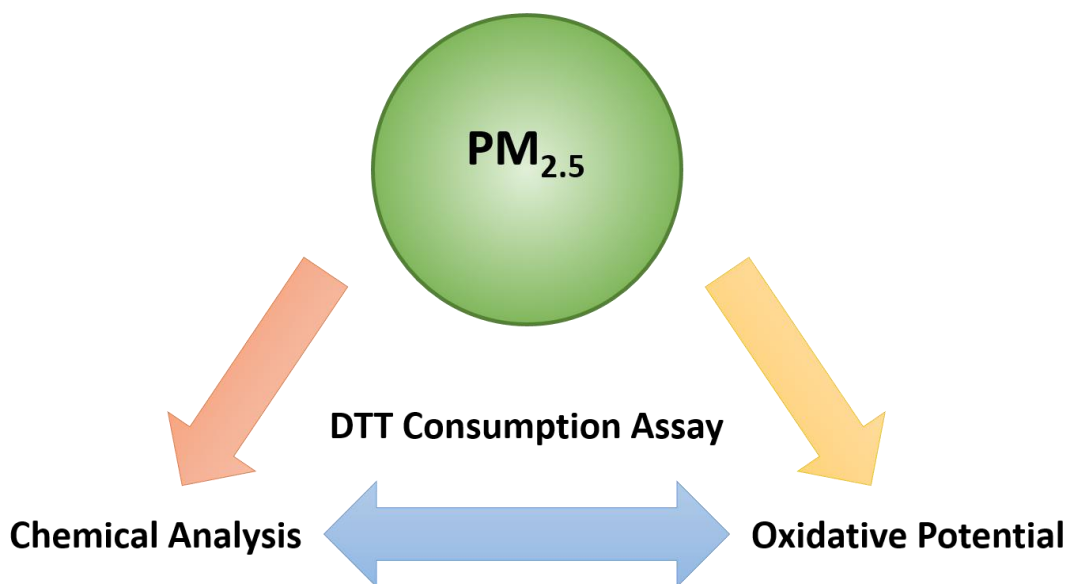


Figure 4.0

**OXIDATIVE POTENTIAL OF PAHS IN AMBIENT
ATMOSPHERIC PM_{2.5} USING DITHIOLTHREITOL (DTT)
CONSUMPTION ASSAY**

Amber L. Kramer^{1,2}, Shelby Dorn¹, Allison Perez², Ivan A. Titaley², Courtney
Roper³, Paul Cheong¹, Staci L. Massey Simonich^{1,2}

1 – Oregon State University Department of Chemistry, 2 – Oregon State University
Department of Environmental and Molecular Toxicology, 3 – University of Mississippi
Department of Biomolecular Sciences

Contributions – Prepared by Amber L. Kramer with editorial comments provided by Shelby Dorn, Ivan Titaley, Courtney Roper and Staci L. Massey Simonich. Allison Perez developed the micro-scale DTT consumption assay method, Amber Kramer performed all DTT assay experiments, statistical analysis, ambient PM_{2.5} collection, extraction and characterization. Shelby Dorn performed ΔG_{rxn} computational analysis.

Written and formatted for submission for publication in – *Environmental Science and Technology Letters (expected submittal winter 2020)*

*Corresponding Author: staci.simonich@oregonstate.edu

4.1 ABSTRACT

The oxidative potential (OP) of atmospheric fine particulate matter (PM_{2.5}) has been linked to the organic content of PM_{2.5}, including polycyclic aromatic hydrocarbons (PAHs). The OP of 135 individual PAHs, belonging to six separate subclasses of PAH, was assessed using the dithiolthreitol (DTT) consumption assay. We assessed if the free energy (ΔG_{rxn}) of the redox reaction, concentration of each compound to use 50% of the DTT (DTT₅₀), and/or the slope of PAH concentration with assay response could be used to predict mixture results in the DTT consumption assay. There were some statistical correlations of these factors with PAH molecular mass, substituent groups, as well as with other factors. Along with ambient PM_{2.5} extracts, mixtures of PAH standards (prepared to match measured PAH concentrations from ambient PM_{2.5} filter extracts) were measured in the assay. Results indicate that for a small number of PAHs, including the 16 PAHs on the Priority Pollutant List, there appeared to be an additive effect of the mixture of PAHs. However, DTT consumption predictions for the whole PAH mixture was higher than the measured results for the PAH mixture or the filter extracts. This suggests a non-additive effect of larger PAH mixtures on the oxidative potential of PM_{2.5}.

4.2 INTRODUCTION

Reactive oxygen species (ROS) have been linked to cardiopulmonary and respiratory diseases, and even cancer through various oxidative stress pathways^{36 132 59 63 133}. Recent studies have indicated that the organic portion of fine particulate matter (PM_{2.5}), in particular the anthropogenic

portion, is directly linked to the oxidative potential of $PM_{2.5}$ ^{134 67 69 41 66 75}. The ability of a sample, or compound, to cause cellular oxidative stress is referred to as oxidative potential (OP)^{60 43 78}. Measuring OP in environmental samples can be done through biological or chemical assays⁴¹⁶⁷. One chemical assay, the dithiolthreitol (DTT) assay, uses a chemical redox reaction to determine the amount of ROS produced from a sample, and has demonstrated affinity with biological assays^{132 61}. While individual compounds found in $PM_{2.5}$, such as polycyclic aromatic hydrocarbons, have been linked to oxidative stress, a full elucidation of the OP of particle components could improve predictive modeling of $PM_{2.5}$ OP^{41 69 68}.

Polycyclic aromatic hydrocarbons (PAHs) are a class of compounds emitted through incomplete combustion which undergo long-range atmospheric transport entrapped in $PM_{2.5}$ ^{85 16}. Unsubstituted PAHs (UPAHs) are directly emitted to the atmosphere, and sixteen UPAHs appear on the US EPA Priority Pollutant List (PPL) due to their well characterized toxicity, and availability of standards at the time of inclusion²⁸. Other subclasses of PAHs have been measured in atmospheric $PM_{2.5}$ samples, but have only limited data on their toxicological implications in $PM_{2.5}$, including OP^{16 114 94 20 72 18 73}⁷⁷. These substituted PAHs, such as heterocyclic PAHs (HPAHs), which contain a non-carbon atom in the ring-structures, oxy PAHs (OPAHs) which contain a carbonyl oxygen substituted outside the UPAH rings, can be directly emitted along with UPAHs^{20 31 114}. UPAHs can also undergo reactions in the atmospheric with reactive species, (such as NO_x , O_3 and OH radicals), light,

and particles, leading to the production of nitro (NPAHs) and hydroxy (OHPAHs) substitutions to a hydrogen on the UPAH rings^{20 12}. All of these subclasses of PAHs have been measured in PM_{2.5} samples along with UPAHs^{94 114 20}.

The objective of this study was to assess, for the first time, if the commonly used dithiolthreitol (DTT) consumption assay was a viable method for determining the contribution of individual PAHs on the OP of PM_{2.5}^{65 74}. A total of 135 individual PAHs, (23 UPAHs, 24 NPAHs, 18 OPAHs, 12 HPAHs, 15 HMWs and 43 OHPAHs), were analyzed with the DTT consumption assay. DTT assay results were used to assess if individual PAH OP measurements could be used to predict PAH mixture results in the DTT assay, as well as to identify molecular properties driving OP, which could help in modeling OP of ambient PM_{2.5} samples. Extracts of ambient PM_{2.5} were compared to standard mixtures prepared to match PM_{2.5} concentrations of PAHs measured in ambient atmospheric samples. We assessed if the free energy (ΔG_{rxn}) of the redox reaction, concentration of each compound to use 50% of the DTT (DTT₅₀), and/or the slope of PAH concentration with assay response could be used to predict mixture results in the DTT consumption assay.

4.3 METHODS AND MATERIAL

4.3.1 Materials. Compound names, CAS numbers, molecular mass, abbreviations, and sources in PM_{2.5}, can be found on Table A3.T1 of the supplemental information. Derivatization of OHPAHs was performed using N-tertbutyldimethylsilyl-N-methyl-trifluoroacetamide (MTBSTFA) as previously

described⁹⁸. Analytical standards were dissolved in dimethylsulfoxide (DMSO) and diluted to ~1 mM concentration. For individual compounds, six point concentration ranges were made by diluting standards to between 20-100 μ M in DMSO. Concentration ranges were measured in triplicate, with control of non-reacted PAH.

4.3.2 DTT assay. DTT was dissolved in 0.05 M monobasic potassium phosphate buffer (PBS), making a 5 mM solution of DTT. As described elsewhere, six point calibration curves of DTT were made by diluting to stock solution to between 0 and 1 mM concentrations^{65 74}. For sample exposure, DTT stock was diluted to 1 mM, and 5 μ L were added to samples in each well. DTT assay reaction can be found in Figures A3.F1. DTNB (5,5-dithio-bis-2-nitrobenzoic acid) was dissolved in methanol to a concentration of 10 mM. For reaction quenching, DTNB was diluted to 1 mM in PBS^{65 74}.

DTT consumption assay was performed in flat bottom 96 well plates. Wells were prepared with 100 μ L of 5.0 mM PBS buffer. For DTT calibration curves, 10 μ L of DMSO and 5 μ L of DTT calibration standards was added. Sample wells were prepared by adding 10 μ L of each compound or mixture, and then 5 μ L of 1 mM DTT. Plates were incubated at 37°C for 15 minutes. After incubation, 10 μ L of 1 mM DTNB was added to all wells to quench DTT reactions, and plates were gently shaken. Absorbance (412 nm) was measured using a BioTek (Winooski Vermont, USA) Synergy HTX multimode reader.

Each 96 well plate contained a triplicate DTT calibration curve to remove variability between plates. Controls of DTNB, PBS, and unreacted samples were run alongside each DTT reaction sample. Assay measurements were corrected for PAH absorbance at 412 nm by subtracting the unreacted sample control measurements from DTT reacted measurements of each PAH or mixture sample. Average measurements and standard deviations are reported. Using linear relationships of PAH concentration to the concentration of DTT consumed in the assay, the concentration (mM) of each PAH required to use 50% of the DTT (DTT₅₀) in the assay was calculated. Also calculated for each PAH was a response factor in the assay. This was calculated using the linear relationship between the concentrations of PAH and the change in measured response in the assay, to determine if such response could be used in modeling OP of PM_{2.5}.

4.3.3 *PM_{2.5} samples.* PM_{2.5} was collected using Tisch Environmental (Village of Cleves Ohio, USA) high volume cascade impact on quartz fiber filters (QFF) for a 24 hour period along the northern coast of the US State of Washington during the spring of 2018. Filters were stored at -20°C until extraction. Filters were extracted using ThermoFisher (USA) Dionex ASE 350 – Accelerated Solvent Extractor. Extraction process is detailed in supplemental information (Appendix section A2.1 and A2.2). Extracts were characterized for PAH content using gas chromatography mass spectrometry (GC/MS) operated in electron Impact (UPAH, HPAH, OPAH, HMW, OHPAH) and in negative chemical ionization (NPAH)^{20 72 12}.

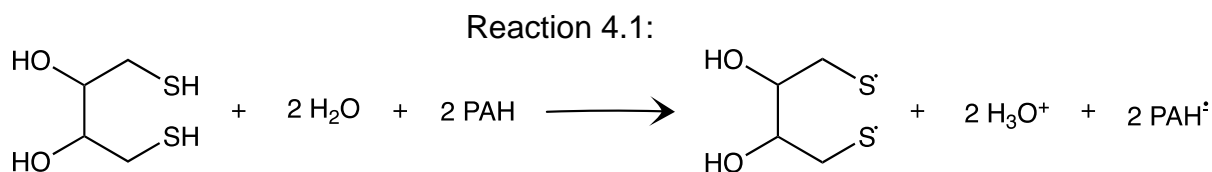
An aliquot of 100 μL of the extract from three $\text{PM}_{2.5}$ filters was evaporated to near dryness under fine nitrogen stream. To help reduce evaporation loss of volatile PAHs from extracts, the aliquots were incased in ice during concentration. Before total dryness was observed, 100 μL of DMSO was added to the aliquots and evaporation continued for ~ 10 minutes to ensure solvent evaporation. From this stock solution, dilutions were made for final concentration of 1.5 mM (± 0.3) for use in assay. For OP analysis, 10 μL of each filter extract was used in the DTT assay. Three filters (A, B, and C) were measured in the DTT consumption assay, alongside mixtures of PAH standards prepared to match PAH concentrations.

To assess if the total OP could be predicted by the individual PAH concentrations, mixtures priority pollutant list PAHS (PPL), and the entire suite of measured PAHs (Whole) were prepared to match concentrations with three (A, B, C) $\text{PM}_{2.5}$ filter extracts (Extracts). Measured PAH concentrations for the Extracts can be found in Table A3.T2. Analytical standards were made by dissolving each compound in DMSO. The Whole and PPL mixtures were measured alongside Extracts the in the DTT consumption assay at a total concentration (based on chemical composition) of 35 - 59 μM . Six replicates of each mixture were analyzed in the DTT consumption assay, with results reported as average (\pm Standard Error) in Table A3.T3.

4.3.4 Statistical analysis. Statistical analysis was performed using R statistical software on the RStudio user platform. Pearson's Correlations, and Student's t-tests were performed and statistical significance is reported as p-

value ≤ 0.05 . To illustrate where data failed to meet the statistically significant criteria, but correlations were $0.05 \leq p\text{-value} \leq 0.10$, are reported as suggestively correlated. While not significant, the correlation data suggests more information could be discovered in these categories.

4.3.5 Computational analysis. From the DTT₅₀ concentrations measured in the assay, free energy (ΔG_{rxn}) of the redox reaction for the PAHs was calculated using reaction 4.1 and Equation 4.1 below. Geometric optimizations were computed using density functional theory (DFT) B3LYP1 with the 6-311++G(d,p) basis set in Gaussian 09^{135 136 137 138 139 140}. All geometry optimizations were performed in the gas phase at 298 K. Refined single-point energies were then computed in the ORCA program, at the DLPNO-CCSD(T)/def2-TZVPP level of theory^{141 142 143 144}. Both steps were performed for all molecules involved in the balanced reaction (reaction 4.1). The Gibbs free energy of reaction was calculated (equation 4.1) for each parent and radical anion pair based on reaction 4.1.



Structural composition was considered for possible differences observed between isomers. Structural components such as a bay region containing only 6-atom rings, versus bay regions that have at least one 5-atom ring in the bay would have differences in electron density, and so were

counted and used for correlation analysis. The structural components considered are illustrated in Figure A3.F2, in short: exterior 2 uninterrupted cyclohexane connections (2CH), 3-ringed bay regions with all 6 membered rings (3RBR-6), 3-ringed bay regions with one 5 membered ring (3RBR-5), 4-ring bay region with all 6 membered rings (4RBR-6), 4-ring bay region with one 5 membered ring (4RBR-5), as well as the number of substituents for subclasses of PAHs.

4.4 RESULTS AND DISCUSSION

4.4.1 *DTT₅₀ Results.* Individual PAH measurements in the DTT consumption assay resulted in a DTT₅₀ concentration range of 0.0003 – 1.219 mM. (Table A3.T2) Overall, the DTT₅₀ (mM) was statistically correlated with a molecular mass (AMU) and the response factor of PAH concentrations within the assay. (Table 4.1) The number of 2CH had suggestively negative correlation with the DTT₅₀ of PAHs. Within subclasses of PAHs the DTT₅₀ was negatively statistically correlated with the response factor and number of 2CH (Figure A3.F2) within OHPAHs. The DTT₅₀ for UPAHs had suggestively positive correlation with the number of 3RBR-5. While smaller, more volatile PAHs can partition into and back out of PM_{2.5} during long-range atmospheric transport, larger, less volatile PAHs will stay partitioned to the PM_{2.5}. The trend of lower DTT₅₀ concentrations with higher PAH molecular masses implies that the OP of PM_{2.5} could be driven by the presence of some of the larger PAHs (Table 4.1).

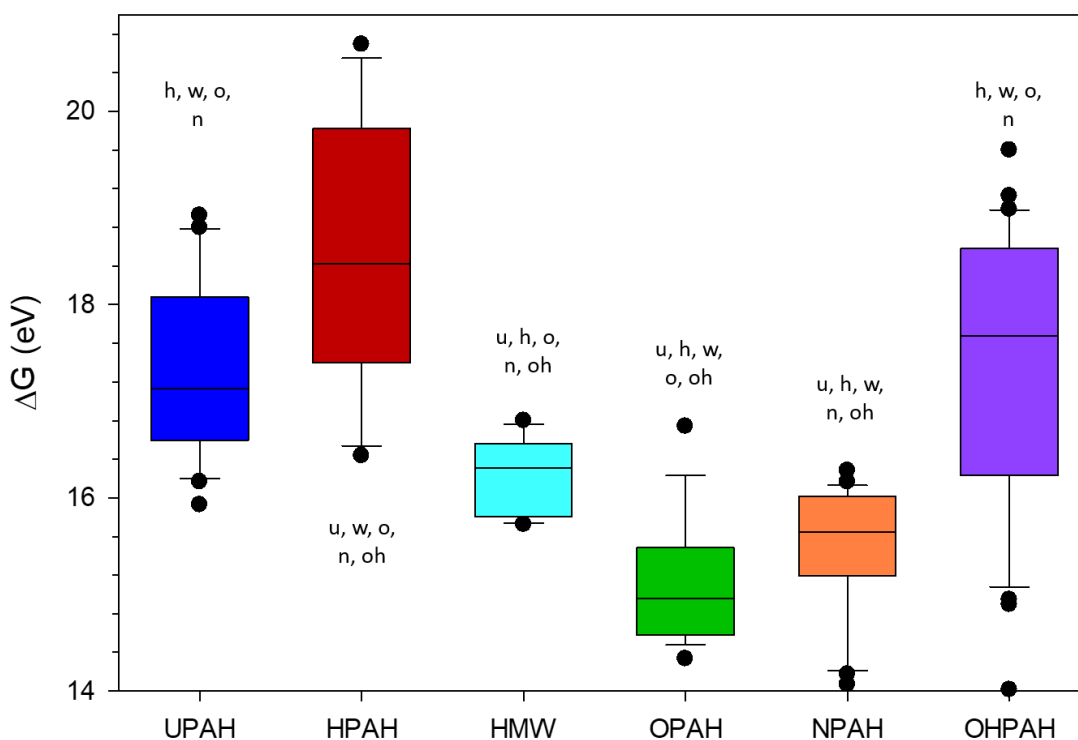
Variable	Correlated factors	ALL PAHs	UPAH	HPAH	HMW	NPAH	OPAH	OHPAH
DTT ₅₀	2CH	$Y = -0.021 x + 0.128$ (p = 0.069)						↓
	Response	$Y = -0.069 x + 0.671$ (p = 0.007)						↓
	AMU	$Y = -0.001 x + 0.277$ (p = 0.027)						
	3RBR-5		↑					
Response Factor	3RBR-6	$Y = 0.125 x + 0.517$ (p = 0.081)				↑	↑	↑
	OH groups	$Y = -0.485 x + 1.325$ (p = 0.020)						
	4RBR-5				↓			
	AMU							↓
ΔG _{rxn}	AMU	$Y = -0.014 x + 19.738$ (p < 0.000)	↓			↓	↑	↓
	Response	$Y = -0.386 x + 16.902$ (p = 0.069)		↓				
	3RBR-5		↓				↑	
	=O groups	$Y = -0.583 x + 16.199$ (p = 0.058)						
	NO ₂ groups	$Y = -1.082 x + 16.767$ (p = 0.001)				↓		

Table 4.1. Statistically significant (p-values ≤ 0.05) correlations for the entire set of 135 PAHs measured with the DTT consumption assay. Variables (Y) are correlated with factors (x) in linear regression modeling (with p values in parentheses). For each subclass of PAH, arrows indicate if the correlation was positive (↑) or negative (↓). Suggested correlations (0.05 ≤ p-value ≤ 0.10) parameters are in gray.

4.4.2 *Response Factor*. The linear slope (response factor) of PAH concentration (mM) with control corrected response in the DTT consumption assay was calculated to assess the reactivity of individual PAHs in the assay, with larger response factors indicating a greater response to changes in PAH concentration. The number of OH groups on the PAH was significantly correlated to the response factor in the DTT consumption assay (Table 4.1). The number of 3RBR-6 was suggestively positive correlations with all PAH data, but statistically correlated within the NPAH, OPAH, and OHPAH subclasses of PAHs. The 4RBR-5 within HMW PAHs, and the molecular mass of OHPAHs were statistically negatively correlated with the response factor in the assay.

4.4.3 ΔG_{rxn} of DTT Reaction. There were statistically significant negative correlations of all PAHs between both molecular mass and the number of NO₂ groups, with the ΔG_{rxn} (Table 4.1). There were suggestive negative correlations of ΔG_{rxn} with both the response factor and the number of carbonyl substituents on the PAH. Individual subclasses of PAHs had ΔG_{rxn} negative significant correlations with molecular mass (UPAH, NPAH, OPAH and OHPAH), response factor (HPAH), 3RBR-5 (UPAH and OPAH), and NO₂ groups (NPAH) (Table 4.1). While most correlations of ΔG_{rxn} and PAH subclasses were negative, OPAHs showed positive correlations for both molecular mass and the number of 3RBR-5. This could be due to the nature of the carbonyl substituent being highly electron donating on an aromatic ring, which could inhibit the ability of the molecule to accept an additional electron

to undergo reduction. While hydroxy substituents are electron donating, the correlations measured here suggest they are more amenable for reduction in the DTT assay than the OPAHs. However, the nitro substituent is electron withdrawing, which is likely to enable reduction over the surface of the



molecule.

Figure 4.1. Box and whisker plots for calculated ΔG_{rxn} per subclass of PAHs. The colored box represents standard deviation of the estimates with the solid line within the box representing the mean value. Whiskers represent the 95th percentile for measurements and the dots are outlying measurements. Statistical differences (p -value < 0.05) were calculated using Student's t-test. Lowercase letters indicate statistically different averages between subclasses. For example, the HPAH (h) average ΔG_{rxn} (red box) is statistically different from all other subclasses of PAHs: UPAHs (u), HMW (w), OPAHs (o), NPAHs (n), and OHPAHs (oh). The only classes of PAHs not statistically different

from each other are UPAH (blue) with OHPAH (purple), and OPAH (green) with NPAH (orange). HMW (teal) was statistically different from all other PAH classes.

4.4.4 Mixture Results. Figure 4.2 shows the results of the mixtures analysis in the DTT consumption assay. Bars (\pm SE) show average measured DTT consumed for each of the three filters (A, B, and C), for priority pollutant PAHS (PPL), entire PAH concentration mixtures (Whole), and filter Extracts. Extract measurements in the DTT consumption assay were significantly different from Whole mixture measurements of filters A and B, and significantly different from the PPL measurements for filter C (Figure 4.3, Table A3.T3). The process of evaporating off solvent to reconstitute in DMSO for the assay likely results in the evaporation of PAHs with high vapor pressures (2-3 ringed PAHs), which could explain the significantly lower DTT consumption measured in the assay. While it has been suggested that PAHs provide a synergistic effect on OP of $PM_{2.5}$ ⁴¹, these results suggest there could also be antagonistic effects of other extracted compounds from the $PM_{2.5}$ that have not been characterized or analyzed for OP.

Using the linear relationships established through the concentration range of PAHs tested and DTT consumed in the assay, DTT consumption was modeled assuming an additive effect with the mixtures (Table A3.T2). The triangles in Figure 4.3 show the predicted responses overlaying the measured responses for PPL and Whole mixtures. For mixtures of PPL, the effect appeared to be additive, though the modeled DTT consumption for filter B was 0.059, just outside the standard error for the measured responses,

0.054 ($\pm .003$), suggesting there may be a more complex mixtures effect than just additive (Table A3.T3).

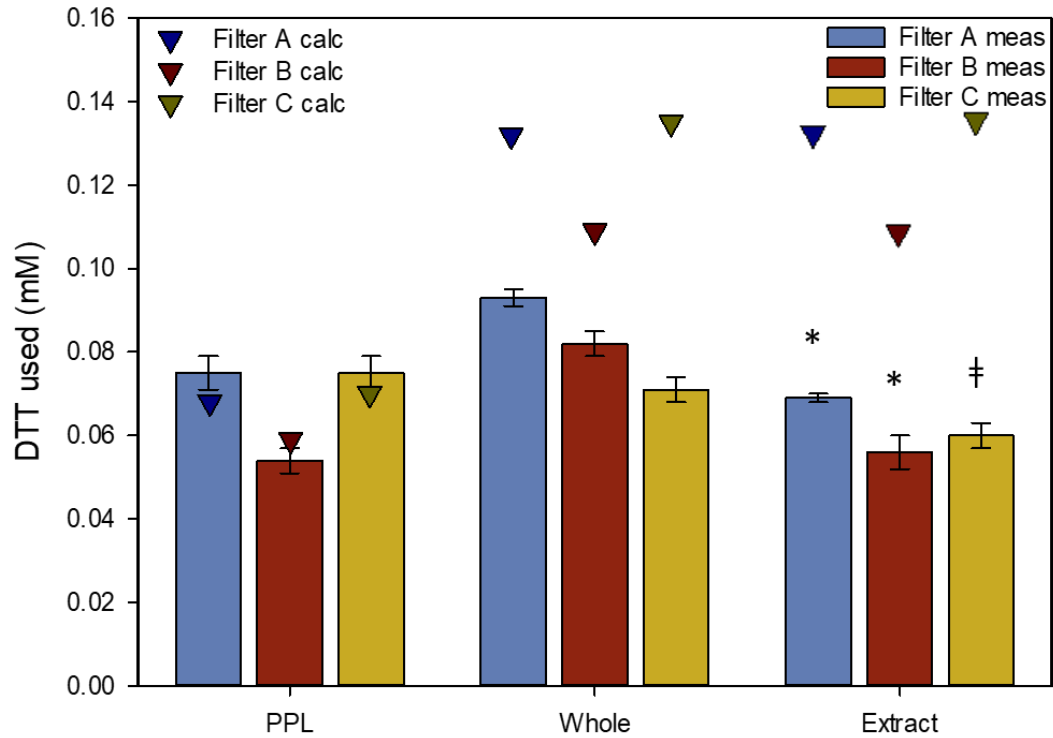


Figure 4.2. DTT assay results for mixtures analysis. Bars represent the DTT consumption for PPL standard mixtures, whole standard mixtures and filter extracts. Mixtures were prepared to match measured concentrations of PAHs found in ambient $PM_{2.5}$ filters A, B and C (\pm SE). The * indicates that Extract measurements were significantly (p -value ≤ 0.05) less than the whole mixture measurements for 2 of the filters. The † indicates that the extract measurement for filter C was significantly lower than the PPL mixture. Triangles represent predicted concentrations using the linear relationships of PAHs measured in the filter extracts, assuming an additive mixture effect. Because the Whole mixture was made to replicate the sample extract concentrations of PAHs, the predicted values are the same.

When comparing the modeled DTT consumption to the Whole and Extract measurements, a different relationship is apparent. There appears to be either an antagonistic effect occurring within the mixtures of PAHs, or a non-additive effect of the mixtures of PAHs that needs to be further explored in the DTT consumption assay.

Overall, the results of this study illustrate that the DTT consumption assay can be used to examine different properties of PM_{2.5} that might be adding to oxidative stress observed upon human inhalation of such particles. The ΔG_{rxn} for the redox reaction of each PAH can be used to compare which portions of the particles are causing the most oxidative stress, as well as the DTT₅₀ found in the assay. These results provide promising information on the OP of individual PAHs, and should be further explored for mixtures synergies.

4.5 ASSOCIATED CONTENT

4.5.1 Supporting Information

Supplemental information for this chapter can be found in Appendix 3.

4.5.2 Corresponding Author

*Tel: (541) 737-9194. Fax: (542) 737 0497. E-mail:

staci.simonich@oregonstate.edu

4.5.3 Notes

The authors declare no conflicts of interest.

4.6 ACKNOWLEDGEMENTS

This publication was made possible in part by Grant Numbers AGS-1411214 from the National Science Foundation (NSF), and P42-ES016465 and P30-

ES00210, from National Institute of Environmental Health Sciences (NIEHS), National Institute of Health (NIH). Its contents are the sole responsibility of the authors and do not represent the official view of the NIEHS or NIH.

5.0 Conclusions and Future Directions

This dissertation has explored the formation of PAH transformation products (TPs) during atmospheric reactions that result in organic aerosols in the atmosphere. These TPs, along with others, were then screened for in ambient $PM_{2.5}$ and used to correlate local weather patterns with diminished air quality over a Tribal Reservation. The presence of TPs measured in ambient $PM_{2.5}$ changes the inhalation cancer risk to communities around the world, in part by changing the oxidative potential of the particles.

Atmospheric $PM_{2.5}$ sampling and/or monitoring usually screens for the PAHs which appear on certain watch lists, like the US EPA Priority Pollutant List. While $PM_{2.5}$ emissions have been quasi-regulated across the globe, the emission of volatile and semi-volatile organic compounds are more difficult regulated, and in many cases remain unregulated. These compounds form, and contribute to increased proportions of organic aerosol in the atmosphere. Chapter 2 of this dissertation illustrates how secondary organic aerosols can aid in the long-range transport of VOC and SVOC pollutants around the globe. Gas-phase atmospheric lifetime estimates for VOC and SVOCs can be calculated, and are used to predict long-range atmospheric transport of emissions around the globe. If these molecules are within organic aerosol shields, as shown in Chapter 2, then it reasons the compounds are entrapped in SOA and being transported differently, and possibly further than modeling estimates. The increased lifetime of SOA particles formed in Chapter 2, illustrate how atmospheric emissions, such as PAHs, are not behaving as

many transport modelling paradigms assume. The synergistic effect on SOA growth observed in Chapter 2 can help explain atmospheric mass loadings of organic aerosol, but needs to be further explored to improve atmospheric modeling predictions.

If a portion of these emission molecules are transforming during incorporation into organic aerosol, as Chapter 2 demonstrated, those TPs are also entrapped from degradation and will travel alongside emitted compounds. These TPs most often do not appear on lists for screening or monitoring. Many of the TPs found in PM_{2.5} in Chapter 3 have incomplete or unknown toxicity profiles. If atmospheric scientists, modelers and chemist can continue to work together to better understand the reactions PAHs undergo during PM_{2.5} incorporation and transportation, the predictions for PAH and PAH TP transport can be improved.

While recent trends in research revolve around long-range atmospheric transport of pollutants, due to the global crisis of PM_{2.5} related deaths, work in Chapter 3 of this dissertation illustrate the gaps in knowledge around local and regional source impacts on air quality. Changing prevailing winds, patterns of extreme weather events, such as inversions, and increases in wildfires around the planet are all predicted in the latest IPCC (Intergovernmental Panel on Climate Change) report [IPCC 2014]. Changes to local and regional air quality will occur due to these climate driven changes. Understanding what air quality impacts these events have is essential to efforts to limit exposure of harmful PM_{2.5} around the globe.

Minority and indigenous communities, around the globe, are disproportionately affected by adverse air quality. These communities, globally, have less access to chemical data about the air they breathe, and they are less equipped to protect themselves due to inequity of resources. Communities, such as the Swinomish Indian Tribal Community (SITC), collaborated with for Chapter 3 of this dissertation, are interested in protecting their people and improving community knowledge about environmental contamination. The pairing of chemical analysis with local atmospheric conditions in vulnerable communities, gives community members the data they need to take action to protect themselves from the harmful effects of $PM_{2.5}$ contamination. Working with these communities to address the concerns they have, and working with them to understand what the data means for them, allows the scientific community to both advance the knowledge we have of local and regional transport of atmospheric emissions, as well as makes science accessible to communities often underrepresented in scientific research.

Many researchers are trying to understand why $PM_{2.5}$ is so dangerous to humans. Toxicologists rely on assays, which may be missing vital chemical information. PAHs are hydrophobic, yet many assays for PAH exposure rely on a water-based extraction. This has led to a large discussion about the bioavailability of chemicals in toxicity assays. This topic remains highly contentious, and there are many ways to examine environmental samples for toxicological effects. A popular paradigm is to extract an

environmental sample, and then split that sample for separate toxicity and chemical analysis. The problem with this, is the extraction itself. If the extraction is optimized for chemical characterization, the toxicity portion of the extract will usually be dried of the extraction solvent and re-suspended in a solvent more amenable to biological assays. During this process, chemicals with high vapor pressures, such as many 2-3 ring PAHs, will be lost to vaporization. And visa versa, if the extraction is optimized for toxicological analysis, many chemical components are being emitted from the analysis. This means the toxicity testing in either situation, will only be viable for a proportion of the compounds found in the environmental samples. Finding a model for predicting toxicological outcomes using chemical data has potential to improve collaborative measures between chemists and toxicologists.

Chapter 4 of this dissertation explored the DTT assay as a means to take chemical data from ambient $PM_{2.5}$ samples to predict oxidative potential in extracts. Assuming an additive effect of oxidative potential in the assay, the research failed to accurately predict sample oxidative potential. This suggests mixtures of PAHs do not behave in an additive manner. This project did find that statistical trends in the oxidative potential of PAHs in the DTT consumption assay might be useful in modeling oxidative potential. Further exploration of the structural components that may change the redox potential of PAHs, could lead to predictive modeling, enabling the ability of the chemical analysis of an environmental sample to more accurately inform toxicology.

As the climate continues to change, the ability to protect communities around the planet, especially vulnerable communities, from toxic air pollution is becoming more difficult. Changing weather patterns carry PAHs to different communities than previous weather patterns did. To fully assess the impact of PAH TPs on particle formation, transportation, and toxicity more studies are needed combining the methods used in this dissertation. Examining SOA particles during formation under various conditions can help inform ambient PM_{2.5} studies as to what PAH TPs to search for. SOA studies with mixtures of PAHs, such as would be present at any emission source, could help establish mechanistic pathways for predicting PAH TPs in PM_{2.5} downwind of sources, and can be used to predict toxicity of such particles. Measuring local and regional transport of PAHs and PAH TP on PM_{2.5} can not only help local communities understand their exposures, but will also help with transportation modeling of PAHs as the climate continues to change. The continued development of a link between chemical analysis and toxicological data can help with community protection. Continuing individual and mixture analysis with the DTT consumption assay will help translate PM_{2.5} chemical data into toxicological outcomes, which can then be used to protect vulnerable communities.

This dissertation shows that more in depth studies to understand PAH incorporation into PM_{2.5} in the atmosphere, how PM_{2.5} transports PAHs on local and regional scales, and how the oxidative potential of PM_{2.5} can be examined through chemical characterization is possible. Collectively the

integration of multiple disciplines can improve our understanding of PAHs in the atmosphere from source to human exposure.

6.0 REFERENCES

1. Landrigan, P. J.; Fuller, R.; Acosta, N. J. R.; Adeyi, O.; Arnold, R.; Basu, N.; Baldé, A. B.; Bertollini, R.; Bose-O'Reilly, S.; Boufford, J. I.; Breyse, P. N.; Chiles, T.; Mahidol, C.; Coll-Seck, A. M.; Cropper, M. L.; Fobil, J.; Fuster, V.; Greenstone, M.; Haines, A.; Hanrahan, D.; Hunter, D.; Khare, M.; Krupnick, A.; Lanphear, B.; Lohani, B.; Martin, K.; Mathiasen, K. V.; McTeer, M. A.; Murray, C. J. L.; Ndahimananjara, J. D.; Perera, F.; Potočník, J.; Preker, A. S.; Ramesh, J.; Rockström, J.; Salinas, C.; Samson, L. D.; Sandilya, K.; Sly, P. D.; Smith, K. R.; Steiner, A.; Stewart, R. B.; Suk, W. A.; van Schayck, O. C. P.; Yadama, G. N.; Yumkella, K.; Zhong, M., The Lancet Commission on pollution and health. *The Lancet* **2018**, *391* (10119), 462-512.
2. Li, C.; Martin, R. V.; van Donkelaar, A.; Boys, B.; Hammer, M.; Xu, J.-W.; Marais, E. A.; Reff, A.; Strum, M.; Ridley, D.; Crippa, M.; Brauer, M.; Zhang, Q., Trends in chemical composition of global and regional population-weighted fine particulate matter estimated for 25 years. *Environmental Science & Technology* **2017**.
3. Shiraiwa, M.; Sosedova, Y.; Rouvière, A. I.; Yang, H.; Zhang, Y.; Abbatt, J. P. D.; Ammann, M.; Pöschl, U., The role of long-lived reactive oxygen intermediates in the reaction of ozone with aerosol particles. *Nature Chemistry* **2011**, *3*, 291.
4. Davidson, C. I.; Phalen, R. F.; Solomon, P. A., Airborne Particulate Matter and Human Health: A Review. *Aerosol Science and Technology* **2005**, *39* (8), 737-749.
5. Fernández, P.; Vilanova, R. M.; Martínez, C.; Appleby, P.; Grimalt, J. O., The Historical Record of Atmospheric Pyrolytic Pollution over Europe Registered in the Sedimentary PAH from Remote Mountain Lakes. *Environmental Science & Technology* **2000**, *34* (10), 1906-1913.
6. Gabrieli, J.; Vallelonga, P.; Cozzi, G.; Gabrielli, P.; Gambaro, A.; Sigl, M.; Decet, F.; Schwikowski, M.; Gäggeler, H.; Boutron, C.; Cescon, P.; Barbante, C., Post 17th-Century Changes of European PAH Emissions Recorded in High-Altitude Alpine Snow and Ice. *Environmental Science & Technology* **2010**, *44* (9), 3260-3266.
7. Yunker, M. B.; Macdonald, R. W.; Vingarzan, R.; Mitchell, R. H.; Goyette, D.; Sylvestre, S., PAHs in the Fraser River basin: a critical appraisal of PAH ratios as indicators of PAH source and composition. *Organic Geochemistry* **2002**, *33* (4), 489-515.
8. Jiang, H.; Wu, G.; Li, T.; He, P.; Chen, R., Characteristics of Particulate Matter Emissions from a Low-Speed Marine Diesel Engine at Various Loads. *Environmental Science & Technology* **2019**.
9. Abdel-Shafy, H. I.; Mansour, M. S. M., A review on polycyclic aromatic hydrocarbons: Source, environmental impact, effect on human health and remediation. *Egyptian Journal of Petroleum* **2016**, *25* (1), 107-123.
10. Hyunok Choi, R. H., Hannu Komulainen, Juana M. Delgado Saborit, *WHO Guidelines for Indoor Air Quality: Selected Pollutants*. World Health Organization, Regional Office for Europe: 2010; p 454.
11. Ravindra, K.; Sokhi, R.; Van Grieken, R., Atmospheric polycyclic aromatic hydrocarbons: Source attribution, emission factors and regulation. *Atmospheric Environment* **2008**, *42* (13), 2895-2921.
12. Kramer, A. L.; Suski, K. J.; Bell, D. M.; Zelenyuk, A.; Massey Simonich, S. L., Formation of Polycyclic Aromatic Hydrocarbon Oxidation Products in α -Pinene Secondary Organic Aerosol Particles Formed through Ozonolysis. *Environmental Science & Technology* **2019**, *53* (12), 6669-6677.
13. Zelenyuk, A.; Imre, D. G.; Wilson, J.; Bell, D. M.; Suski, K. J.; Shrivastava, M.; Beranek, J.; Alexander, M. L.; Kramer, A. L.; Massey Simonich, S. L., The effect of gas-phase polycyclic

- aromatic hydrocarbons on the formation and properties of biogenic secondary organic aerosol particles. *Faraday Discussions* **2017**, *200* (0), 143-164.
14. Lafontaine, S.; Schrlau, J.; Butler, J.; Jia, Y.; Harper, B.; Harris, S.; Bramer, L. M.; Waters, K. M.; Harding, A.; Simonich, S. L. M., Relative Influence of Trans-Pacific and Regional Atmospheric Transport of PAHs in the Pacific Northwest, U.S. *Environmental Science & Technology* **2015**, *49* (23), 13807-13816.
 15. Friedman, C. L.; Selin, N. E., Long-Range Atmospheric Transport of Polycyclic Aromatic Hydrocarbons: A Global 3-D Model Analysis Including Evaluation of Arctic Sources. *Environmental Science & Technology* **2012**, *46* (17), 9501-9510.
 16. Genualdi, S. A.; Killin, R. K.; Woods, J.; Wilson, G.; Schmedding, D.; Simonich, S. L. M., Trans-Pacific and Regional Atmospheric Transport of Polycyclic Aromatic Hydrocarbons and Pesticides in Biomass Burning Emissions to Western North America. *Environmental Science & Technology* **2009**, *43* (4), 1061-1066.
 17. Shrivastava, M.; Lou, S.; Zelenyuk, A.; Easter, R. C.; Corley, R. A.; Thrall, B. D.; Rasch, P. J.; Fast, J. D.; Massey Simonich, S. L.; Shen, H.; Tao, S., Global long-range transport and lung cancer risk from polycyclic aromatic hydrocarbons shielded by coatings of organic aerosol. *Proceedings of the National Academy of Sciences* **2017**, *114* (6), 1246-1251.
 18. Geier, M. C.; Chlebowski, A. C.; Truong, L.; Massey Simonich, S. L.; Anderson, K. A.; Tanguay, R. L., Comparative developmental toxicity of a comprehensive suite of polycyclic aromatic hydrocarbons. *Arch Toxicol* **2018**, *92* (2), 571-586.
 19. Davie-Martin, C. L.; Stratton, K. G.; Teeguarden, J. G.; Waters, K. M.; Simonich, S. L. M., Implications of Bioremediation of Polycyclic Aromatic Hydrocarbon-Contaminated Soils for Human Health and Cancer Risk. *Environmental Science & Technology* **2017**, *51* (17), 9458-9468.
 20. Jariyasopit, N.; McIntosh, M.; Zimmermann, K.; Arey, J.; Atkinson, R.; Cheong, P. H.-Y.; Carter, R. G.; Yu, T.-W.; Dashwood, R. H.; Massey Simonich, S. L., Novel Nitro-PAH Formation from Heterogeneous Reactions of PAHs with NO₂, NO₃/N₂O₅, and OH Radicals: Prediction, Laboratory Studies, and Mutagenicity. *Environmental Science & Technology* **2014**, *48* (1), 412-419.
 21. Oja, V.; Suuberg, E. M., Vapor Pressures and Enthalpies of Sublimation of Polycyclic Aromatic Hydrocarbons and Their Derivatives. *Journal of Chemical & Engineering Data* **1998**, *43* (3), 486-492.
 22. Yunker, M. B.; Snowdon, L. R.; Macdonald, R. W.; Smith, J. N.; Fowler, M. G.; Skibo, D. N.; McLaughlin, F. A.; Danyushevskaya, A. I.; Petrova, V. I.; Ivanov, G. I., Polycyclic Aromatic Hydrocarbon Composition and Potential Sources for Sediment Samples from the Beaufort and Barents Seas. *Environmental Science & Technology* **1996**, *30* (4), 1310-1320.
 23. Panda, S. K.; Schrader, W.; al-Hajji, A.; Andersson, J. T., Distribution of Polycyclic Aromatic Sulfur Heterocycles in Three Saudi Arabian Crude Oils as Determined by Fourier Transform Ion Cyclotron Resonance Mass Spectrometry. *Energy & Fuels* **2007**, *21* (2), 1071-1077.
 24. Forsey, S. P.; Thomson, N. R.; Barker, J. F., Oxidation kinetics of polycyclic aromatic hydrocarbons by permanganate. *Chemosphere* **2010**, *79* (6), 628-636.
 25. Titley, I. A.; Chlebowski, A.; Truong, L.; Tanguay, R. L.; Massey Simonich, S. L., Identification and Toxicological Evaluation of Unsubstituted PAHs and Novel PAH Derivatives in Pavement Sealcoat Products. *Environmental Science & Technology Letters* **2016**, *3* (6), 234-242.

26. Alam, M. S.; Delgado-Saborit, J. M.; Stark, C.; Harrison, R. M., Using atmospheric measurements of PAH and quinone compounds at roadside and urban background sites to assess sources and reactivity. *Atmospheric Environment* **2013**, *77*, 24-35.
27. Johansson, K. O.; Campbell, M. F.; Elvati, P.; Schrader, P. E.; ZÅjdor, J.; Richards-Henderson, N. K.; Wilson, K. R.; Violi, A.; Michelsen, H. A., Photoionization Efficiencies of Five Polycyclic Aromatic Hydrocarbons. *The Journal of Physical Chemistry A* **2017**, *121* (23), 4447-4454.
28. Agency, U. S. E. P., Priority Pollutant List. 2014.
29. Agency, U. S. E. P. Development of a Relative Potency Factor (Rpf) Approach for Polycyclic Aromatic Hydrocarbon (PAH) Mixtures (External Review Draft). .
https://cfpub.epa.gov/si/si_public_record_report.cfm?Lab=NCEA&dirEntryId=194584
 (accessed 2 September).
30. Friedman, C. L.; Pierce, J. R.; Selin, N. E., Assessing the Influence of Secondary Organic versus Primary Carbonaceous Aerosols on Long-Range Atmospheric Polycyclic Aromatic Hydrocarbon Transport. *Environmental Science & Technology* **2014**, *48* (6), 3293-3302.
31. Zhao, Y.; Hong, B.; Fan, Y.; Wen, M.; Han, X., Accurate analysis of polycyclic aromatic hydrocarbons (PAHs) and alkylated PAHs homologs in crude oil for improving the gas chromatography/mass spectrometry performance. *Ecotoxicology and Environmental Safety* **2014**, *100* (Supplement C), 242-250.
32. Liu, L.-Y.; Wang, J.-Z.; Wei, G.-L.; Guan, Y.-F.; Wong, C. S.; Zeng, E. Y., Sediment Records of Polycyclic Aromatic Hydrocarbons (PAHs) in the Continental Shelf of China: Implications for Evolving Anthropogenic Impacts. *Environmental Science & Technology* **2012**, *46* (12), 6497-6504.
33. Oliveira, C.; Martins, N.; Tavares, J.; Pio, C.; Cerqueira, M.; Matos, M.; Silva, H.; Oliveira, C.; Camões, F., Size distribution of polycyclic aromatic hydrocarbons in a roadway tunnel in Lisbon, Portugal. *Chemosphere* **2011**, *83* (11), 1588-1596.
34. Rene P. Schwarzenbach, P. M. G. a. D. M. I., *Environmental Organic Chemistry*. 3rd ed.; John Wiley and Sons: 2016.
35. Harrison, R. M.; Yin, J., Particulate matter in the atmosphere: which particle properties are important for its effects on health? *Science of The Total Environment* **2000**, *249* (1), 85-101.
36. Thurston, G. D.; Kipen, H.; Annesi-Maesano, I.; Balmes, J.; Brook, R. D.; Cromar, K.; De Matteis, S.; Forastiere, F.; Forsberg, B.; Frampton, M. W.; Grigg, J.; Heederik, D.; Kelly, F. J.; Kuenzli, N.; Laumbach, R.; Peters, A.; Rajagopalan, S. T.; Rich, D.; Ritz, B.; Samet, J. M.; Sandstrom, T.; Sigsgaard, T.; Sunyer, J.; Brunekreef, B., A joint ERS/ATS policy statement: what constitutes an adverse health effect of air pollution? An analytical framework. *European Respiratory Journal* **2017**, *49* (1), 1600419.
37. Liu, X.; Li, H.; Wang, J.; Fan, Y.; Xu, Y.; Xie, M.; Yuan, Y.; Qian, X., Particulate matter exposure history affects antioxidant defense response of mouse lung to haze episodes. *Environmental Science & Technology* **2019**.
38. Delfino, R. J.; Staimer, N.; Tjoa, T.; Gillen, D. L.; Schauer, J. J.; Shafer, M. M., Airway inflammation and oxidative potential of air pollutant particles in a pediatric asthma panel. *J Expos Sci Environ Epidemiol* **2013**, *23* (5), 466-473.
39. Hatzis, C.; Godleski, J. J.; González-Flecha, B.; Wolfson, J. M.; Koutrakis, P., Ambient Particulate Matter Exhibits Direct Inhibitory Effects on Oxidative Stress Enzymes. *Environmental Science & Technology* **2006**, *40* (8), 2805-2811.

40. Hong, Y.-C.; Park, E.-Y.; Park, M.-S.; Ko, J. A.; Oh, S.-Y.; Kim, H.; Lee, K.-H.; Leem, J.-H.; Ha, E.-H., Community level exposure to chemicals and oxidative stress in adult population. *Toxicology Letters* **2009**, *184* (2), 139-144.
41. Bae, S.; Pan, X. C.; Kim, S. Y.; Park, K.; Kim, Y. H.; Kim, H.; Hong, Y. C., Exposures to Particulate Matter and Polycyclic Aromatic Hydrocarbons and Oxidative Stress in Schoolchildren. *Environ Health Persp* **2010**, *118* (4), 579-583.
42. Block, G.; Dietrich, M.; Norkus, E. P.; Morrow, J. D.; Hudes, M.; Caan, B.; Packer, L., Factors Associated with Oxidative Stress in Human Populations. *American Journal of Epidemiology* **2002**, *156* (3), 274-285.
43. Crobeddu, B.; Aragao-Santiago, L.; Bui, L.-C.; Boland, S.; Baeza Squiban, A., Oxidative potential of particulate matter 2.5 as predictive indicator of cellular stress. *Environmental Pollution* **2017**, *230*, 125-133.
44. Zelenyuk, A.; Imre, D.; Beranek, J.; Abramson, E.; Wilson, J.; Shrivastava, M., Synergy between Secondary Organic Aerosols and Long-Range Transport of Polycyclic Aromatic Hydrocarbons. *Environmental Science & Technology* **2012**, *46* (22), 12459-12466.
45. Jokinen, T.; Berndt, T.; Makkonen, R.; Kerminen, V.-M.; Junninen, H.; Paasonen, P.; Stratmann, F.; Herrmann, H.; Guenther, A. B.; Worsnop, D. R.; Kulmala, M.; Ehn, M.; Sipilä, M., Production of extremely low volatile organic compounds from biogenic emissions: Measured yields and atmospheric implications. *Proceedings of the National Academy of Sciences* **2015**, *112* (23), 7123.
46. Ehn, M.; Thornton, J. A.; Kleist, E.; Sipilä, M.; Junninen, H.; Pullinen, I.; Springer, M.; Rubach, F.; Tillmann, R.; Lee, B.; Lopez-Hilfiker, F.; Andres, S.; Acir, I.-H.; Rissanen, M.; Jokinen, T.; Schobesberger, S.; Kangasluoma, J.; Kontkanen, J.; Nieminen, T.; Kurtz, T.; Nielsen, L. B.; Jørgensen, S.; Kjaergaard, H. G.; Canagaratna, M.; Maso, M. D.; Berndt, T.; Petäjä, T.; Wahner, A.; Kerminen, V.-M.; Kulmala, M.; Worsnop, D. R.; Wildt, J. r.; Mentel, T. F., A large source of low-volatility secondary organic aerosol. *Nature* **2014**, *506*, 476.
47. Jarvinen, E.; Ignatius, K.; Nichman, L.; Kristensen, T. B.; Fuchs, C.; Hoyle, C. R.; Hoppel, N.; Corbin, J. C.; Craven, J.; Duplissy, J.; Ehrhart, S.; El Haddad, I.; Frege, C.; Gordon, H.; Jokinen, T.; Kallinger, P.; Kirkby, J.; Kiselev, A.; Naumann, K. H.; Petäjä, T.; Pinterich, T.; Prevot, A. S. H.; Saathoff, H.; Schiebel, T.; Sengupta, K.; Simon, M.; Slowik, J. G.; Tröstl, J.; Virtanen, A.; Vochezer, P.; Vogt, S.; Wagner, A. C.; Wagner, R.; Williamson, C.; Winkler, P. M.; Yan, C.; Baltensperger, U.; Donahue, N. M.; Flagan, R. C.; Gallagher, M.; Hansel, A.; Kulmala, M.; Stratmann, F.; Worsnop, D. R.; Müller, O.; Leisner, T.; Schnaiter, M., Observation of viscosity transition in α -pinene secondary organic aerosol. *Atmos. Chem. Phys.* **2016**, *16* (7), 4423-4438.
48. Grayson, J. W.; Zhang, Y.; Mutzel, A.; Renbaum-Wolff, L.; Böge, O.; Kamal, S.; Herrmann, H.; Martin, S. T.; Bertram, A. K., Effect of varying experimental conditions on the viscosity of α -pinene derived secondary organic material. *Atmos. Chem. Phys.* **2016**, *16* (10), 6027-6040.
49. Hinks, M. L.; Montoya-Aguilera, J.; Ellison, L.; Lin, P.; Laskin, A.; Laskin, J.; Shiraiwa, M.; Dabdub, D.; Nizkorodov, S. A., Effect of relative humidity on the composition of secondary organic aerosol from the oxidation of toluene. *Atmos. Chem. Phys.* **2018**, *18* (3), 1643-1652.
50. Zhou, S.; Lee, A. K. Y.; McWhinney, R. D.; Abbatt, J. P. D., Burial Effects of Organic Coatings on the Heterogeneous Reactivity of Particle-Borne Benzo[a]pyrene (BaP) toward Ozone. *The Journal of Physical Chemistry A* **2012**, *116* (26), 7050-7056.

51. Kroll, J. H.; Seinfeld, J. H., Chemistry of secondary organic aerosol: Formation and evolution of low-volatility organics in the atmosphere. *Atmospheric Environment* **2008**, *42* (16), 3593-3624.
52. Abramson, E.; Imre, D.; Beránek, J.; Wilson, J.; Zelenyuk, A., Experimental determination of chemical diffusion within secondary organic aerosol particles. *Physical Chemistry Chemical Physics* **2013**, *15* (8), 2983-2991.
53. Socorro, J.; Lakey, P. S. J.; Han, L.; Berkemeier, T.; Lammel, G.; Zetzsch, C.; Pöschl, U.; Shiraiwa, M., Heterogeneous OH Oxidation, Shielding Effects, and Implications for the Atmospheric Fate of Terbutylazine and Other Pesticides. *Environmental Science & Technology* **2017**, *51* (23), 13749-13754.
54. Zhang, X.; McVay, R. C.; Huang, D. D.; Dalleska, N. F.; Aumont, B.; Flagan, R. C.; Seinfeld, J. H., Formation and evolution of molecular products in α -pinene secondary organic aerosol. *Proceedings of the National Academy of Sciences* **2015**, *112* (46), 14168.
55. Kristensen, K.; Jensen, L. N.; Glasius, M.; Bilde, M., The effect of sub-zero temperature on the formation and composition of secondary organic aerosol from ozonolysis of alpha-pinene. *Environmental Science: Processes & Impacts* **2017**, *19* (10), 1220-1234.
56. Basnayake, T. L.; Morgan, L. C.; Chang, A. B., The global burden of respiratory infections in indigenous children and adults: A review. *Respirology* **2017**, *22* (8), 1518-1528.
57. Jin, L.; Xie, J.; Wong, C. K.-C.; Chan, S. K. Y.; Abbaszade, G.; Schnelle-Kreis, J.; Zimmermann, R.; Li, J.; Zhang, G.; Fu, P.; Li, X., Contributions of city-specific PM_{2.5} to differential in vitro oxidative stress and toxicity implications between Beijing and Guangzhou of China. *Environmental Science & Technology* **2019**.
58. Chowdhury, P. H.; He, Q.; Lasitzka Male, T.; Brune, W. H.; Rudich, Y.; Pardo, M., Exposure of Lung Epithelial Cells to Photochemically Aged Secondary Organic Aerosol Shows Increased Toxic Effects. *Environmental Science & Technology Letters* **2018**, *5* (7), 424-430.
59. Saffari, A.; Daher, N.; Shafer, M. M.; Schauer, J. J.; Sioutas, C., Global Perspective on the Oxidative Potential of Airborne Particulate Matter: A Synthesis of Research Findings. *Environmental Science & Technology* **2014**, *48* (13), 7576-7583.
60. Abrams, J. Y.; Weber, R. J.; Klein, M.; Samat, S. E.; Chang, H. H.; Strickland, M. J.; Verma, V.; Fang, T.; Bates, J. T.; Mulholland, J. A.; Russell, A. G.; Tolbert, P. E., Associations between Ambient Fine Particulate Oxidative Potential and Cardiorespiratory Emergency Department Visits. *Environ Health Persp* **2017**, *125* (10), 107008-107008.
61. Tong, H.; Lakey, P. S. J.; Arangio, A. M.; Socorro, J.; Shen, F.; Lucas, K.; Brune, W. H.; Pöschl, U.; Shiraiwa, M., Reactive Oxygen Species Formed by Secondary Organic Aerosols in Water and Surrogate Lung Fluid. *Environmental Science & Technology* **2018**, *52* (20), 11642-11651.
62. Manfrin, A.; Nizkorodov, S. A.; Malecha, K. T.; Getzinger, G. J.; McNeill, K.; Borduas-Dedekind, N., Reactive Oxygen Species Production from Secondary Organic Aerosols: The Importance of Singlet Oxygen. *Environmental Science & Technology* **2019**.
63. Danielsen, P. H.; Møller, P.; Jensen, K. A.; Sharma, A. K.; Wallin, H.; Bossi, R.; Autrup, H.; Mølhav, L.; Ravanat, J.-L.; Briedé, J. J.; de Kok, T. M.; Loft, S., Oxidative Stress, DNA Damage, and Inflammation Induced by Ambient Air and Wood Smoke Particulate Matter in Human A549 and THP-1 Cell Lines. *Chemical Research in Toxicology* **2011**, *24* (2), 168-184.
64. Circu, M. L.; Aw, T. Y., Reactive oxygen species, cellular redox systems, and apoptosis. *Free Radical Biology and Medicine* **2010**, *48* (6), 749-762.
65. Patel, A.; Rastogi, N., Oxidative potential of ambient fine aerosol over a semi-urban site in the Indo-Gangetic Plain. *Atmospheric Environment* **2018**, *175*, 127-134.

66. Tuet, W. Y.; Chen, Y.; Fok, S.; Champion, J. A.; Ng, N. L., Inflammatory responses to secondary organic aerosols (SOA) generated from biogenic and anthropogenic precursors. *Atmos. Chem. Phys.* **2017**, *17* (18), 11423-11440.
67. Bortey-Sam, N.; Ikenaka, Y.; Akoto, O.; Nakayama, S. M. M.; Asante, K. A.; Baidoo, E.; Obirikorang, C.; Saengtienchai, A.; Isoda, N.; Nimako, C.; Mizukawa, H.; Ishizuka, M., Oxidative stress and respiratory symptoms due to human exposure to polycyclic aromatic hydrocarbons (PAHs) in Kumasi, Ghana. *Environmental Pollution* **2017**, *228*, 311-320.
68. Liu, H.-H.; Lin, M.-H.; Chan, C.-I.; Chen, H.-L., Oxidative damage in foundry workers occupationally co-exposed to PAHs and metals. *International Journal of Hygiene and Environmental Health* **2010**, *213* (2), 93-98.
69. Lu, S.-y.; Li, Y.-x.; Zhang, J.-q.; Zhang, T.; Liu, G.-h.; Huang, M.-z.; Li, X.; Ruan, J.-j.; Kannan, K.; Qiu, R.-I., Associations between polycyclic aromatic hydrocarbon (PAH) exposure and oxidative stress in people living near e-waste recycling facilities in China. *Environment International* **2016**, *94*, 161-169.
70. Wei, H.; Feng, Y.; Liang, F.; Cheng, W.; Wu, X.; Zhou, R.; Wang, Y., Role of oxidative stress and DNA hydroxymethylation in the neurotoxicity of fine particulate matter. *Toxicology* **2017**, *380*, 94-103.
71. Roper, C.; Delgado, L. S.; Barrett, D.; Massey Simonich, S. L.; Tanguay, R. L., PM2.5 Filter Extraction Methods: Implications for Chemical and Toxicological Analyses. *Environmental Science & Technology* **2019**, *53* (1), 434-442.
72. Chibwe, L.; Geier, M. C.; Nakamura, J.; Tanguay, R. L.; Aitken, M. D.; Simonich, S. L. M., Aerobic Bioremediation of PAH Contaminated Soil Results in Increased Genotoxicity and Developmental Toxicity. *Environmental Science & Technology* **2015**, *49* (23), 13889-13898.
73. Trine, L. S. D.; Davis, E. L.; Roper, C.; Truong, L.; Tanguay, R. L.; Simonich, S. L. M., Formation of PAH Derivatives and Increased Developmental Toxicity during Steam Enhanced Extraction Remediation of Creosote Contaminated Superfund Soil. *Environmental Science & Technology* **2019**, *53* (8), 4460-4469.
74. Kramer, A. J.; Rattanavaraha, W.; Zhang, Z.; Gold, A.; Surratt, J. D.; Lin, Y.-H., Assessing the oxidative potential of isoprene-derived epoxides and secondary organic aerosol. *Atmospheric Environment* **2016**, *130*, 211-218.
75. Tuet, W. Y.; Chen, Y.; Xu, L.; Fok, S.; Gao, D.; Weber, R. J.; Ng, N. L., Chemical oxidative potential of secondary organic aerosol (SOA) generated from the photooxidation of biogenic and anthropogenic volatile organic compounds. *Atmos. Chem. Phys.* **2017**, *17* (2), 839-853.
76. Xiong, Q.; Yu, H.; Wang, R.; Wei, J.; Verma, V., Rethinking Dithiothreitol-Based Particulate Matter Oxidative Potential: Measuring Dithiothreitol Consumption versus Reactive Oxygen Species Generation. *Environmental Science & Technology* **2017**, *51* (11), 6507-6514.
77. Fang, T.; Zeng, L.; Gao, D.; Verma, V.; Stefaniak, A. B.; Weber, R. J., Ambient Size Distributions and Lung Deposition of Aerosol Dithiothreitol-Measured Oxidative Potential: Contrast between Soluble and Insoluble Particles. *Environmental Science & Technology* **2017**, *51* (12), 6802-6811.
78. Lin, Y.-H.; Arashiro, M.; Martin, E.; Chen, Y.; Zhang, Z.; Sexton, K. G.; Gold, A.; Jaspers, I.; Fry, R. C.; Surratt, J. D., Isoprene-Derived Secondary Organic Aerosol Induces the Expression of Oxidative Stress Response Genes in Human Lung Cells. *Environmental Science & Technology Letters* **2016**, *3* (6), 250-254.
79. Hemmingsen, J. G.; Møller, P.; Nøjgaard, J. K.; Roursgaard, M.; Loft, S., Oxidative Stress, Genotoxicity, And Vascular Cell Adhesion Molecule Expression in Cells Exposed to

- Particulate Matter from Combustion of Conventional Diesel and Methyl Ester Biodiesel Blends. *Environmental Science & Technology* **2011**, *45* (19), 8545-8551.
80. Luo, P.; Bao, L.-J.; Li, S.-M.; Zeng, E. Y., Size-dependent distribution and inhalation cancer risk of particle-bound polycyclic aromatic hydrocarbons at a typical e-waste recycling and an urban site. *Environmental Pollution* **2015**, *200*, 10-15.
81. Jia, Y.; Stone, D.; Wang, W.; Schrlau, J.; Tao, S.; Massey Simonich Staci, L., Estimated Reduction in Cancer Risk due to PAH Exposures If Source Control Measures during the 2008 Beijing Olympics Were Sustained. *Environ Health Persp* **2011**, *119* (6), 815-820.
82. Ramirez-Andreotta, M., Chapter 31 - Environmental Justice. In *Environmental and Pollution Science (Third Edition)*, Brusseau, M. L.; Pepper, I. L.; Gerba, C. P., Eds. Academic Press: 2019; pp 573-583.
83. Indians, N. C. o. A., Tribal Nations and the United States: An Introduction. Embassy of Tribal Nations: 2015.
84. Dippel, C., FORCED COEXISTENCE AND ECONOMIC DEVELOPMENT: EVIDENCE FROM NATIVE AMERICAN RESERVATIONS. *Econometrica* **2014**, *82* (6), 2131-2165.
85. Primbs, T.; Piekarz, A.; Wilson, G.; Schmedding, D.; Higginbotham, C.; Field, J.; Simonich, S. M., Influence of Asian and Western United States Urban Areas and Fires on the Atmospheric Transport of Polycyclic Aromatic Hydrocarbons, Polychlorinated Biphenyls, and Fluorotelomer Alcohols in the Western United States. *Environmental Science & Technology* **2008**, *42* (17), 6385-6391.
86. Knecht, A. L.; Goodale, B. C.; Truong, L.; Simonich, M. T.; Swanson, A. J.; Matzke, M. M.; Anderson, K. A.; Waters, K. M.; Tanguay, R. L., Comparative developmental toxicity of environmentally relevant oxygenated PAHs. *Toxicology and Applied Pharmacology* **2013**, *271* (2), 266-275.
87. Thackray, C. P.; Friedman, C. L.; Zhang, Y.; Selin, N. E., Quantitative Assessment of Parametric Uncertainty in Northern Hemisphere PAH Concentrations. *Environmental Science & Technology* **2015**, *49* (15), 9185-9193.
88. Wang, R.; Liu, G.; Zhang, J., Variations of emission characterization of PAHs emitted from different utility boilers of coal-fired power plants and risk assessment related to atmospheric PAHs. *Science of The Total Environment* **2015**, *538*, 180-190.
89. Shiraiwa, M.; Ueda, K.; Pozzer, A.; Lammel, G.; Kampf, C. J.; Fushimi, A.; Enami, S.; Arangio, A. M.; Fröhlich-Nowoisky, J.; Fujitani, Y.; Furuyama, A.; Lakey, P. S. J.; Lelieveld, J.; Lucas, K.; Morino, Y.; Pöschl, U.; Takahama, S.; Takami, A.; Tong, H.; Weber, B.; Yoshino, A.; Sato, K., Aerosol Health Effects from Molecular to Global Scales. *Environmental Science & Technology* **2017**, *51* (23), 13545-13567.
90. Chu, S. N.; Sands, S.; Tomasik, M. R.; Lee, P. S.; McNeill, V. F., Ozone Oxidation of Surface-Adsorbed Polycyclic Aromatic Hydrocarbons: Role of PAH-Surface Interaction. *Journal of the American Chemical Society* **2010**, *132* (45), 15968-15975.
91. Wang, W. T.; Jariyasopit, N.; Schrlau, J.; Jia, Y. L.; Tao, S.; Yu, T. W.; Dashwood, R. H.; Zhang, W.; Wang, X. J.; Simonich, S. L. M., Concentration and Photochemistry of PAHs, NPAHs, and OPAHs and Toxicity of PM_{2.5} during the Beijing Olympic Games. *Environmental Science & Technology* **2011**, *45* (16), 6887-6895.
92. Shahpoury, P.; Lammel, G.; Albinet, A.; Sofuoğlu, A.; Dumanoğlu, Y.; Sofuoğlu, S. C.; Wagner, Z.; Zdimal, V., Evaluation of a Conceptual Model for Gas-Particle Partitioning of Polycyclic Aromatic Hydrocarbons Using Polyparameter Linear Free Energy Relationships. *Environmental Science & Technology* **2016**, *50* (22), 12312-12319.
93. Sindelarova, K.; Granier, C.; Bouarar, I.; Guenther, A.; Tilmes, S.; Stavrakou, T.; Muller, J. F.; Kuhn, U.; Stefani, P.; Knorr, W., Global data set of biogenic VOC emissions

- calculated by the MEGAN model over the last 30 years. *Atmospheric Chemistry and Physics* **2014**, *14* (17), 9317-9341.
94. Walgraeve, C.; Demeestere, K.; Dewulf, J.; Zimmermann, R.; Van Langenhove, H., Oxygenated polycyclic aromatic hydrocarbons in atmospheric particulate matter: Molecular characterization and occurrence. *Atmospheric Environment* **2010**, *44* (15), 1831-1846.
95. Ehn, M.; Thornton, J. A.; Kleist, E.; Sipilä, M.; Junninen, H.; Pullinen, I.; Springer, M.; Rubach, F.; Tillmann, R.; Lee, B.; Lopez-Hilfiker, F.; Andres, S.; Acir, I.-H.; Rissanen, M.; Jokinen, T.; Schobesberger, S.; Kangasluoma, J.; Kontkanen, J.; Nieminen, T.; Kurtén, T.; Nielsen, L. B.; Jørgensen, S.; Kjaergaard, H. G.; Canagaratna, M.; Maso, M. D.; Berndt, T.; Petäjä, T.; Wahner, A.; Kerminen, V.-M.; Kulmala, M.; Worsnop, D. R.; Wildt, J.; Mentel, T. F., A large source of low-volatility secondary organic aerosol. *Nature* **2014**, *506*, 476.
96. Perraudin, E.; Budzinski, H. I. n.; Villenave, E., Identification and quantification of ozonation products of anthracene and phenanthrene adsorbed on silica particles. *Atmospheric Environment* **2007**, *41* (28), 6005-6017.
97. Archibald, A.; Arnold, S.; Bejan, L.; Brown, S.; Brüggemann, M.; Carpenter, L. J.; Collins, W.; Evans, M.; Finlayson-Pitts, B.; George, C.; Hastings, M.; Heard, D.; Hewitt, C. N.; Isaacman-VanWertz, G.; Kalberer, M.; Keutsch, F.; Kiendler-Scharr, A.; Knopf, D.; Lelieveld, J.; Marais, E.; Petzold, A.; Ravishankara, A.; Reid, J.; Rovelli, G.; Scott, C.; Sherwen, T.; Shindell, D.; Tinel, L.; Unger, N.; Wahner, A.; Wallington, T. J.; Williams, J.; Young, P.; Zelenyuk, A., Atmospheric chemistry and the biosphere: general discussion. *Faraday Discussions* **2017**, *200* (0), 195-228.
98. Schummer, C.; Delhomme, O.; Appenzeller, B. M. R.; Wennig, R.; Millet, M., Comparison of MTBSTFA and BSTFA in derivatization reactions of polar compounds prior to GC/MS analysis. *Talanta* **2009**, *77* (4), 1473-1482.
99. Vaden, T. D.; Imre, D.; Beránek, J.; Shrivastava, M.; Zelenyuk, A., Evaporation kinetics and phase of laboratory and ambient secondary organic aerosol. *Proceedings of the National Academy of Sciences* **2011**, *108* (6), 2190.
100. Nah, T.; Sanchez, J.; Boyd, C. M.; Ng, N. L., Photochemical Aging of α -pinene and β -pinene Secondary Organic Aerosol formed from Nitrate Radical Oxidation. *Environmental Science & Technology* **2016**, *50* (1), 222-231.
101. DeCarlo, P. F.; Kimmel, J. R.; Trimborn, A.; Northway, M. J.; Jayne, J. T.; Aiken, A. C.; Gonin, M.; Fuhrer, K.; Horvath, T.; Docherty, K. S.; Worsnop, D. R.; Jimenez, J. L., Field-Deployable, High-Resolution, Time-of-Flight Aerosol Mass Spectrometer. *Analytical Chemistry* **2006**, *78* (24), 8281-8289.
102. Kroll, J. H.; Lim, C. Y.; Kessler, S. H.; Wilson, K. R., Heterogeneous Oxidation of Atmospheric Organic Aerosol: Kinetics of Changes to the Amount and Oxidation State of Particle-Phase Organic Carbon. *The Journal of Physical Chemistry A* **2015**, *119* (44), 10767-10783.
103. Lambe, A. T.; Ahern, A. T.; Williams, L. R.; Slowik, J. G.; Wong, J. P. S.; Abbatt, J. P. D.; Brune, W. H.; Ng, N. L.; Wright, J. P.; Croasdale, D. R.; Worsnop, D. R.; Davidovits, P.; Onasch, T. B., Characterization of aerosol photooxidation flow reactors: heterogeneous oxidation, secondary organic aerosol formation and cloud condensation nuclei activity measurements. *Atmos Meas Tech* **2011**, *4* (3), 445-461.
104. Berset, J. D.; Ejem, M.; Holzer, R.; Lischer, P., Comparison of different drying, extraction and detection techniques for the determination of priority polycyclic aromatic hydrocarbons in background contaminated soil samples. *Analytica Chimica Acta* **1999**, *383* (3), 263-275.

105. Gao, S.; Zhang, Y.; Meng, J.; Shu, J., Online investigations on ozonation products of pyrene and benz[a]anthracene particles with a vacuum ultraviolet photoionization aerosol time-of-flight mass spectrometer. *Atmospheric Environment* **2009**, *43* (21), 3319-3325.
106. Miet, K.; Le Menach, K.; Flaud, P. M.; Budzinski, H.; Villenave, E., Heterogeneous reactions of ozone with pyrene, 1-hydroxypyrene and 1-nitropyrene adsorbed on particles. *Atmospheric Environment* **2009**, *43* (24), 3699-3707.
107. Cochran, R. E.; Jeong, H.; Haddadi, S.; Fisseha Derseh, R.; Gowan, A.; Beránek, J.; Kubátová, A., Identification of products formed during the heterogeneous nitration and ozonation of polycyclic aromatic hydrocarbons. *Atmospheric Environment* **2016**, *128*, 92-103.
108. Berndt, T.; Herrmann, H.; Kurtz, T., Direct Probing of Criegee Intermediates from Gas-Phase Ozonolysis Using Chemical Ionization Mass Spectrometry. *Journal of the American Chemical Society* **2017**, *139* (38), 13387-13392.
109. Krapf, M.; El Haddad, I.; Bruns, Emily A.; Molteni, U.; Daellenbach, Kaspar R.; Prévôt, André S. H.; Baltensperger, U.; Dommen, J., Labile Peroxides in Secondary Organic Aerosol. *Chem* **2016**, *1* (4), 603-616.
110. Titaley, I. A.; Ogba, O. M.; Chibwe, L.; Hoh, E.; Cheong, P. H. Y.; Simonich, S. L. M., Automating data analysis for two-dimensional gas chromatography/time-of-flight mass spectrometry non-targeted analysis of comparative samples. *Journal of Chromatography A* **2018**, *1541*, 57-62.
111. Schrlau, J. E.; Kramer, A. L.; Chlebowski, A.; Truong, L.; Tanguay, R. L.; Simonich, S. L. M.; Semprini, L., Formation of Developmentally Toxic Phenanthrene Metabolite Mixtures by Mycobacterium sp. ELW1. *Environmental Science & Technology* **2017**, *51* (15), 8569-8578.
112. Silva, K. T.; Oliveira-Castro, R. A.; Rodrigues, V. c. C.; de Lima, W. G.; Rodrigues, C. V.; Castro-Borges, W.; Andrade, M. H. r. G., DBT- and DBTO₂-Induced Dysplasia and Their Associated Proteomic Alterations in the Small Intestines of Wistar Rats. *Journal of Proteome Research* **2015**, *14* (1), 385-396.
113. Agency, U. S. E. P., Integrated Risk Information System (IRIS) Chemical Assessment Summary: Benz[a]anthracene; CASRN 56-55-3.
114. Wang, W.; Jariyasopit, N.; Schrlau, J.; Jia, Y.; Tao, S.; Yu, T.-W.; Dashwood, R. H.; Zhang, W.; Wang, X.; Simonich, S. L. M., Concentration and Photochemistry of PAHs, NPAHs, and OPAHs and Toxicity of PM_{2.5} during the Beijing Olympic Games. *Environmental Science & Technology* **2011**, *45* (16), 6887-6895.
115. Hu, C.; Hou, J.; Zhou, Y.; Sun, H.; Yin, W.; Zhang, Y.; Wang, X.; Wang, G.; Chen, W.; Yuan, J., Association of polycyclic aromatic hydrocarbons exposure with atherosclerotic cardiovascular disease risk: A role of mean platelet volume or club cell secretory protein. *Environmental Pollution* **2018**, *233*, 45-53.
116. Minick, D. J.; Paulik, L. B.; Smith, B. W.; Scott, R. P.; Kile, M. L.; Rohlman, D.; Anderson, K. A., A passive sampling model to predict PAHs in butter clams (*Saxidomus giganteus*), a traditional food source for Native American tribes of the Salish Sea Region. *Marine Pollution Bulletin* **2019**, *145*, 28-35.
117. Rohlman, D.; Donatuto, J.; Heidt, M.; Barton, M.; Campbell, L.; Anderson, A. K.; Kile, L. M., A Case Study Describing a Community-Engaged Approach for Evaluating Polycyclic Aromatic Hydrocarbon Exposure in a Native American Community. *Int J Environ Res Public Health* **2019**, *16* (3).
118. Navarro, K. M.; Cisneros, R.; O'Neill, S. M.; Schweizer, D.; Larkin, N. K.; Balmes, J. R., Air-Quality Impacts and Intake Fraction of PM_{2.5} during the 2013 Rim Megafire. *Environmental Science & Technology* **2016**, *50* (21), 11965-11973.

119. Gillies, R. R.; Wang, S.-Y.; Booth, M. R., Atmospheric Scale Interaction on Wintertime Intermountain West Low-Level Inversions. *Weather and Forecasting* **2010**, *25* (4), 1196-1210.
120. Hou, P.; Wu, S., Long-term Changes in Extreme Air Pollution Meteorology and the Implications for Air Quality. *Scientific Reports* **2016**, *6* (1), 23792.
121. Commission, T. E., Air Quality Standards. 07/18/2019 ed.; 2019.
122. Hites, R. A., Correcting for Censored Environmental Measurements. *Environmental Science & Technology* **2019**.
123. Claus P. Haslauer, J. R. M., Andras Bardossy, and Beth L. Parker, Estimating a Representative Value and Proportion of True Zeros for Censored Analytical Data with Application to Contaminated Site Assessment. *Environmental Science & Technology* **2017**, *51* (13), 7502-7510.
124. US EPA, C. M. T., Definition and Procedure for the Determination of the Method Detection Limit, Revision 2. (4303T), E. a. A. S. B. E., Ed. US Environmental Protection Agency: www.epa.gov, 2010.
125. Ramdahl, T., Retene—a molecular marker of wood combustion in ambient air. *Nature* **1983**, *306* (5943), 580-582.
126. Yau, P. S.; Lee, S. C.; Cheng, Y.; Huang, Y.; Lai, S. C.; Xu, X. H., Contribution of ship emissions to the fine particulate in the community near an international port in Hong Kong. *Atmospheric Research* **2013**, *124*, 61-72.
127. Galarneau, E., Source specificity and atmospheric processing of airborne PAHs: Implications for source apportionment. *Atmospheric Environment* **2008**, *42* (35), 8139-8149.
128. Esen, F.; Tasdemir, Y.; Cindoruk, S. S., Evaluation of NO_x and O₃ Concentrations in the Atmosphere of Bursa, Turkey. *Environmental Forensics* **2005**, *6* (3), 311-317.
129. Mote, P. W.; Salathé, E. P., Future climate in the Pacific Northwest. *Climatic Change* **2010**, *102* (1), 29-50.
130. IPCC Climate Change 2014: Synthesis Report. Contributions of Working Groups I, II, and III to the Fifth Assessment Report of the Intergovernmental Panel on Climate Change (Core writing team, R.K. Pachauri, L. A Meyer). https://www.ipcc.ch/site/assets/uploads/2018/02/SYR_AR5_FINAL_full.pdf (accessed 30 August 2019).
131. Navarro, K. M.; Cisneros, R.; Noth, E. M.; Balmes, J. R.; Hammond, S. K., Occupational Exposure to Polycyclic Aromatic Hydrocarbon of Wildland Firefighters at Prescribed and Wildland Fires. *Environmental Science & Technology* **2017**, *51* (11), 6461-6469.
132. Ayres, J. G.; Borm, P.; Cassee, F. R.; Castranova, V.; Donaldson, K.; Ghio, A.; Harrison, R. M.; Hider, R.; Kelly, F.; Kooter, I. M.; Marano, F.; Maynard, R. L.; Mudway, I.; Nel, A.; Sioutas, C.; Smith, S.; Baeza-Squiban, A.; Cho, A.; Duggan, S.; Froines, J., Evaluating the Toxicity of Airborne Particulate Matter and Nanoparticles by Measuring Oxidative Stress Potential—A Workshop Report and Consensus Statement. *Inhalation Toxicology* **2008**, *20* (1), 75-99.
133. Chowdhury, P.-H.; He, Q.; Carmieli, R.; Li, C.; Rudich, Y.; Pardo, M., Connecting the oxidative potential of secondary organic aerosols with Reactive Oxygen Species in exposed lung cells. *Environmental Science & Technology* **2019**.
134. Athanasios Valavanidis, T. V., Konstantinos Fiotakis, Spyrdion Loidas, Pulmonary Oxidative Stress, Inflammation and Cancer: Respirable Particulate Matter, Fibrous Dust and Ozone as Major Causes of Lung Carcinogenesis through Reactive Oxygen Species Mechanisms. *Int J Environ Res Public Health* **2013**, *10* (9), 3886-3907.

135. Becke, A. D., Density-functional thermochemistry. III. The role of exact exchange. *The Journal of Chemical Physics* **1993**, *98* (7), 5648-5652.
136. McLean, A. D.; Chandler, G. S., Contracted Gaussian basis sets for molecular calculations. I. Second row atoms, $Z=11-18$. *The Journal of Chemical Physics* **1980**, *72* (10), 5639-5648.
137. Krishnan, R.; Binkley, J. S.; Seeger, R.; Pople, J. A., Self-consistent molecular orbital methods. XX. A basis set for correlated wave functions. *The Journal of Chemical Physics* **1980**, *72* (1), 650-654.
138. Clark, T.; Chandrasekhar, J.; Spitznagel, G. W.; Schleyer, P. V. R., Efficient diffuse function-augmented basis sets for anion calculations. III. The 3-21+G basis set for first-row elements, Li-F. *Journal of Computational Chemistry* **1983**, *4* (3), 294-301.
139. Frisch, M. J.; Pople, J. A.; Binkley, J. S., Self-consistent molecular orbital methods 25. Supplementary functions for Gaussian basis sets. *The Journal of Chemical Physics* **1984**, *80* (7), 3265-3269.
140. M. J. Frisch, G. W. T., H. B. Schlegel, G. E. Scuseria, M. A. Robb, J. R. Cheeseman, G. Scalmani, V. Barone, G. A. Petersson, H. Nakatsuji, X. Li, M. Caricato, A. Marenich, J. Bloino, B. G. Janesko, R. Gomperts, B. Mennucci, H. P. Hratchian, J. V. Ortiz, A. F. Izmaylov, J. L. Sonnenberg, D. Williams-Young, F. Ding, F. Lipparini, F. Egidi, J. Goings, B. Peng, A. Petrone, T. Henderson, D. Ranasinghe, V. G. Zakrzewski, J. Gao, N. Rega, G. Zheng, W. Liang, M. Hada, M. Ehara, K. Toyota, R. Fukuda, J. Hasegawa, M. Ishida, T. Nakajima, Y. Honda, O. Kitao, H. Nakai, T. Vreven, K. Throssell, J. A. Montgomery, Jr., J. E. Peralta, F. Ogliaro, M. Bearpark, J. J. Heyd, E. Brothers, K. N. Kudin, V. N. Staroverov, T. Keith, R. Kobayashi, J. Normand, K. Raghavachari, A. Rendell, J. C. Burant, S. S. Iyengar, J. Tomasi, M. Cossi, J. M. Millam, M. Klene, C. Adamo, R. Cammi, J. W. Ochterski, R. L. Martin, K. Morokuma, O. Farkas, J. B. Foresman, and D. J. Fox *Gaussian 09*, Gaussian, Inc: Wallingford, CT, USA, 2016.
141. Neese, F., The ORCA program system. *Wiley Interdisciplinary Reviews: Computational Molecular Science* **2012**, *2* (1), 73-78.
142. Neese, F., Software update: the ORCA program system, version 4.0. *Wiley Interdisciplinary Reviews: Computational Molecular Science* **2018**, *8* (1), e1327.
143. Raghavachari, K.; Trucks, G. W.; Pople, J. A.; Head-Gordon, M., A fifth-order perturbation comparison of electron correlation theories. *Chemical Physics Letters* **1989**, *157* (6), 479-483.
144. Weigend, F., Accurate Coulomb-fitting basis sets for H to Rn. *Physical Chemistry Chemical Physics* **2006**, *8* (9), 1057-1065.

Appendix 1

CHAPTER 2 SUPPORTING INFORMATION

**Formation of polycyclic aromatic hydrocarbon oxidation products in
 α -pinene secondary organic aerosol particles formed through
ozonolysis**

Amber L. Kramer[†], Kaitlyn J. Suski[‡], David M. Bell^{†‡}, Alla Zelenyuk^{‡2},
Staci L. Massey Simonich^{††1}

[†] Department of Chemistry, [†]Department of Environmental and Molecular
Toxicology, Oregon State University, Corvallis Oregon 97331, United
States

[‡] Atmospheric Sciences and Global Change, Pacific Northwest National
Laboratory, Richland Washington 99354, United States

¹ David M. Bell is now a researcher at Paul Scherrer Institute, Switzerland

Table A1.T1: Analytical standard names, abbreviations, CAS numbers, physical properties estimated using EPISUITE 4.1, and manufacturer purchased from. * Indicates where experimental values from EPISUITE 4.1 were used instead of estimated values.

Parent Compound Oxidation product	Abbreviation	Molecular weight (g/mol)	CAS Number	Vapor Pressure (Pa at 25°C)	Boiling Point (°C)	Manufacturer
α-pinene	α-P	136.24	7785-70-8	*633	*155.9	Sigma Aldrich
verbenol	v-ol	152.24	18881-04-4	2.51	220.98	Sigma Aldrich
verbenone	v-one	150.22	1196-01-6	18.13	215.05	Sigma Aldrich
Phenanthrene	PHE	178.23	85-01-8	*1.61 x 10 ⁻²	*340	Sigma Aldrich
1-hydroxyphenanthrene	1-OHPHE	194.23	2433-56-9	2.15 x 10 ⁻³	363.13	Toronto Research Chemicals
2-hydroxyphenanthrene	2-OHPHE	194.23	605-56-0	2.15 x 10 ⁻³	363.13	Toronto Research Chemicals
3-hydroxyphenanthrene	3-OHPHE	195.23	605-87-8	2.15 x 10 ⁻³	363.13	Toronto Research Chemicals
4-hydroxyphenanthrene	4-OHPHE	196.23	7561-86-7	2.15 x 10 ⁻³	363.13	Toronto Research Chemicals
9-hydroxyphenanthrene	9-OHPHE	197.23	484-17-3	2.15 x 10 ⁻³	363.13	Sigma Aldrich
<i>cis</i> -9,10-dihydroxyphenanthrene	<i>cis</i> -9,10-OHPHE	210.23	2510-71-6	6.69 x 10 ⁻³	397.97	Toronto Research Chemicals
<i>trans</i> -9,10-dihydroxyphenanthrene	<i>trans</i> -9,10-OHPHE	211.23	572-41-8	6.69 x 10 ⁻³	397.97	Toronto Research Chemicals
1,9-dihydroxyphenanthrene	1,9-OHPHE	210.23	85337-40-2	6.69 x 10 ⁻³	397.97	Sigma Aldrich
phenanthren-1,4-dione	1,4-PHEone	208.22	569-15-3	1.02 x 10 ⁻²	377.67	Sigma Aldrich
9,10-phenanthrequinone	9,10-PHEQ	209.22	84-11-7	1.02 x 10 ⁻³	377.67	Sigma Aldrich
Dibenzothiophene	DBT	184.26	132-65-0	*2.73 x 10 ⁻²	*332.5	Sigma Aldrich
Dibenzothiophene sulfone	DBTS	216.26	1016-05-3	6.17 x 10 ⁻³	369.08	Sigma Aldrich
diphenyl sulfoxide	DPS	202.27	945-51-7	2.36 x 10 ⁻²	*340	Sigma Aldrich
Pyrene	PYR	202.25	129-00-0	*6.0 x 10 ⁻⁴	*404	Sigma Aldrich
1-hydroxypyrene	1-OHPYR	218.26	5315-79-7	*6.44 x 10 ⁻⁷	406.69	Accu Standard
4H-cyclopenta[def]phenanthren-4-one	4H-CPP	204.23	5737-13-3	4.25 x 10 ⁻³	375.83	Toronto Research Chemicals
6H-benzo(cd)pyrene-6-one	6H-BcdP	254.29	3074-00-8	7.89 x 10 ⁻⁵	446.73	European Community Bureau of Reference

Benz(a)anthracene	BaA	228.29	56-55-3	$*2.8 \times 10^{-5}$	*437.6	Sigma Aldrich
3-hydroxybenz(a)anthracene	3-OHBaA	244.31	4834-35-9	2.92×10^{-5}	434.03	Toronto Research Chemicals
benz(a)anthracene-7,12-dione	7,12-BaAone	258.28	2498-66-0	1.59×10^{-4}	434.48	Accu Standard

Figure A1.F1. Chromatograms from GC/MS non-targeted analysis α -P SOA (A), DBT influenced SOA (B), PHE influenced SOA (C), and PYR influenced SOA (D), with peaks for known compounds labeled. Individual peaks were examined for fragmentation patterns, compared to NIST library database, and are not at this point classified as PAH-OPs.

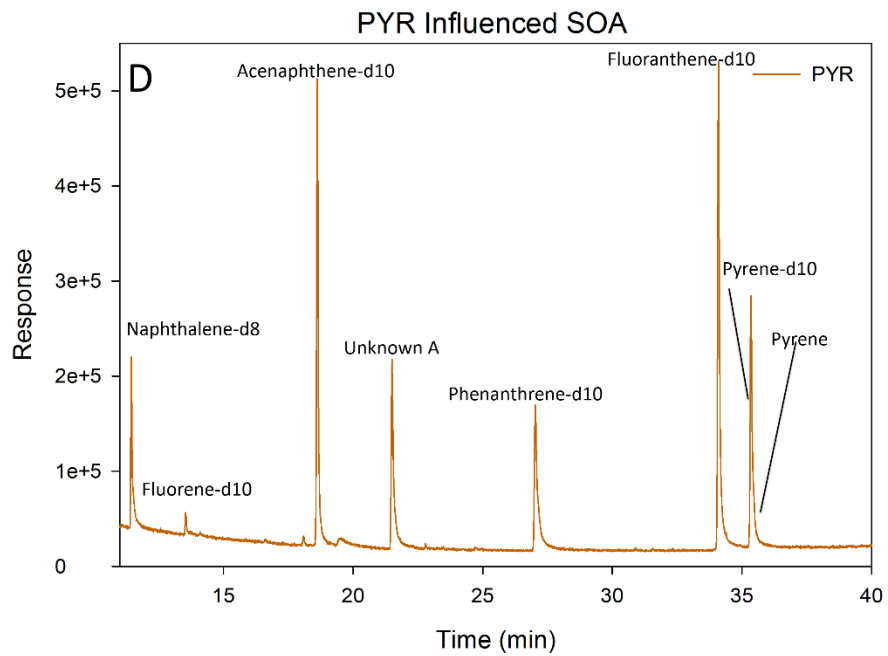
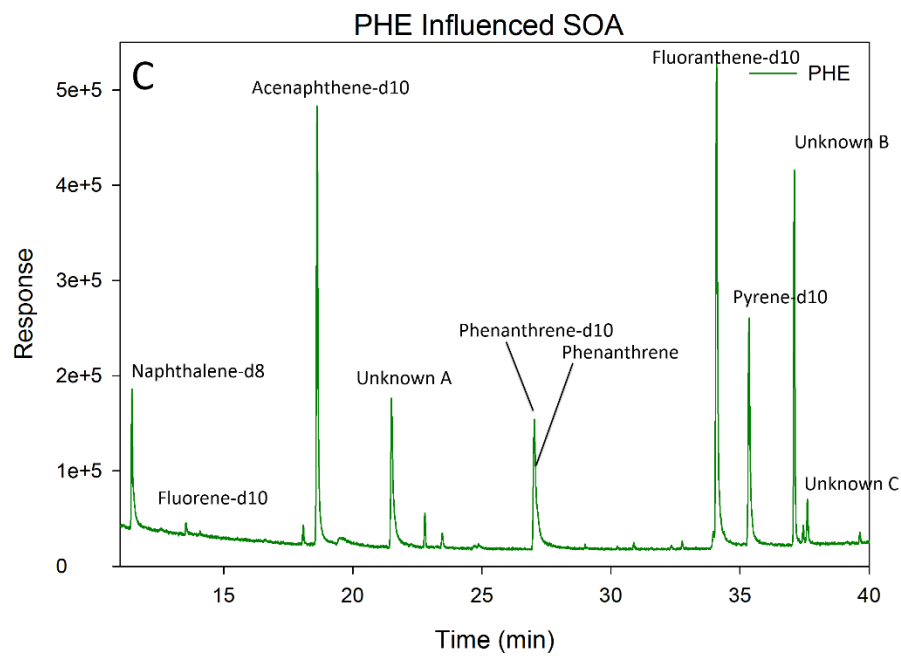
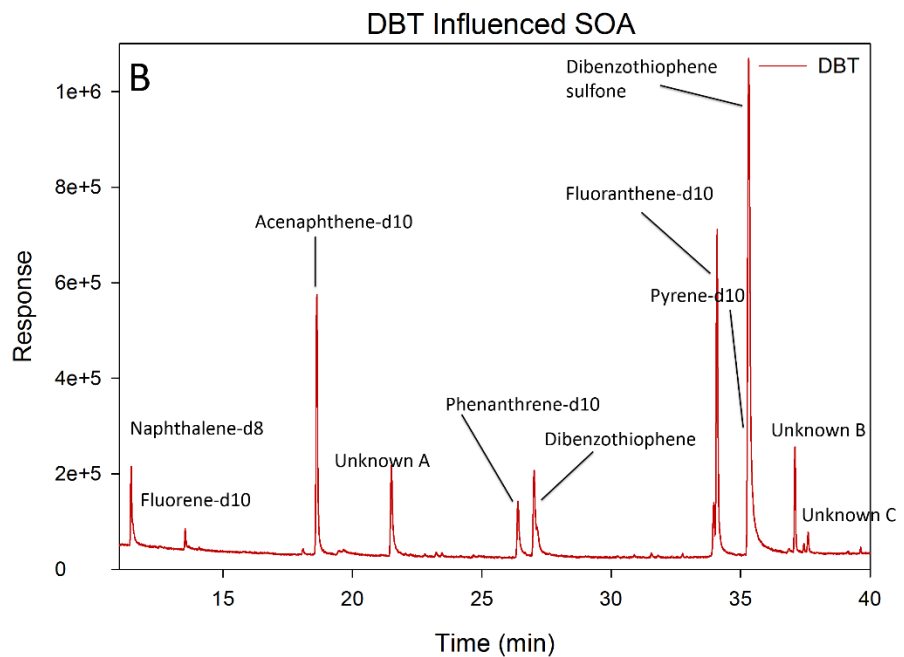
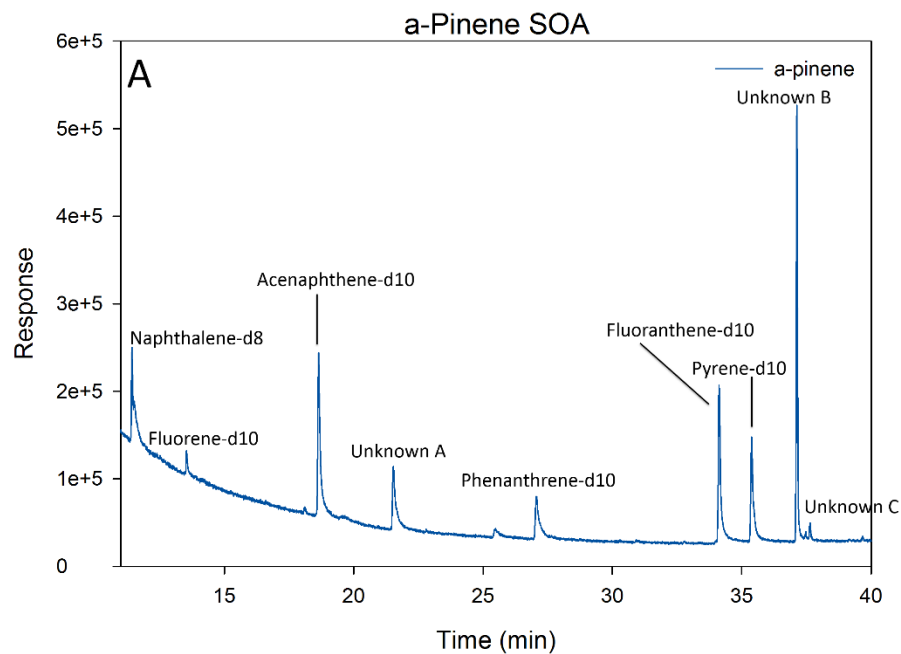


Table A1.T2. Comparison of average weight percent (\pm SE) for each for ozone exposure with two charcoal denuders inline before PAM reactor, and ozone exposure without denuders inline before the PAM reactor was performed using Students T-test. No statistical differences (p -value > 0.05) was found between ozone exposure with the use of charcoal denuders before PAM reactor or without. Table S2 shows p -values for measured PHE compounds (shaded in purple), DBT compounds (orange), and PYR compounds (blue).

Compound	PHE	9-OHPHE	Trans-9,10	1,9-OHPHE	DBT	DTBS	PYR	1-OHPYR	6H
w/ Denuders	0.79 % (\pm 0.40)	9.57% (\pm 4.77)	0.07 % (\pm 0.04)	10.10 % (\pm 5.91)	5.09 % (\pm 2.01)	2.85 % (\pm 0.95)	10.64 % (\pm 4.20)	9.84% (\pm 3.10)	0.88 % (\pm 0.40)
w/out Denuders	0.28 % (\pm 0.12)	2.97% (\pm 0.93)	0.02 % (\pm 0.02)	1.93% (\pm 1.07)	8.64 % (\pm 3.16)	1.72 % (\pm 0.10)	3.38% (\pm 2.30)	3.65% (\pm 0.20)	0.51 % (\pm 0.10)
p-value	0.374 3	0.2992	0.628 9	0.2993	0.406 0	0.354 8	0.2327	0.1805	0.312 3

Table A1.T3. Isotope labeled compounds used as internal and surrogate standards for quantification, the compounds each are used to quantify. Labeled compounds were purchased through Cambridge Isotope Laboratories.

Isotope Labeled	Used as	Used to quantify
Acenaphthene-d10	Internal Standard	Fluorene-d10 Naphthalene-d8 Phenanthrene-d10 1-hydroxynaphthalene-d8 4-hydroxyphenanthrene-13C4
Fluoranthene-d10	Internal Standard	Pyrene-d10 1-hydroxypyrene-d9
Naphthalene-d8	Surrogate	α -pinene verbanol verbenone
Benzo(k)fluoranthene-d12	Internal Standard	1-hydroxybenz(a)anthracene-13C6
9-fluorenone-d8	Internal Standard	Anthraquinone-d8
Fluorene-d10	Surrogate	DBT DBTS
Penanthrene-d10	Surrogate	PHE
Pyrene-d10	Surrogate	PYR
1-hydroxynaphthalene-d8	Surrogate	1-OHPHE 2-OHPHE 3-OHPHE 4-OHPHE 9-OHPHE
1-hydroxypyrene-9	Surrogate	1-OHPYR
1-hydroxybenz(a)anthracene-13C6	Surrogate	3-OHBaA
4-hydroxyphenanthrene-13C4	Surrogate	<i>cis</i> -9,10-OHPHE <i>trans</i> -9,10-OHPHE 1,9-OHPHE
Anthraquinone-d8	Surrogate	4H-CPP 6HBcdP 7,12-BaAO

Table A1.T4. Extraction recovery of acetone sonication extraction. Extraction was performed in triplicate and laboratory blank corrected by subtracting concentrations measured from the extraction of an unexposed QFF subjected to the same extraction process. Extraction was performed in 4 mL amber vials with 2 mL of acetone, analysis was performed using GC/MS methods detailed above.

Analyte	Average (\pm SE) Percent recovered
DBT	35 (3.8)
DBTS	46 (4.9)
PHE	39 (3.5)
PYR	46 (3.0)
BaA	42 (3.2)
4-OHPHE	103 (3.0)
9-OHPHE	105 (2.6)
3-OHPHE	81 (2.1)
1-OHPHE	86 (1.8)
2-OHPHE	74 (1.0)
<i>cis</i> -9,10-OHPHE	66 (2.9)
<i>trans</i> -9,10-OHPHE	70 (1.8)
1,9-OHPHE	36 (19.7)
1-OHPYR	117 (5.0)
3-OHBaA	88 (3.8)

A1.1 Detailed Methodology

A1.1.1 GC-MS Parameters.

An injection volume of 1 μL was used from a 10 μL syringe in an Agilent 7639 auto sampler. Syringes were cleaned with 3 pumps of 3 μL ethyl acetate and then 3 pumps of 3 μL acetone both before and after each injection.

Parent analysis. Inlet temperature was set to 300 $^{\circ}\text{C}$ in splitless mode with total flow of 21.4 mL/min. Septum purge flow was set to 1 mL/min and gas saver went to 50 after 2 min. The GC oven started at 60 $^{\circ}\text{C}$ for 1 minute, followed by a 6 $^{\circ}\text{C}/\text{min}$ ramp to 150 $^{\circ}\text{C}$ with a 2 minute hold. Then the ramp was changed to 4 $^{\circ}\text{C}/\text{min}$ up to 250 $^{\circ}\text{C}$, with another hold for 2 minutes. The final ramp was 12 $^{\circ}\text{C}/\text{min}$ up to 320 $^{\circ}\text{C}$, with a 5 minute hold time. Column flow was set to 0.4091 mL/min. Auxiliary MSD transfer line was set to 280 $^{\circ}\text{C}$. Mass spec source temperature was held at 230 $^{\circ}\text{C}$, and the quadrupole temperature was 150 $^{\circ}\text{C}$. A 4.8 minute solvent delay was employed to allow acetone to leave the system before the filaments fired up for detection. A 9-point calibration curve ranging from 1000 to 1 pg/ μL was used for quantification, and check standards within the calibration curve were run after every 10 samples to ensure stability of the system.

Mono-hydroxy PAH analysis. Inlet temperature was set to 300 $^{\circ}\text{C}$ in splitless mode with total flow of 23 mL/min. Septum purge flow was set to 1 mL/min and gas saver went to 50 after 2 min. The GC oven started at 60 $^{\circ}\text{C}$ for 1 minute, followed by an 8 $^{\circ}\text{C}/\text{min}$ ramp to 175 $^{\circ}\text{C}$, with a 1 minute hold.

The ramp was then changed to 3⁰C/min up to 275⁰C, with another hold for 1 minute. The final ramp was 7⁰C/min up to 320⁰C, with a 2 minute hold time. Column flow was set to 2 mL/min. Auxiliary MSD transfer line was set to 280⁰C. Mass spec source temperature was held at 230⁰C, and the quadrupole temperature was 150⁰C. An 8.5 minute solvent delay was employed to allow solvents to leave the system before the filaments fired up for detection. An 8-point calibration curve ranging from 1000 to 1 pg/μL was used for quantification, and check standards within the calibration curve were run after every 10 samples to ensure stability of the system.

Poly-hydroxy PAH analysis. Inlet temperature was set to 300⁰C in splitless mode with total flow of 22.5 mL/min. Septum purge flow was set to 1 mL/min and gas saver went to 36 after 0.75 min. The GC oven started at 60⁰C for 1 minute, followed by a 10⁰C/min ramp to 120⁰C, with no temperature hold. Then the ramp was changed to 2⁰C/min up to 210⁰C, with a hold for 1 minute. The final ramp was 10⁰C/min up to 320⁰C, with a 2 minute hold time. Column flow was set to 1.5 mL/min. Auxiliary MSD transfer line was set to 280⁰C. Mass spec source temperature was held at 230⁰C, and the quadrupole temperature was 150⁰C. A 12.0 minute solvent delay was employed to allow solvents to leave the system before the filaments fired up for detection. A 6-point calibration curve ranging from 750 to 1 pg/μL was used for quantification, and check standards within the calibration curve were run after every 10 samples to ensure stability of the system.

Oxy-PAH analysis. Inlet temperature was set to 40⁰C in splitless mode using liquid nitrogen cryo to achieve temperature, and increasing at 600⁰C/min to 350⁰C, with total flow of 21.9 mL/min. Septum purge flow was set to 1 mL/min and gas saver went to 65 after 1 min. The GC oven started at 60⁰C for 1 minute, followed by a 40⁰C/min ramp to 150⁰C, with a 5 minute hold. Then the ramp was changed to 4⁰C/min up to 265⁰C, with no old. The final ramp was 40⁰C/min up to 320⁰C, with a 5 minute hold time. Column flow was set to 0.91 mL/min. Auxiliary MSD transfer line was set to 300⁰C. Mass spec source temperature was held at 230⁰C, and the quadrupole temperature was 150⁰C. A 4.75 minute solvent delay was employed to allow acetone to leave the system before the filaments fired up for detection. A 9-point calibration curve ranging from 1000 to 1 pg/ μ L was used for quantification, and check standards within the calibration curve were run after every 10 samples to ensure stability of the system.

A1.1.2 Real-time In-Situ Characterization

Scanning Mobility Particle Sizer (SMPS) was performed by pairing differential mobility analyzer (DMA), TSI model 3080, to Ultra-fine condensation particle counter (CPC), TSI model 3786, to qualify and quantify particle number and size distributions. This allowed for mass loading measurements in each RTIS characterization step. Flow rate was set with TXI (Shoreview MN) 4100 series flow meter and pump. Single particle mass spectrometer (MiniSPLAT) was used to measure individual particle shape, density, and chemical fingerprint utilizing time-of-flight mass spectrometry.

Full detailed method descriptions can be found in manuscript references 15 and 18.

A1.1.3 Sample aliquots

For parent analysis, 250 μL of the filter extracts were transferred to 500 μL glass inserts in amber GC vials. Internal standards were added for a final concentration of 500 $\text{pg}/\mu\text{L}$, and the final volume was adjusted to 300 μL . Hydroxy aliquots were prepared in 300 μL spring insert in amber GC vials. 100 μL of acetonitrile, 20 μL of toluene, and internal standards (final concentration 500 $\text{pg}/\mu\text{L}$) were added to 50 μL of filter extracts and the volume was concentrated to 20 μL total. 30 μL of the appropriate derivatizing agent was added and aliquots were incubated before GC-MS analysis. Oxy analysis was performed by transferring 270 μL of the filter extracts into 500 μL glass inserts in amber GC vials. Internal standards (final concentration 500 $\text{pg}/\mu\text{L}$) were added and volume was corrected to 300 μL with acetone. Both SIM and full scan analysis was performed on the *Parent*, *mono-hydroxy*, and *poly-hydroxy* prepared aliquots to assess if unidentified peaks were present in each derivatization method.

A1.1.4 Phenanthrene standard purity testing

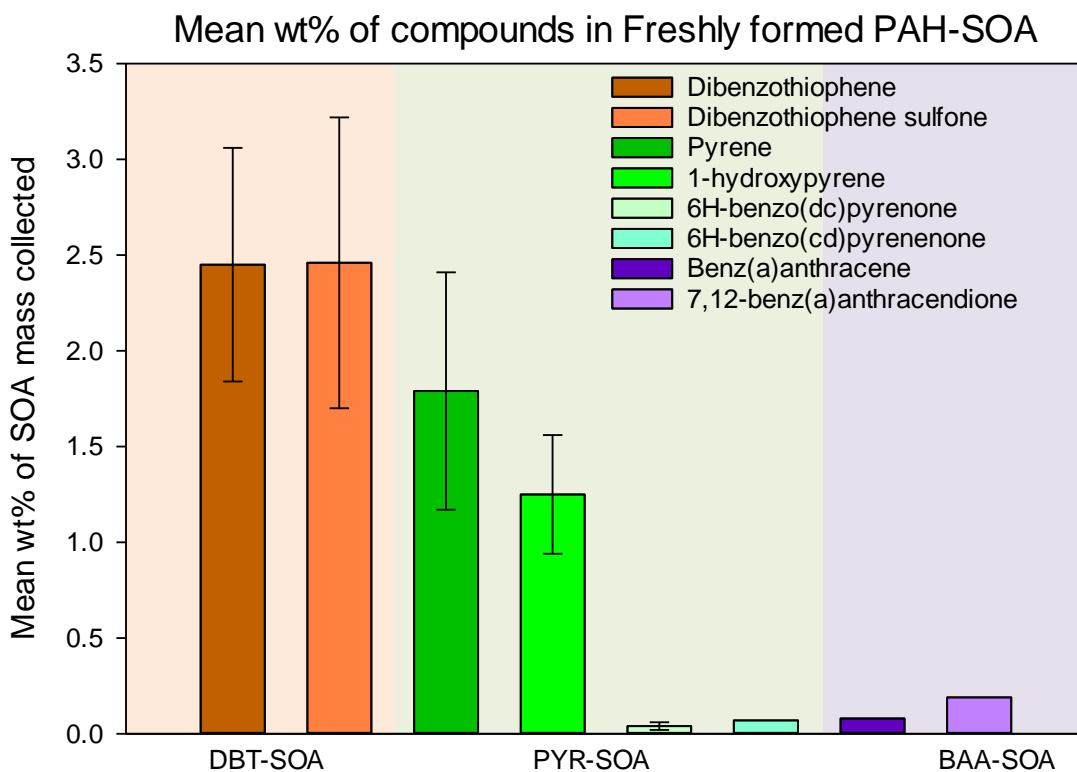
In all of the PHE PAH-SOA samples, both DBT and the oxidation product of DBT (dibenzothiophene sulfone - DBTS) were detected. To determine if DBT was somehow being produced in the PAH-SOA or was present in the PHE standard used, 1.66 mg of the standard PHE was dissolved in acetone and analyzed. DBT was found to be 0.0054 mg, or

roughly 0.003% of the PHE mass. This impurity in the standard explains the presence of DBT and DBTS on the PHE PAH-SOA filters, as the DBT with a higher vapor pressure than the PHE would have volatilized along with the PHE, been incorporated into the growing PAH-SOA, and oxidized along with the PHE at a much smaller w/w% of the PAH-SOA. Measured DBT and DBTS amounts were then subtracted out and not included in the analysis of PHE and PHE-OPs.

A1.1.5 Sonication Extraction Efficiency

Extraction efficiency was determined by spiking mixtures of analytes dissolved in acetone onto clean QFF in 4 mL amber vials, then adding 2 mL of solvent and sonicating for 60 minutes at room temperature. Solvents tested included a 1:1 mixture of dichloromethane and acetone, ethyl acetate, and acetone. Extracts were analyzed and the highest average recovery solvent across tested analytes was acetone with individual results listed in Table S3.

Figure A1.F2. Mean wt% (± 1 standard error) of compounds measured in collected *freshly* formed PAH-SOA. DBT influenced SOA contained equal wt% of DBT and DBTS (left-hand panel), PYR influenced SOA (c panel) had equal parts OPs with PYR, and BaA influenced SOA (right-hand panel) was measured to have more OP in the one measurable sample.



A1.2.1 Vapor phase PAH concentration Calculations.

Experimental values for PAH vapor pressure at 25°C, were obtained using EpiSuite (USEPA v. 4.1) (Table S1). To estimate the saturation vapor pressure of each parent PAH under laboratory conditions with room-temperature of 20±2°C, the Clausius-Clapeyron equation (equation 1) was used. Enthalpy of sublimation for each compound was obtained through a NIST database search with the most recent entry from experimentation used, though all entries were found around 300°C which could add some error. Gas constant R was used in the Joules/mol*K format (8.3145 J/mol*K).

Equation A1.1.1:

$$\ln\left(\frac{P_1}{P_2}\right) = \frac{\Delta H_{sub}}{R} * \left(\frac{1}{T_2} - \frac{1}{T_1}\right)$$

Table A1.T5. Parent PAH enthalpy of sublimation measurements listed on NIST.GOV, subcooled liquid vapor pressures at 25°C obtained through EPISUITE 4.1 search, and calculated subcooled liquid vapor pressures at 20°C.

Parent PAH	ΔH_{sub} obtained on webbook.nist.gov (KJ/mol)	EpiSuite vapor pressure at 25°C (Pa)	Calculated vapor pressure at 20°C (Pa)
Phenanthrene	92.1	1.61×10^{-2}	8.54×10^{-3}
Dibenzothiophene	91.2	2.73×10^{-2}	1.46×10^{-2}
Pyrene	103.3	6.00×10^{-4}	2.95×10^{-4}
Benz(a)anthracene	115.5	2.80×10^{-5}	1.26×10^{-5}

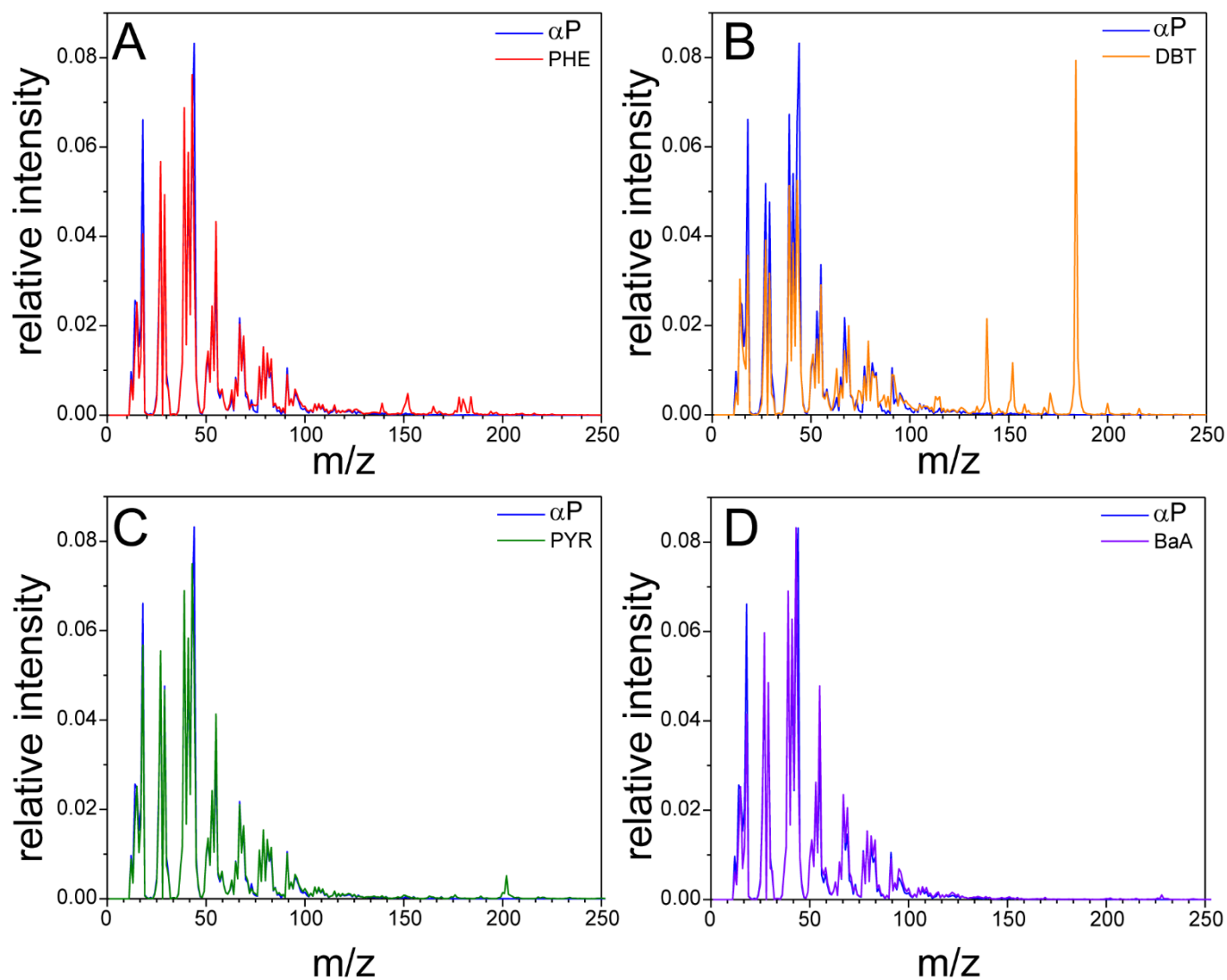
Because there was a significant amount of residual solid PAH left in each bag, saturation of vapor-phase PAH was assumed. Using the ideal gas

law and the newly calculated vapor pressure of each PAH, and assuming standard conditions in each ~70 L Teflon bag, the mixing ratio (ppb) of each PAH was estimated:

Table A1.T6. Parent PAH vapor pressure (atm), and calculated mixing ratios (ppb).

Parent PAH	P_2(atm)	Concentration (ppb)
Phenanthrene	8.43×10^{-8}	84.3
Dibenzothiophene	1.44×10^{-7}	144
Pyrene	2.91×10^{-9}	2.91
Benz(a)anthracene	1.25×10^{-10}	0.125

Figure A1.F3. Linear scaled High Resolution Time of Flight Aerosol Mass Spectrometer (HR-ToF-AMS) spectra for each PAH used in study. Linear scale illustrates the increases in peak signature observed in the α -P SOA (blue plot on each graph) to each PAH (A-D color plots).



Appendix 2

CHAPTER 3 SUPPORTING INFORMATION

**Impact of Local and Regional Sources of PAHs on Tribal
Reservation Air Quality in the U.S. Pacific Northwest**

Amber L. Kramer_{a,b}, Larry Campbell_c, Jamie Donatuto_c, Myk Heidt_c, Molly
Kile_d, Staci L. Massey Simonich_{a,b}¹

a – Oregon State University Department of Chemistry, Corvallis OR

b – Oregon State University Department of Environmental and Molecular
Toxicology, Corvallis OR

c – Swinomish Indian Tribal Community, La Caonner WA

d - Oregon State University School of Biological and Population Health
Sciences, Corvallis OR

¹ Corresponding Author: Phone (541) 737-9194; fax: (541) 737-0497; e-mail:
staci.simonich@oregonstate.edu

Table A2.T1. List of all analytes quantified in this study. Table includes chemical name, CAS number, molecular mass, abbreviation, main emission source to the atmosphere (CR = Crude fossil fuels, COMB = Combustion byproduct, TP = Transformation Product), PAH subclass, and Method Detection Limit (MDL). Co-eluding compounds share an MDL value.

Compound name	CAS No.	AMU	Abbrev.	Source	PAH class	MDL (pg/u L)
Naphthalene	91-20-3	128.171	NAP	CR, CMB	UPAH	0.08
Acenaphthylene	208-96-8	152.196	ACY	CR, CMB	UPAH	0.05
Acenaphthene	83-32-9	154.212	ACN	CR, CMB	UPAH	0.09
Fluorene	86-73-7	166.223	FLO	CR, CMB	UPAH	0.13
Phenanthrene	85-01-8	178.234	PHE	CR, CMB	UPAH	0.07
Anthracene	120-12-7	178.234	ANT	CR, CMB	UPAH	0.07
Fluoranthene	206-44-0	202.256	FLN	CR, CMB	UPAH	0.06
Pyrene	129-00-0	202.256	PYR	CR, CMB	UPAH	0.06
Retene	483-65-8	234.336	RET	CR, CMB	UPAH	0.16
Benzo(c)fluorene	205-12-9	216.283	BcF	CR, CMB	UPAH	0.10
Benzo(a)anthracene	56-55-3	228.288	BaA	CR, CMB	UPAH	0.06
Chrysene	218-01-9	228.294	Cry	CR, CMB	UPAH	0.06
Triphenylene	217-59-4	228.294	Tri	CR, CMB	UPAH	
Benzo(b)fluoranthene	205-99-2	252.309	BbF	CR, CMB	UPAH	0.05
Benzo(k)fluoranthene	207-08-9	252.309	BkF	CR, CMB	UPAH	0.06
Benz(e)pyrene	192-97-2	252.316	BeP	CR, CMB	UPAH	0.06
Benzo(a)pyrene	50-32-8	252.316	BaP	CR, CMB	UPAH	0.08
Dibenz(a,h)anthracene	53-70-3	278.347	DahA	CR, CMB	UPAH	0.02
Dibenz(a,c)anthracene	215-58-7	278.347	DacA	CR, CMB	UPAH	
Indeno(1,2,3-cd)pyrene	193-39-5	276.331	IcdP	CR, CMB	UPAH	0.06
Benzo(ghi)perylene	191-24-2	276.338	BghiP	CR, CMB	UPAH	0.06
Picene	213-46-7	278.347	PIC	CR, CMB	HMW	53.90
Naphtho[1,2-b]fluoranthene	111189-32-3	302.376	N1,2-bF	CR, CMB	HMW	1.20
Naphtho[2,3-j]fluoranthene	205-83-4	302.376	N2,3-jF	CR, CMB	HMW	1.10
Naphtho[1,2-k]fluoranthene	238-04-0	302.376	N1,2-kF	CR, CMB	HMW	1.30
Naphtho[2,3-b]fluoranthene	206-06-4	302.376	N2,3-bF	CR, CMB	HMW	
Dibenzo[a,e]fluoranthene	5385-75-1	302.376	DaeF	CR, CMB	HMW	1.00
Dibenzo[b,k]fluoranthene	205-97-0	302.376	DbkF	CR, CMB	HMW	1.50
Dibenzo[a,k]fluoranthene	84030-79--5	302.376	DakF	CR, CMB	HMW	
Dibenzo[j,l]fluoranthene	203-18-9	302.368	Djlf	CR, CMB	HMW	1.10
Dibenzo[a,l]pyrene	191-30-0	302.376	DalP	CR, CMB	HMW	1.60
Naphtho[2,3-k]fluoranthene	207-18-1	302.376	N2,3-kF	CR, CMB	HMW	1.50
Naphtho[2,3-e]pyrene	193-09-9	302.376	N2,3-eP	CR, CMB	HMW	1.50
Dibenzo[a,e]pyrene	192-65-4	302.367	DaeP	CR, CMB	HMW	1.20
Coronene	191-07-1	300.36	COR	CR, CMB	HMW	1.10
Dibenzo[a,i]pyrene	189-55-9	302.367	DaiP	CR, CMB	HMW	2.20
Dibenzo[a,h]pyrene	189-64-0	302.367	DahP	CR, CMB	HMW	2.60
1-nitronaphthalene	86-57-7	173.171	1NNap	CMB, TP	NPAH	0.30
2-nitronaphthalene	581-89-5	173.171	2NNap	CMB, TP	NPAH	0.30
2-nitrobiphenyl	86-00-0	199.209	2NBP	CMB, TP	NPAH	0.30
3-nitrobiphenyl	2113-58-8	199.209	3NBP	CMB, TP	NPAH	0.30
4-nitrobiphenyl	92-93-3	199.209	4NBP	CMB, TP	NPAH	2.20
3-nitrodibenzofuran	5410-97-9	214.192	3NDBF	CMB, TP	NPAH	1.40
5-nitroacenaphthene	602-87-9	199.209	5NAcn	CMB, TP	NPAH	1.40
2-nitrofluorene	607-57-8	211.220	2NFlo	CMB, TP	NPAH	0.90
9-nitroanthracene	602-60-8	223.231	9NAnt	CMB, TP	NPAH	0.50
9-nitrophenanthrene	954-46-1	223.231	9NPhe	CMB, TP	NPAH	0.50
2-nitrodibenzothiophene	6639-36-7	229.253	2NDBT	CMB, TP	NPAH	0.50
3-nitrophenanthrene	17024-19-0	223.231	3NPhe	CMB, TP	NPAH	0.80
2-nitrofluoranthene	13177-29-2	247.253	2NFln	CMB, TP	NPAH	0.60
3-nitrofluoranthene	892-21-7	247.253	3NFln	CMB, TP	NPAH	

1-nitropyrene	5522-43-0	247.253	1NPyr	CMB, TP	NPAH	0.50
2,8-dinitrodibenzothiophene	109041-38-5	274.25	28NDBT	CMB, TP	NPAH	6.10
7-nitrobenz[a]anthracene	20268-51-3	273.291	7NBaA	CMB, TP	NPAH	1.00
6-nitrochrysene	7496-02-8	273.291	6NCry	CMB, TP	NPAH	0.70
3-nitrobenzanthrone	17117-34-9	275.263	3NBZN	CMB, TP	NPAH	2.90
1,3-dinitropyrene	75321-20-9	292.25	13NPyr	CMB, TP	NPAH	2.90
1,6-dinitropyrene	42397-64-8	292.25	16NPyr	CMB, TP	NPAH	4.00
1,8-dinitropyrene	42397-65-9	292.25	18NPyr	CMB, TP	NPAH	11.20
6-nitrobenzo(a)pyrene	63041-90-7	297.313	6NBaP	CMB, TP	NPAH	1.90
p-benzoquinone	106-51-4	108.096	BZQ	CMB, TP	OPAH	1.00
1,4-naphthoquinone	130-15-4	158.156	14NapQ	CMB, TP	OPAH	13.20
1,2-naphthoquinone	524-42-5	158.156	12NapQ	CMB, TP	OPAH	1.50
2,3-benzo-4-pyrone (chromone)	491-38-3	146.145	Chro	CMB, TP	OPAH	0.80
9,10-anthraquinone	84-65-1	208.216	910AntQ	CMB, TP	OPAH	2.10
1,4-phenanthrenedione	569-15-3	208.216	14PheONE	CMB, TP	OPAH	
9-fluorenone	486-25-9	180.206	9FIONE	CMB, TP	OPAH	8.80
xanthone	90-47-1	196.19	XONE	CMB, TP	OPAH	0.50
perinaphthenone	548-39-0	180.206	PNap	CMB, TP	OPAH	1.40
1,4-anthraquinone	635-12-1	208.216	1,4AntQ	CMB, TP	OPAH	9.70
Acenaphthalenquinone	82-86-0	182.178	AcnQ	CMB, TP	OPAH	3.50
1,2-acenaphthalindione	82-86-0	182.175	1,2AcyONE	CMB, TP	OPAH	
4H-cyclopenta[def]phenanthrenone	5737-13-3	204.228	4HCdefP	CMB, TP	OPAH	0.30
2-methyl-9,10-anthraquinone	84-54-8	222.239	2-ME-AntQ	CMB, TP	OPAH	1.10
9,10-phenanthrenequinone	84-11-7	208.216	9,10-PheQ	CMB, TP	OPAH	3.40
2-ethyl-9,10-anthraquinone	84-51-5	236.27	2ETANTQ	CMB, TP	OPAH	1.00
benzo(a)fluorenone	116232-62-3	230.261	BAFONE	CMB, TP	OPAH	0.60
Benzanthrone	82-05-3	230.266	BZN	CMB, TP	OPAH	0.80
7,12-benz[a]anthracenequinone	2498-66-0	258.271	7,12-BaAQ	CMB, TP	OPAH	3.60
benzo[c]phenanthrone	Unknown	245.295	BcPhONE	CMB, TP	OPAH	
5,12-naphthacenequinone	1090-13-7	258.271	5,12-NapQ	CMB, TP	OPAH	1.70
6H-benzo(cd)pyren-6-one	3074-00-8	245.288	6HBPONE	CMB, TP	OPAH	0.70
aceanthrenequinone	6373-11-1	232.23	AcyAntQ	CMB, TP	OPAH	6.50
1,6-benzo(a)pyrendione	3067-13-8	282.298	16-BaPONE	CMB, TP	OPAH	0.30
3,6-benzo(a)pyrendione	3067-14-9	282.298	36-BaPONE	CMB, TP	OPAH	0.10
1-Hydroxynaphthalene	90-15-3	144.173	1-OHNap	TP	OHPAH	0.10
2-Hydroxynaphthalene	135-19-3	144.173	2-OHNap	TP	OHPAH	0.10
2,3-Dihydroxynaphthalene	92-44-4	160.172	2,3-OHNap	TP	OHPAH	0.20
1,3-dihydroxynaphthalene	132-86-5	160.172	1,2-OHNap	TP	OHPAH	1.30
1,5-dihydroxynaphthalene	83-56-7	160.172	1,5-OHNap	TP	OHPAH	
1,6-Dihydroxynaphthalene	575-44-0	160.172	1,6-OHNap	TP	OHPAH	0.10
2,7-Dihydroxynaphthalene	582-17-2	160.172	2,7-OHNap	TP	OHPAH	0.10
2,6-Dihydroxynaphthalene	581-43-1	160.172	2,6-OHNap	TP	OHPAH	0.10
4-Hydroxyphenanthrene	7651-86-7	194.233	4-OHPhe	TP	OHPAH	0.10
9-Hydroxyphenanthrene	484-17-3	194.233	9-OHPhe	TP	OHPAH	0.10
3-Hydroxyphenanthrene	605-87-8	194.233	3-OHPhe	TP	OHPAH	0.10
1-Hydroxyphenanthrene	2433-56-9	194.233	1-OHPhe	TP	OHPAH	0.10
2-Hydroxyphenanthrene	605-55-0	194.233	2-OHPhe	TP	OHPAH	0.10
2-Hydroxyanthraquinone	605-32-3	224.215	2-OHAntQ	TP	OHPAH	5.20
3-Hydroxyfluoranthene	17798-09-3	218.255	3-OHFln	TP	OHPAH	0.10
9-Hydroxyfluorene	1689-64-1	182.222	9-OHFlo	TP	OHPAH	0.30
3-Hydroxyfluorene	6344-67-8	182.222	3-OHFlo	TP	OHPAH	0.10
2-Hydroxyfluorene	2443-58-5	182.222	2-OHFlo	TP	OHPAH	0.10
1-Hydroxy-9-fluorenone	6344-60-1	196.205	1-OH9Flone	TP	OHPAH	0.02

2-Hydroxy-9-fluorenone	6949-73-1	196.205	2-OH9Flone	TP	OHPAH	0.10
1-Hydroxypyrene	5315-79-7	218.255	1-OHPyp	TP	OHPAH	0.10
3-Hydroxybenzo(a)anthracene	4834-35-9	244.293	3-OHBaA	TP	OHPAH	0.10
3-Hydroxybenzo(c)phenanthrene	22717-95-9	244.293	3-OHBcP	TP	OHPAH	1.50
10-Hydroxybenzo(a)pyrene	56892-31-0	268.315	10-OHBaP	TP	OHPAH	0.10
12-Hydroxybenzo(a)pyrene	56892-33-2	268.315	12-OHBaP	TP	OHPAH	0.20
7-Hydroxybenzo(a)pyrene	37994-82-4	268.315	7-OHBaP	TP	OHPAH	0.10
9-Hydroxybenzo(a)pyrene	17573-21-6	268.315	9-OHBaP	TP	OHPAH	0.10
3-Hydroxybenzo(e)pyrene	77508-02-2	268.315	3-OHBeP	TP	OHPAH	
3-Hydroxybenzo(a)pyrene	13345-21-6	268.315	3-OHBaP	TP	OHPAH	0.20
1-Hydroxyindeno[1,2,3-c,d]pyrene	99520-65-7	292.337	1-OHlcdP	TP	OHPAH	0.70
4-Hydroxychrysene	63019-40-9	244.293	4-OHCry	TP	OHPAH	0.30
6-Hydroxychrysene	37515-51-8	244.293	6-OHCry	TP	OHPAH	0.30
3-Hydroxychrysene	63019-39-6	244.293	3-OHCry	TP	OHPAH	0.30
11-Hydroxybenzo(b)fluoranthene	Unknown	269.316	11-OHBbF	TP	OHPAH	0.40
9-Hydroxybenzo(k)fluoranthene	Unknown	269.316	9-OHBkF	TP	OHPAH	0.50
11-Hydroxybenzo(g)chrysene	Unknown	294.307	11-OHBgC	TP	OHPAH	0.40
10-Hydroxybenzo(c)chrysene	Unknown	294.307	10-OHBcC	TP	OHPAH	0.70
2-Methylbenzofuran	4265-25-2	132.162	2-Me-BZF	CR, CMB	HPAH	0.15
Thianaphthene (benzothiophene)	95-15-8	134.196	TNAP	CR, CMB	HPAH	0.12
Quinoline	91-22-5	129.162	QUIN	CR, CMB	HPAH	0.13
Dibenzofuran	132-64-9	168.195	DBF	CR, CMB	HPAH	0.08
Indole	120-72-9	117.151	IND	CR, CMB	HPAH	0.14
8-Methylquinoline	611-32-5	143.189	8-Me-Qu	CR, CMB	HPAH	0.12
Xanthene	92-83-1	182.222	XAN	CR, CMB	HPAH	0.09
Acridine	260-94-6	179.222	ACR	CR, CMB	HPAH	0.10
5,6-benzoquinoline	85-02-9	179.222	5,6-BQ	CR, CMB	HPAH	0.14
Carbazole	86-74-8	167.211	CARB	CR, CMB	HPAH	0.08
Dibenzothiophene	132-65-0	184.256	DBT	CR, CMB	HPAH	0.09
Dibenzothiophene sulfone	1016-05-3	216.254	DBTS	CR, CMB	HPAH	0.04

A2.1 Detailed GC-MS Parameters

An injection volume of 1 μL was used from a 10 μL syringe in an Agilent 7639 auto sampler. Syringes were cleaned with 3 pumps of 3 μL acetone and then 3 pumps of 3 μL ethyl acetate both before and after each injection.

UPAH analysis. Inlet temperature was set to 300 $^{\circ}\text{C}$ in splitless mode with total flow of 21.9 mL/min. Septum purge flow was set to 0.5 mL/min and gas saver went to 36 after 1 min. The GC oven started at 60 $^{\circ}\text{C}$ for 1 minute, followed by a 10 $^{\circ}\text{C}/\text{min}$ ramp to 150 $^{\circ}\text{C}$ with a 1-minute hold. The ramp then changed to 4 $^{\circ}\text{C}/\text{min}$ up to 226 $^{\circ}\text{C}$, then switching to 2 $^{\circ}\text{C}/\text{min}$ up to 244 $^{\circ}\text{C}$, and then back to 4 $^{\circ}\text{C}/\text{min}$ to 264 $^{\circ}\text{C}$. A 2 $^{\circ}\text{C}/\text{min}$ ramp then went to 284 $^{\circ}\text{C}$ followed by a final 10 $^{\circ}\text{C}/\text{min}$ to 320 $^{\circ}\text{C}$ with a 1-minute hold. Column flow was set to 1.2 mL/min. Auxiliary MSD transfer line was set to 300 $^{\circ}\text{C}$. Mass spec source temperature was held at 230 $^{\circ}\text{C}$, and the quadrupole temperature was 150 $^{\circ}\text{C}$. A 7-minute solvent delay was employed to allow ethyl acetate to leave the system before the filaments fired up for detection. A 9-point calibration curve ranging from 1000 to 1 pg/ μL was used for quantification, and check standards within the calibration curve were run after every 10 samples to ensure stability of the system.

OHPAH analysis. Inlet temperature was set to 280 $^{\circ}\text{C}$ in splitless mode with total flow of 52.2 mL/min. Septum purge flow was set to 1 mL/min and gas saver went to 35 after 2.25 min. The GC oven started at 70 $^{\circ}\text{C}$ for 1 minute, followed by an 4 $^{\circ}\text{C}/\text{min}$ ramp to 250 $^{\circ}\text{C}$. The ramp then changed to 2 $^{\circ}\text{C}/\text{min}$ up to 280 $^{\circ}\text{C}$, and finished with a ramp of 30 $^{\circ}\text{C}/\text{min}$ up to 320 $^{\circ}\text{C}$, with

a 6-minute hold time. Column flow was set to 1.3 mL/min. Auxiliary MSD transfer line was set to 280⁰C. Mass spec source temperature was held at 230⁰C, and the quadrupole temperature was 150⁰C. A 10-minute solvent delay was employed to allow solvents to leave the system before the filaments fired up for detection. An 9-point calibration curve ranging from 1000 to 1 pg/μL was used for quantification, and check standards within the calibration curve were run after every 10 samples to ensure stability of the system.

OPAH analysis. Inlet temperature was set to 40⁰C in splitless mode using liquid nitrogen cryo to achieve temperature, and increasing at 600⁰C/min to 350⁰C, with total flow of 22.1 mL/min. Septum purge flow was set to 1 mL/min and gas saver went to 65 after 1 min. The GC oven started at 60⁰C for 1 minute, followed by a 30⁰C/min ramp to 120⁰C, with a 1-minute hold. Then the ramp was changed to 3⁰C/min up to 250⁰C, with no old. The ramp then changed to 2⁰C/min up to 256⁰C, with a final 30⁰C/min ramp to 320⁰C with a 3-minute hold time. Column flow was set to 1.1 mL/min.

Auxiliary MSD transfer line was set to 300⁰C. Mass spec source temperature was held at 230⁰C, and the quadrupole temperature was 150⁰C. A 4-minute solvent delay was employed to allow solvents to leave the system before the filaments fired up for detection. An 8-point calibration curve ranging from 1000 to 1 pg/μL was used for quantification, and check standards within the calibration curve were run after every 10 samples to ensure stability of the system.

NPAH analysis. Inlet temperature was set to 40⁰C in splitless mode using liquid nitrogen cryo to achieve temperature, and increasing at 600⁰C/min to 350⁰C, with total flow of 507.1 mL/min. Septum purge flow was set to 503 mL/min and gas saver went to 20 after 2 min. The GC oven started at 60⁰C for 1 minute, followed by a 40⁰C/min ramp to 150⁰C, with a 5-minute hold. Then the ramp was changed to 4⁰C/min up to 300⁰C, with a 6-minute hold. Column flow was set to 1.1 mL/min. Auxiliary MSD transfer line was set to 300⁰C. Mass spec source temperature was held at 150⁰C, and the quadrupole temperature was 150⁰C. An 8-minute solvent delay was employed to allow ethyl acetate to leave the system before the filaments fired up for detection. A 7-point calibration curve ranging from 500 to 1 pg/ μ L was used for quantification, and check standards within the calibration curve were run after every 10 samples to ensure stability of the system.

HPAH analysis. Inlet temperature was set to 300⁰C in splitless mode with total flow of 21.2 mL/min. Septum purge flow was set to 0.5 mL/min and gas saver went to 36 after 1 min. The GC oven started at 60⁰C for 1 minute, followed by a 6⁰C/min ramp to 230⁰C, followed by a ramp of 25⁰C/min up to 300⁰C, with a 1-minute hold. Column flow was set to 0.49 mL/min. Auxiliary MSD transfer line was set to 280⁰C. Mass spec source temperature was held at 230⁰C, and the quadrupole temperature was 150⁰C. A 7-minute solvent delay was employed to allow ethyl acetate to leave the system before the filaments fired up for detection. A 9-point calibration curve ranging from 1000 to 1 pg/ μ L was used for quantification, and check standards within the

calibration curve were run after every 10 samples to ensure stability of the system.

HMW analysis. Inlet temperature was set to 260⁰C in splitless mode with total flow of 22.2 mL/min. Septum purge flow was set to 2 mL/min and gas saver went to 15 after 0.75 min. The GC oven started at 100⁰C for 1 minute, followed by a 40⁰C/min ramp to 200⁰C. Then the ramp changed to 2⁰C/min up to 310⁰C, with a 58-minute. The final ramp was 45⁰C/min up to 320⁰C, with a 6-minute hold time. Column flow was set to 1.1 mL/min.

Auxiliary MSD transfer line was set to 300⁰C. Mass spec source temperature was held at 230⁰C, and the quadrupole temperature was 150⁰C. A 50-minute solvent delay was employed to allow ethyl acetate to leave the system before the filaments fired up for detection. A 7-point calibration curve ranging from 1000 to 1 pg/ μ L was used for quantification, and check standards within the calibration curve were run after every 10 samples to ensure stability of the system.

A2.2 Derivatization of Hydroxy PAHs

Due to low volatility of hydroxy substituted PAHs, derivatization to increase volatility is required for gas phase analysis. This process includes *flooding* an aliquot of the sample with MTBSFTA (N-tert-Butyldimethylsilyl-N-methyltrifluoroacetamide), and incubating at 65°C for 25 minutes just prior to GC/MS analysis. To accomplish this, 50 μL of extracts were spiked with internal standards, and concentrated under fine nitrogen stream to 20 μL . Then 30 μL of MTBSTFA was added to the sample and vortexed to fully mix before incubation.

Table A2.T2. PAHs with significant (p-value < 0.05) changes measured between low (< 20% of the sampling time) and high (> 80% of the sampling time), winds coming from labeled direction. * indicates that for the wind coming from the NW, the high measurements were > 70% of the sampling time, to have a large enough number of samples to run statistical analysis. Numbers in red indicate significant decreases, and numbers in green indicate significant increases.

COMPOUND(S) NAME	FENCE			TOWN		
	NW	SW	SE	NW	SW	SE
ACENAPHTHYLENE	-72.6%	-64.7%		-69.5%		
PHENANTHRENE				-80.7%		
FLUORANTHENE		-90.4%			-86.8%	
PYRENE		-87.4%				
RETENE		-87.9%		-73.6%	-81.2%	
BENZ(C)FLUORENE		-90.4%			-89.0%	
BENZO(A)ANTHRACENE		-96.4%			-98.7%	
CHRYSENE & TRIPHENYLENE		-94.1%			-94.1%	
BENZO(B)FLUORANTHENE		-96.2%			-96.6%	
BENZO(K)FLUORANTHENE		-97.6%			-97.3%	
BENZ(E)PYRENE		-95.6%			-96.2%	
BENZO(A)PYRENE		-96.1%			-96.2%	
DIBENZ[A,H] & [A,C]ANTHRACENE		-96.8%			-78.1%	
INDENO(1,2,3-CD)PYRENE		-95.0%			-94.0%	
BENZO(GHI)PERYLENE		-93.3%			-93.0%	
Σ UPAHS		-90.8%			-87.2%	
1,4-NAPHTHOQUINONE			-65.4%			
1,2-NAPHTHOQUINONE			-89.8%	-99.6%		-90.4%
CHROMONE		52.2%				
9,10-ANTHRAQUINONE & 1,4-PHENANTHRENE DIONE			-65.4%			
9-FLUORENONE			-85.6%	-97.3%		-65.7%
PERINAPHTHENE		-70.9%				
1,4-ANTHRAQUINONE			-86.6%	-84.0%	314.3%	-79.5%
ACENAPHTHALENQUINONE & 1,2-ACENAPHTHALYNE DIONE				-91.0%		
2-METHYL-9,10-ANTHRAQUINONE				-66.1%		
9,10-PHENANTHRENEQUINONE			-91.0%	-97.3%	465.3%	-90.2%
2-ETHYL-9,10-ANTHRAQUINONE		-91.4%			-94.5%	
BENZO(A)FLUORENONE		-96.4%			-97.9%	
BENZANTHRONE		-90.5%			-89.6%	
7,12-BENZ[A]ANTHRACENEQUINONE + BENZO[C]FLUORENONE			-70.5%			
6H-BENZO(CD)PYREN-6-ONE				-76.9%		
ACEANTHRENEQUINONE			-89.3%	-92.7%		-70.0%
Σ OPAHS			-69.3%			-55.0%
3-NITROBIPHENYL	-96.3%					
9-NITROPHENANTHRENE					-97.3%	
2,8-DINITRODIBENZOTHIOPHENE		-71.8%		-77.5%	-73.2%	
7-NITROBENZ[A]ANTHRACENE		-73.0%				
6-NITROCHRYSENE		-88.6%			-89.5%	

3-NITROBENZANTHRONE		-97.0%		-97.3%
1,3-DINITROPYRENE		-98.4%		-98.4%
1,6-DINITROPYRENE		-92.0%	-74.8%	-95.0%
1,8-DINITROPYRENE		-87.6%		-91.6%
6-NITROBENZO(A)PYRENE		-97.0%		
Σ NPAHS		-75.8%		-80.0%
PICENE		-89.9%		-92.5%
NAPHTHO[1,2-B]FLUORANTHENE				-87.7%
NAPHTHO[2,3-J]/[1,2-K]FLUORANTHENE		-82.2%		-47.4%
NAPHTHO[2,3-B]FLUORANTHENE		-88.6%		-79.4%
DIBENZO[A,E] & [B,K]FLUORANTHENE				-57.7%
DIBENZO[A,K]FLUORANTHENE	-67.3%	-72.4%	-77.8%	-76.0%
DIBENZO[J,L]FLUORANTHENE		-92.3%		-89.6%
DIBENZO[A,L]PYRENE				-64.4%
NAPHTHO[2,3-E]PYRENE		-76.8%		-87.1%
DIBENZO[A,E]PYRENE		-90.5%		-89.7%
CORONENE	-57.4%	-84.4%		-85.6%
DIBENZO[A,I]PYRENE		-59.2%	-68.4%	
Σ HMWS		-86.7%		-87.9%
2-METHYLBENZOFURAN				-79.4%
THIANAPHTHENE		-41.2%		
DIBENZOFURAN	-98.1%			
DIBENZOTHIOPHENE			-79.0%	
DIBENZOTHIOPHENE SULFONE	-88.2%	-89.0%		
INDOLE		-97.7%	-84.1%	
8-METHYLQUINOLINE				-76.6%
XANTHENE			-77.1%	
ACRIDINE		-72.9%		-76.1%
Σ HPAHS				
1-HYDROXYNAPHTHALENE			-74.2%	-62.6%
2-HYDROXYNAPHTHALENE				-96.3%
1,6-DIHYDROXYNAPHTHALENE				-90.6%
2,7-DIHYDROXYNAPHTHALENE	-87.7%		-97.9%	-98.7%
2,6-DIHYDROXYNAPHTHALENE			222.6%	
4-HYDROXYPHENANTHRENE			-77.6%	
3-HYDROXYPHENANTHRENE		-69.9%	-98.2%	
1-HYDROXYPHENANTHRENE			-97.2%	
2-HYDROXYPHENANTHRENE			-92.4%	-82.8%
2-HYDROXYANTHRAQUINONE			-68.3%	-81.7%
9-HYDROXYFLUORENE		-41.8%		
3-HYDROXYFLUORENE				-66.7%
2-HYDROXYFLUORENE			140.1%	-65.8%
1-HYDROXY-9-FLUORENONE			-88.8%	

2-HYDROXY-9-FLUORENONE		-82.9%	
1-HYDROXYPYRENE		-86.6%	
3-HYDROXYBENZO(A)ANTHRACENE		131.7%	-69.7%
3-HYDROXYBENZO(C)PHENANTHRENE		-88.6%	-88.0%
12-HYDROXYBENZO(A)PYRENE			-64.9%
3-HYDROXYBENZO(A)PYRENE	-74.3%		
1-HYDROXYINDENO[1,2,3-C,D]PYRENE	-79.9%		-96.2%
4-HYDROXYCHRYSENE	-92.3%		
3-HYDROXYCHRYSENE		-71.4%	-62.4%
Σ OHPAHS		-43.7%	-53.2%

Table A2.T3. Correlation results table. Atmospheric reactants and compounds with significant correlations with SE or SW wind direction are listed with slope value, intercept value and p-value. NW and NE wind directions had less than 10 individual compound correlations for each location, therefore data not included. Ozone was negatively correlated with the NW wind at both locations

Measured Analyte pg/m ³ air sampled	SE winds						SW winds						
	Fence			Town			Fence			Town			
	Slope	Intercept	p-value	Slope	Intercept	p-value	Slope	Intercept	p-value	Slope	Intercept	p-value	
O ₃ (ppm)	0.0153	0.0221	0.0376	0.0187	0.0221	.00450							
NO ₂ (ppm)				-3.457	0.2657	.03330							
NO (ppm)				-1.767	1.9734	0.0474							
ACY	25.57	0.87	0.0024	23.14	8.96	0.0249							
FLO				7.71	1.90	0.0489							
FLN										-36.14	34.32	0.0124	
RET				91.95	15.16	0.0066							
BCF				6.85	1.63	0.0293							
BaA				33.72	7.38	0.0321							
CrTr				87.13	16.85	0.0284	-102.68	82.05	0.0474				
BbF				372.54	12.52	0.0079							
BkF				113.37	2.01	0.0065							
BeP				172.67	9.48	0.0146							
BaP				47.03	10.99	0.0406							
IcdP				171.65	9.68	0.0116							
BghiP				163.61	14.24	0.0137							
Pic				540.07	167.72	0.0051	-544.10	417.25	0.0038	-	539.50	510.71	0.0091
N1,2-bF							-8.33	8.85	0.0142	-9.19	9.92	0.0006	
N2,3-j/1,3-kF							-17.96	22.40	0.0067	-13.04	23.51	0.0318	
N2,3-bF				4.97	4.03	0.0366	-8.11	8.21	0.0047	-8.09	8.21	0.0009	
DBae/bkF							-15.19	20.80	0.0119	-14.03	22.49	0.0127	
DBakF	3.49	0.41	0.0124	6.12	0.54	0.0002							
DBjlF				9.30	4.40	0.0095	-11.56	9.70	0.0018	-10.53	10.72	0.0056	
N2,3-eP							-8.80	7.73	0.0049	-7.91	8.48	0.0074	
DBaeP							-10.29	8.75	0.0023	-9.34	9.59	0.0031	
Cor	18.14	8.39	0.0287	20.94	7.88	0.0058	-27.78	23.80	0.0041	-20.87	21.16	0.0103	
DBaiP				3.72	2.41	0.0267							

1-NNap									8.12	6.00	0.0048
2-NNap						2.16	5.55	0.0017	3.08	5.64	0.0008
3-NDBF						-5.54	11.35	0.0047	-4.42	12.12	0.0138
2-NFlo						-23.45	22.74	0.0059	-20.29	19.52	0.0130
2&3-NFln	-6.09	16.01	0.0357			-1.32	13.70	0.0016	-1.97	12.40	0.0428
7-NBaA									-7.08	8.63	0.0160
1,3-NPyr	43.00	42.53	0.0323			-149.60	101.51	0.0043	-7.08	8.63	0.0210
BnzQ				-42.22	230.63	0.0398					
1,2-NapQ	-			-815	952.67	0.0118			596.75	506.88	0.0163
9,10-AntQ / 1,4- PheDlone	528.85	3.28	0.0430	58.48	101.14	0.0275	-176.50	272.59	0.0463		
Xan				55.02	56.55	0.0269					
Per									-39.18	51.13	0.0306
1,4-AntQ							659.33	158.00	0.0264	592.93	98.74
9,10-PheQ							535.13	63.15	0.0030	473.59	51.08
2-Et-9,10- AntQ	3.28	62.04	0.0131				-72.95	83.06	0.0195	-38.08	79.84
BaFone	85.26	20.67	0.0001	113.07	24.01	< 0E-4	-104.90	86.19	0.0223	-88.53	87.76
AceAntQ	-									245.94	49.57
3,6-BaPone	177.80	212.05	0.0276	8.97	1.81	0.0098					
2-OHNap							71.66	3.78	0.0070		
1,3- & 1,5- OHNap	-4.14	7.74	0.0312				4.77	4.64	0.0368		
1,6-OHNap										2.87	0.13
9-OHPhe	-30.38	26.88	0.0241								
3-OHFlo							13.98	2.30	0.0098		
2-OHFlo	-16.43	17.70	0.0158	-10.37	14.04	0.0466					
3-OHBaA							-4.02	5.02	0.0400	-5.02	5.61
3-OHBcP							5.49	-0.33	0.0057	1.87	0.24
12-OHBaP										-2.91	4.31
3-OHBaP							45.58	3.29	0.0064		
1-OHlcdP										-3.81	3.48
11-OHBbF				-5.93	18.81	0.0258				31.83	6.48
2-MeBzF				154.76	21.07	0.0258				-	310.81
DBF							23.41	5.13	0.0279	269.90	
Ind				-16.53	24.41	0.0116				-14.80	32.13
8-MeQuin										32.28	9.62

Table A2.T4. Table of compound correlations with atmospheric reactants.

Each correlation is in the $y = mx + b$ format, with the $y =$ assumed. Only 3-nitrobenzanthrone had correlations with NO_2 at both sample locations. No other PAH was correlated with the same atmospheric reactant at both locations.

Fence	NO	NO₂	O₃
Benzo(a)pyrene		20.1 x - 29.8	
Picene		67.9 x + 12.8	-153.8 x + 745.3
Naphtho[1,2-b]fluoranthene		1.7 x + 3.7	-399.7 x + 19.1
Dibenzo[a,k]fluoranthene	0.85 x + 0.78	0.46 x + 0.03	-124.1 x + 5.6
Dibenzo[a,i]pyrene	1.1 x + 1.9	0.58 x + 1.0	-149.9 x + 7.8
Dibenzo[a,h]pyrene			-78.4 x + 4.2
9-nitroanthracene			-574.3 x + 25.9
2,8-dinitrodibenzothiophene		4.8 x + 12.1	
3-nitrobenzanthrone	39.1 x + 24.7	18.3 x + 2.5	48.2 x + 220.0
1,2-naphthoquinone		196.3 x + 74.5	
9,10-anthraquinone & 1,4-phenanthrenedio	49.7 x + 134.4		-72.4 x + 416.0
5,12-naphthacenequinone	22.4 x + 2.6	11.4 x - 13.7	-29.36 x + 119.7
6H-benzo(cd)pyren-6-one	28.6 x + 17.4		-40.5 x + 175.8
3-Hydroxyphenanthrene			-390.8 x + 17.0
1-Hydroxyphenanthrene			-353.1 x + 13.9
2-Hydroxyphenanthrene			-524.2 x + 22.7
Indole	12.9 x + 11.6	7.3 x - 0.82	-1961 x + 87.2
Xanthene	7.7 x + 6.8		-1112 x + 53.7
Town			
Naphtho[2,3-k]fluoranthene		0.31 x + 0.04	
Dibenzo[a,h]pyrene		0.55 x 0.08	
3-nitrobenzanthrone		16.9 x + 0.12	
1,3-dinitropyrene		16.8 x - 15.5	
1-Hydroxy-9-fluorenone			-55.5 x + 2.8
12-Hydroxybenzo(a)pyrene		0.75 x + 1.3	

Table A2.T5. List of Relative Potency Factors (RPF) available for PAHs.

UPAHs are shaded in green, and HMWs are shaded in orange [Agency 2010].

Analyte	Available RPF
Phenanthrene	0
Anthracene	0
Fluoranthene	0.08
Pyrene	0
Benzo(c)fluorene	20
Benzo(a)anthracene	0.2
Chrysene	0.1
Benzo(b)fluoranthene	0.8
Benzo(k)fluoranthene	0.03
Benzo(a)pyrene	1
Dibenz(ah)anthracene	10
Indeno(1,23-cd)pyrene	0.07
Benzo(ghi)perylene	0.009
Dibenz(ae)fluoranthene	0.9
Dibenz(al)pyrene	30
Naphtho(2,3-e)pyrene	0.3
Dibenz(ae)pyrene	0.4
Dibenz(ai)pyrene	0.6
Dibenz(ah)pyrene	0.9

Table A2.T6. Full results for the average (Avg), geometric mean (Mean), median (Med), maximum (Max) and minimum (Min) measured concentrations (pg/m³ air) for all compounds at both sampling locations. Also included is the frequency (Freq), as a percentage, of each compound being above the quantification limit listed in Table S1.

Compound name	Fence						Town					
	Avg	Mean	Med	Max	Min	Freq	Avg	Mean	Med	Max	Min	Freq
Naphthalene	12.39	2.03	2.51	122.32	ND	84%	15.03	2.54	2.27	103.96	ND	88%
Acenaphthylene	12.64	6.99	6.65	85.32	0.46	100%	15.73	7.60	6.92	107.19	0.64	100%
Acenaphthene	9.82	1.85	1.60	178.62	ND	96%	7.02	1.17	1.02	80.81	ND	93%
Fluorene	4.76	1.96	1.70	42.11	ND	96%	4.69	1.62	1.43	50.91	ND	96%
Phenanthrene	39.31	16.82	18.39	262.91	0.53	100%	27.75	10.83	11.09	328.21	0.09	100%
Anthracene	11.74	4.44	4.42	140.64	0.11	100%	4.44	1.75	1.76	56.08	ND	98%
Fluoranthene	62.05	24.44	29.28	493.54	0.21	100%	34.93	9.49	8.51	619.74	0.15	100%
Pyrene	45.67	18.48	21.86	316.22	0.14	100%	36.15	9.13	8.30	613.59	ND	96%
Retene	58.76	16.17	10.85	956.36	0.69	100%	56.73	15.32	12.73	383.77	ND	98%
Benz(c)fluorene	4.96	1.58	1.46	51.03	ND	95%	5.87	1.29	1.15	102.32	ND	95%
Benzo(a)anthracene	25.67	6.78	6.64	296.00	0.39	100%	29.84	4.56	3.82	569.71	ND	95%
Chrysene+Triphenylene	72.33	23.28	17.50	579.28	1.63	100%	71.54	12.07	8.15	1178.33	ND	98%
Benzo(b)fluoranthene	133.02	32.18	23.16	1535.96	0.66	100%	178.02	26.11	21.27	2258.94	0.07	100%
Benzo(k)fluoranthene	42.13	8.83	6.33	520.17	0.74	100%	51.94	7.00	5.33	677.01	0.08	100%
Benz(e)pyrene	65.99	14.82	9.01	792.53	0.48	100%	85.50	12.12	7.61	1106.52	0.32	100%
Benzo(a)pyrene	37.03	8.21	6.46	483.52	ND	98%	41.95	7.12	5.49	838.15	ND	96%
Dibenz(a,h)+(a,c)anthracene	4.69	1.82	2.53	18.53	ND	96%	5.58	1.92	2.44	40.72	ND	98%
Indeno(1,2,3-cd)pyrene	63.28	16.27	11.19	953.60	0.41	100%	82.67	14.29	8.66	1097.98	0.30	100%
Benzo(ghi)perylene	70.22	20.59	15.23	1020.86	0.54	100%	83.28	17.35	11.70	1081.42	0.83	100%
Picene	389.55	150.75	119.24	4859.17	ND	80%	456.81	159.31	122.33	4972.14	ND	77%
Naphtho[1,2-b]fluoranthene	7.15	4.30	6.16	27.41	ND	98%	7.32	4.29	6.43	24.40	ND	95%
Naphtho[2,3-j]/[1,2-k]fluoranthene	20.11	14.51	11.93	82.48	ND	95%	21.88	16.16	12.26	89.02	ND	98%
Naphtho[2,3-b]fluoranthene	6.97	3.94	5.57	30.95	ND	82%	6.64	3.28	5.28	34.33	ND	68%
Dibenzo[a,e]fluoranthene+Dibenzo[b,k]fl	19.01	13.94	11.99	77.23	ND	95%	20.38	15.13	11.71	88.72	ND	96%

Dibenzo[a,k]fluoranthene	2.58	1.27	0.76	20.66	ND	27%	3.05	1.38	0.76	20.80	ND	32%
Dibenzo[j,l]fluoranthene	8.44	3.97	5.46	64.12	ND	59%	9.25	3.84	5.63	70.75	ND	57%
Dibenzo[a,l]pyrene	1.69	1.08	0.80	16.41	ND	9%	2.41	1.25	0.80	21.84	ND	14%
Naphtho[2,3-k]fluoranthene	1.25	0.84	0.73	14.70	ND	5%	1.38	0.87	0.73	15.65	ND	7%
Naphtho[2,3-e]pyrene	6.54	3.38	1.53	34.52	ND	79%	6.85	3.22	1.53	38.22	ND	70%
Dibenzo[a,e]pyrene	7.42	3.58	4.63	48.64	ND	89%	8.09	3.69	5.34	53.93	ND	82%
Coronene	21.12	9.63	8.97	198.46	ND	98%	18.56	6.86	6.92	165.26	ND	98%
Dibenzo[a,i]pyrene	3.48	2.14	1.11	24.44	ND	41%	4.34	2.52	1.67	30.73	ND	50%
Dibenzo[a,h]pyrene	1.80	1.50	1.32	10.50	ND	9%	1.87	1.48	1.32	14.74	ND	5%
1-nitronaphthalene	12.20	1.81	6.84	244.94	ND	61%	15.43	1.49	3.47	311.23	ND	55%
2-nitronaphthalene	7.54	3.19	7.69	75.60	ND	79%	8.06	3.22	8.19	81.19	ND	77%
2-nitrobiphenyl	5.60	0.87	0.17	96.10	ND	41%	6.53	0.90	0.17	101.59	ND	39%
3-nitrobiphenyl	5.21	0.88	0.13	26.65	ND	43%	5.65	0.96	0.13	36.31	ND	45%
4-nitrobiphenyl	15.76	4.45	1.12	221.45	ND	45%	17.52	4.73	1.12	297.54	ND	46%
3-nitrodibenzofuran	11.41	7.61	11.06	45.73	ND	84%	11.96	8.79	11.31	59.17	ND	89%
5-nitroacenaphthene	29.40	7.26	12.02	420.24	ND	73%	20.61	8.09	12.57	270.05	ND	80%
2-nitrofluorene	15.61	6.65	8.17	430.95	ND	91%	12.69	4.26	6.43	353.67	ND	79%
9-nitroanthracene	18.38	6.64	9.66	167.68	ND	88%	13.18	4.92	8.60	108.29	ND	80%
9-nitrophenanthrene	7.29	2.30	7.29	44.57	ND	59%	7.60	2.24	7.59	63.92	ND	59%
2-nitrodibenzothiophene	9.93	2.89	7.78	70.90	ND	66%	8.14	1.31	0.25	98.02	ND	43%
3-nitrophenanthrene	14.70	3.15	5.85	473.17	ND	68%	10.35	1.99	1.33	287.55	ND	52%
2 + 3-nitrofluoranthene	22.73	6.09	15.86	460.75	ND	84%	19.36	4.56	15.69	299.07	ND	71%
1-nitropyrene	7.74	2.81	5.76	81.18	ND	77%	6.88	1.59	1.03	109.64	ND	52%
2,8-dinitrodibenzothiophene	33.88	16.55	15.85	303.89	ND	79%	35.83	15.89	14.86	281.07	ND	75%
7-nitrobenz[a]anthracene	16.50	2.37	0.77	480.74	ND	50%	12.84	2.49	1.30	306.20	ND	52%
6-nitrochrysene	2.48	0.83	0.34	20.44	ND	32%	3.23	1.06	0.34	28.03	ND	45%
3-nitrobenzanthrone	44.11	8.13	4.65	329.39	ND	36%	36.43	7.43	1.46	235.73	ND	48%
1,3-dinitropyrene	56.15	7.64	1.47	314.81	ND	39%	49.65	6.09	1.47	245.87	ND	34%
1,6-dinitropyrene	58.80	13.87	14.08	270.97	ND	61%	64.38	14.14	13.86	296.16	ND	57%
1,8-dinitropyrene	54.84	19.02	9.25	261.85	ND	50%	55.07	18.27	5.61	258.90	ND	45%
6-nitrobenzo(a)pyrene	26.74	3.57	0.96	298.86	ND	43%	21.37	3.03	0.96	303.04	ND	39%

p-benzoquinone	254.52	53.64	129.85	4222.90	ND	82%	213.09	43.57	103.28	2268.12	ND	82%
1,4-naphthoquinone	277.97	146.51	307.85	914.91	ND	86%	783.57	172.12	323.94	18051.52	ND	84%
1,2-naphthoquinone	612.73	91.55	289.54	3032.89	ND	93%	613.13	90.74	211.22	2889.71	ND	93%
2,3-benzo-4-pyrone	9.12	5.02	4.54	104.81	ND	93%	14.65	4.88	5.12	412.96	ND	95%
9,10-anthraquinone & 1,4-phenanthrenedio	218.79	133.16	166.94	1030.59	ND	98%	109.79	67.80	75.56	442.96	ND	98%
9-fluorenone	274.76	75.75	172.05	1573.49	ND	71%	253.83	72.55	169.43	1132.84	ND	73%
xanthone	74.89	11.07	14.58	599.34	ND	88%	67.95	9.70	12.04	576.32	ND	71%
perinaphthenone	35.60	16.50	15.48	198.27	ND	89%	37.34	14.34	13.34	539.95	ND	91%
1,4-anthraquinone	304.97	109.12	101.90	1125.80	ND	86%	275.23	105.98	97.77	1064.02	ND	89%
acenaphthalenquinone & 1,2-acenaphthalyn	134.33	64.50	89.26	465.14	ND	91%	129.59	51.42	68.18	443.91	ND	93%
4H-cyclopenta[def]phenanthre	72.37	14.77	11.49	1694.67	0.76	100%	74.95	9.97	6.90	1980.58	ND	98%
2-methyl-9,10-anthraquinone	39.16	24.69	26.56	190.44	ND	98%	25.93	9.97	12.54	507.83	ND	91%
9,10-phenanthrenequinone	187.91	42.41	32.27	814.89	ND	86%	190.32	39.14	38.78	870.59	ND	86%
2-ethyl-9,10-anthraquinone	59.61	26.55	25.13	260.56	1.58	100%	64.15	25.32	31.05	211.55	1.38	100%
benzo(a)fluorenone	67.54	22.73	21.24	295.69	ND	96%	67.66	12.38	11.27	333.60	ND	89%
benzanthrone	36.75	11.52	11.79	313.99	ND	91%	35.58	9.15	9.66	367.52	ND	91%
7,12-benz[a]anthracenequinone + benzo[c]	83.91	37.89	48.31	515.11	1.82	100%	84.13	35.02	54.11	600.90	1.82	100%
5,12-naphthacenequinone	46.88	10.25	11.82	1239.28	ND	82%	46.46	8.00	11.54	1451.62	ND	71%
6H-benzo(cd)pyren-6-one	43.28	12.31	10.35	215.70	ND	91%	44.00	11.85	13.49	253.23	ND	93%
aceanthrenequinone	124.54	44.26	37.61	653.59	ND	82%	118.06	39.75	30.87	467.67	ND	77%
1,6-benzo(a)pyrendione	13.72	0.33	0.16	584.35	ND	14%	14.90	0.34	0.16	632.17	ND	14%
3,6-benzo(a)pyrendione	4.45	0.16	0.07	49.57	ND	14%	3.94	0.15	0.07	74.28	ND	14%
1-Hydroxynaphthalene	7.87	2.76	3.20	69.56	ND	89%	7.41	3.76	3.94	44.74	ND	95%
2-Hydroxynaphthalene	21.40	3.69	4.18	246.96	ND	84%	25.16	3.15	3.38	323.75	ND	88%
2,3-Dihydroxynaphthalene	1.07	0.31	0.23	16.68	ND	86%	1.95	0.31	0.23	66.24	ND	86%
1,3- & 1,5-dihydroxynaphthalene	7.13	4.65	6.45	59.42	ND	75%	7.53	5.29	7.43	32.63	ND	84%
1,6-Dihydroxynaphthalene	1.62	0.19	0.12	12.77	ND	71%	1.13	0.16	0.12	10.34	ND	79%
2,7-Dihydroxynaphthalene	3.71	0.36	0.07	37.44	ND	39%	3.57	0.40	0.07	32.94	ND	41%
2,6-Dihydroxynaphthalene	1.20	0.23	0.04	9.91	ND	43%	1.14	0.21	0.04	10.05	ND	39%
4-Hydroxyphenanthrene	3.52	0.52	0.63	69.29	ND	50%	3.69	0.88	1.67	22.45	ND	63%

9-Hydroxyphenanthrene	15.59	3.57	3.96	182.68	ND	84%	25.47	4.31	5.56	628.68	ND	88%
3-Hydroxyphenanthrene	4.34	1.05	2.09	35.46	ND	95%	5.41	1.56	3.33	41.09	ND	95%
1-Hydroxyphenanthrene	3.44	0.78	1.50	39.24	ND	63%	3.58	0.82	1.64	38.99	ND	64%
2-Hydroxyphenanthrene	5.62	1.43	2.12	52.94	ND	75%	7.41	1.59	2.29	56.23	ND	71%
2-Hydroxyanthraquinone	34.47	12.92	11.01	414.93	ND	73%	33.73	13.58	13.33	213.68	ND	68%
3-Hydroxyfluoranthene	6.29	3.72	5.21	27.24	ND	91%	6.74	3.94	5.21	29.52	ND	91%
9-Hydroxyfluorene	15.84	12.86	13.54	55.09	1.19	100%	19.73	15.86	18.40	57.89	2.12	100%
3-Hydroxyfluorene	6.76	1.62	2.61	58.72	ND	73%	5.35	1.69	2.26	29.58	ND	79%
2-Hydroxyfluorene	10.55	3.97	6.03	85.69	ND	96%	10.62	4.79	6.02	55.62	ND	98%
1-Hydroxy-9-fluorenone	1.44	0.39	0.11	23.71	0.11	100%	1.28	0.48	0.75	9.01	0.11	100%
2-Hydroxy-9-fluorenone	7.52	1.60	2.19	199.92	ND	98%	5.91	2.53	3.82	22.48	ND	96%
1-Hydroxypyrene	4.76	0.35	1.08	61.94	ND	52%	3.86	0.56	1.63	19.83	ND	61%
3-Hydroxybenzo(a)anthracene	4.11	1.62	4.87	19.46	ND	82%	3.97	1.17	5.10	25.01	ND	79%
3-Hydroxybenzo(c)phenanthrene	1.62	0.26	0.12	32.15	ND	20%	0.78	0.24	0.12	8.88	ND	18%
10-Hydroxybenzo(a)pyrene	1.63	0.42	0.58	14.96	ND	71%	1.73	0.40	0.11	23.12	ND	75%
12-Hydroxybenzo(a)pyrene	4.20	2.98	3.60	48.48	1.09	100%	3.43	2.79	3.77	15.65	1.46	100%
7-Hydroxybenzo(a)pyrene	0.87	0.27	0.11	10.45	0.11	100%	12.65	0.40	0.11	593.89	0.11	100%
9-Hydroxybenzo(a) + 3-Hydroxybenzo(e)pyr	6.02	1.27	2.23	124.73	ND	95%	7.40	1.70	2.69	152.77	ND	93%
3-Hydroxybenzo(a)pyrene	14.84	3.06	5.10	153.02	ND	77%	17.79	2.27	2.91	574.57	ND	77%
1-Hydroxyindeno[1,2,3-c,d]pyrene	3.10	0.85	1.78	25.84	ND	55%	2.77	0.75	1.30	23.93	ND	54%
4-Hydroxychrysene	3.20	0.81	0.23	15.67	ND	36%	2.71	0.69	0.23	14.99	ND	34%
6-Hydroxychrysene	4.65	2.31	2.36	50.60	0.69	100%	4.45	2.32	1.54	14.07	0.69	100%
3-Hydroxychrysene	1.08	0.42	0.27	16.90	ND	18%	1.12	0.52	0.27	8.27	ND	29%
11-Hydroxybenzo(b)fluoranthene	14.74	6.89	7.13	122.27	ND	95%	15.67	4.55	4.18	341.16	ND	88%
9-Hydroxybenzo(k)fluoranthene	13.61	1.02	0.34	299.05	ND	38%	5.68	1.35	1.25	146.86	ND	57%
11-Hydroxybenzo(g)chrysene	1.94	0.81	0.42	22.00	0.42	100%	1.85	0.92	0.42	13.85	0.42	100%
10-Hydroxybenzo(c)chrysene	2.72	1.25	0.49	23.27	ND	48%	3.20	1.21	0.49	34.80	ND	36%
2-Methylbenzofuran	225.24	79.08	120.39	829.54	ND	96%	229.12	75.35	106.02	828.89	ND	96%
Thianaphthene	15.13	7.24	9.42	120.54	ND	95%	12.71	5.11	8.89	47.91	ND	84%
Quinoline	33.16	17.85	21.23	259.11	ND	96%	19.53	8.35	19.34	91.50	ND	88%
Dibenzofuran	11.31	0.88	1.85	279.65	ND	86%	10.06	0.69	1.14	281.28	ND	93%

Dibenzothiophene	6.12	2.06	1.67	62.28	0.11	100%	3.40	1.31	1.35	24.49	ND	95%
Dibenzothiophene sulfone	1.33	0.39	0.46	9.99	ND	86%	2.11	0.34	0.33	40.79	ND	86%
Indole	17.78	1.32	1.50	175.40	ND	55%	23.86	2.86	3.32	164.91	ND	68%
8-Methylquinoline	32.54	8.33	12.43	297.85	ND	93%	18.47	5.70	7.44	125.90	ND	93%
Xanthene	25.11	7.34	11.16	234.78	ND	89%	32.39	10.39	16.58	343.51	ND	89%
Acridine	31.01	10.24	15.36	355.99	ND	89%	19.30	8.53	12.73	125.82	ND	91%
5,6-benzoquinoline	61.61	23.50	29.30	568.77	ND	96%	57.64	11.21	20.60	614.23	ND	86%
Carbazole	23.87	6.05	15.40	191.60	ND	86%	23.04	5.60	14.46	150.89	ND	82%

Figure A2.F1. Retene analysis results for Normal days, Fire impacted samples and Inversion event samples for the two sampling locations (red = Fence, blue = Town). * indicates a statistically significant (p-value ≤ 0.05) higher concentration of Retene at both locations during Inversion events when compared to Normal days.

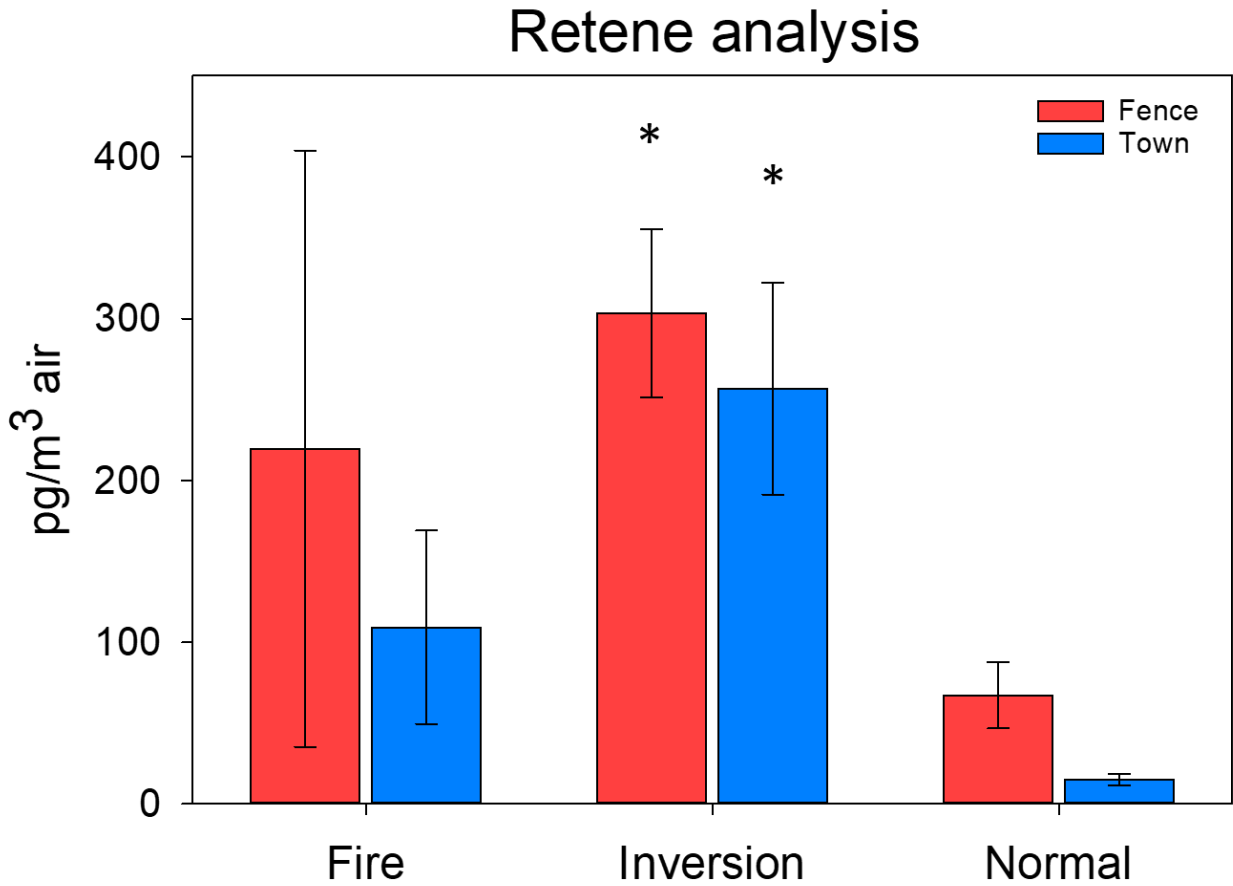
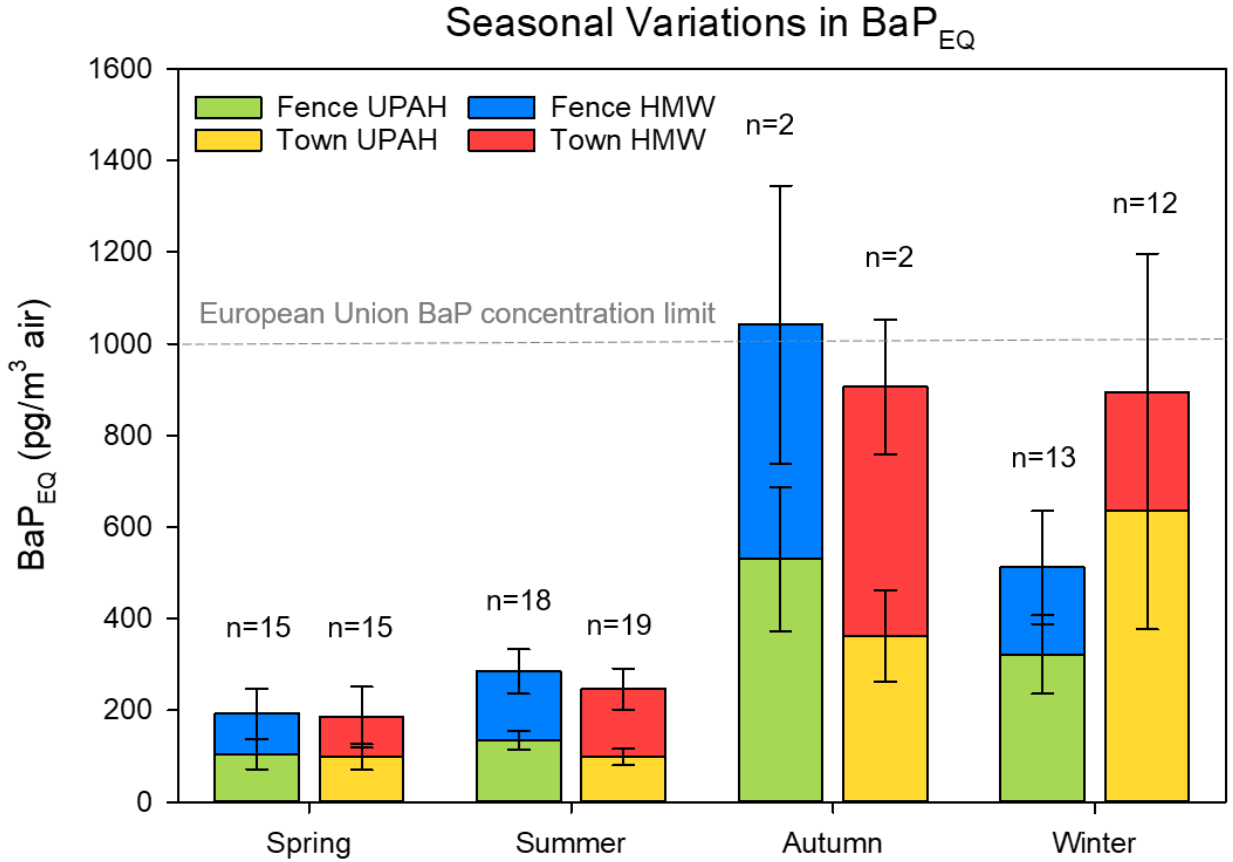


Table A2.T7. Table of BaP_{EQ} concentrations during various wind patterns. The two sampling locations have averages (\pm SE) and median concentrations, for UPAHs and HMWs, as well as average (\pm SE) and median concentrations for total BaP_{EQ}.

		Fence		Town	
		Average	Median	Average	Median
NW \leq 20%	UPAH	242.1 (\pm 109.8)	72.6	359.5 (\pm 141.8)	79.9
	HMW	77.6 (\pm 20.7)	43.5	160.1 (\pm 80.3)	35.7
	Total	319.6 (\pm 115.4)	136.4	519.5 (\pm 163.8)	138.0
NW \geq 70%	UPAH	180.2 (\pm 28.4)	161.0	115.1 (\pm 52.6)	93.9
	HMW	118.8 (\pm 76.7)	47.7	36.2 (\pm 13.8)	32.1
	Total	299.0 (\pm 71.0)	272.7	151.4 (\pm 46.5)	155.9
SW \leq 20%	UPAH	360.9 (\pm 110.8)	194.1	305.4 (\pm 75.6)	192.1
	HMW	90.5 (\pm 17.5)	60.9	216.7 (\pm 88.9)	72.9
	Total	451.3 (\pm 112.8)	303.9	522.1 (\pm 113.8)	356.1
SW \geq 80%	UPAH	19.8 (\pm 9.1)	12.6	27.1 (\pm 7.7)	22.2
	HMW	34.6 (\pm 4.1)	36.5	100.3 (\pm 54.2)	25.7
	Total	54.5 (\pm 10.4)	49.4	127.4 (53.1)	70.6
SE \leq 20%	UPAH	152.3 (\pm 47.9)	135.6	119.3 (\pm 20.7)	93.9
	HMW	55.2 (\pm 9.9)	39.6	75.5 (\pm 18.4)	28.5
	Total	207.5 (\pm 50.1)	193.9	194.8 (\pm 24.5)	181.2
SE \geq 80%	UPAH	223.3 (\pm 73.9)	161.6	365.7 (\pm 146.7)	195.0
	HMW	48.4 (\pm 5.0)	55.8	27.6 (\pm 10.5)	16.1
	Total	271.8 (\pm 77.9)	197.8	393.2 (\pm 157.1)	211.1
Fires	UPAH	163.9 (\pm 36.4)	206.6	247.8 (\pm 197.3)	50.0
	HMW	57.9 (\pm 6.0)	54.9	121.1 (\pm 69.3)	52.9
	Total	221.8 (\pm 38.9)	263.2	368.9 (\pm 226.5)	111.6
Inversions	UPAH	2502.7 (\pm 310.0)	2657.5	2812.7 (\pm 1298.1)	1609.2
	HMW	352.0 (\pm 158.2)	371.8	454.4 (\pm 206.6)	478.2
	Total	2854.9 (\pm 376.1)	2726.1	3267.0 (\pm 1479.1)	2087.4

Figure A2.F2. BaPEQ concentrations for days with no prevalent wind direction broken down by season. 'n' represents the number of samples which fell into each season. Seasons are defined as Spring (22 Mar – 21 Jun), Summer (22 Jun – 21 Sep), Autumn (22 Sep – 21 Dec), Winter (22 Dec – 21 Mar). Dashed line indicates the BaP concentration limit recommended by the European Union to avoid excess lifetime cancer risks.



Appendix 3

CHAPTER 4 SUPPORTING INFORMATION

**Oxidative Potential of PAHs in Ambient Atmospheric PM_{2.5}
using Dithiolthreitol (DTT) Consumption Assay**

Amber L. Kramer^{1,2}, Shelby Dorn¹, Allison Perez², Ivan A. Titaley², Courtney
Roper³, Paul Cheong¹, Staci L. Massey Simonich^{1,2}

1 – Oregon State University Department of Chemistry, 2 – Oregon State University
Department of Environmental and Molecular Toxicology, 3 – University of Mississippi
Department of Biomolecular Sciences

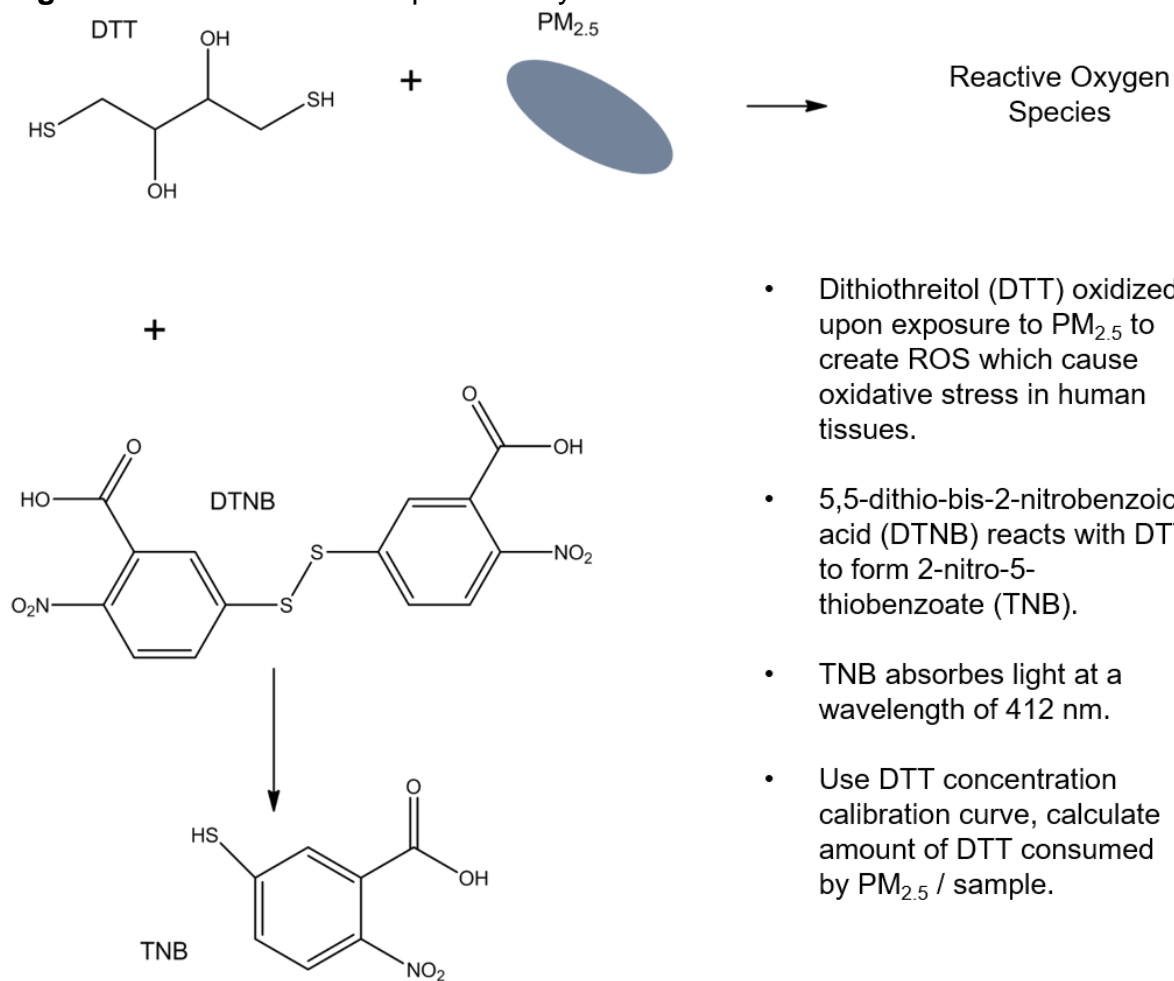
Table A3.T1. Analytical standards used for DTT consumption assay. Each standard was dissolved in DMSO and diluted to a concentration of ~1 mM before use in assay. CAS number, molecular mass (AMU), abbreviation, and PAH subclass are listed.

Compound name	CAS No.	AMU	Abbrev.	PAH class
Naphthalene	91-20-3	128.171	NAP	UPAH
Acenaphthylene	208-96-8	152.196	ACY	UPAH
Acenaphthene	83-32-9	154.212	ACN	UPAH
Fluorene	86-73-7	166.223	FLO	UPAH
Phenanthrene	85-01-8	178.234	PHE	UPAH
Anthracene	120-12-7	178.234	ANT	UPAH
Fluoranthene	206-44-0	202.256	FLN	UPAH
Pyrene	129-00-0	202.256	PYR	UPAH
Retene	483-65-8	234.336	RET	UPAH
Benzo(c)fluorene	205-12-9	216.283	BcF	UPAH
Benzo(a)anthracene	56-55-3	228.288	BaA	UPAH
Chrysene	218-01-9	228.294	Cry	UPAH
Triphenylene	217-59-4	228.294	Tri	UPAH
Benzo(b)fluoranthene	205-99-2	252.309	BbF	UPAH
Benzo(k)fluoranthene	207-08-9	252.309	BkF	UPAH
Benz(e)pyrene	192-97-2	252.316	BeP	UPAH
Benzo(a)pyrene	50-32-8	252.316	BaP	UPAH
Dibenz(a,h)anthracene	53-70-3	278.347	DahA	UPAH
Dibenz(a,c)anthracene	215-58-7	278.347	DacA	UPAH
Indeno(1,2,3-cd)pyrene	193-39-5	276.331	IcdP	UPAH
Benzo(ghi)perylene	191-24-2	276.338	BghiP	UPAH
Picene	213-46-7	278.347	PIC	HMW
Naphtho[1,2-b]fluoranthene	111189-32-3	302.376	N1,2-bF	HMW
Naphtho[2,3-j]fluoranthene	205-83-4	302.376	N2,3-jF	HMW
Naphtho[1,2-k]fluoranthene	238-04-0	302.376	N1,2-kF	HMW
Naphtho[2,3-b]fluoranthene	206-06-4	302.376	N2,3-bF	HMW
Dibenzo[a,e]fluoranthene	5385-75-1	302.376	DaeF	HMW
Dibenzo[b,k]fluoranthene	205-97-0	302.376	DbkF	HMW
Dibenzo[a,k]fluoranthene	84030-79--5	302.376	DakF	HMW
Dibenzo[j,l]fluoranthene	203-18-9	302.368	Djlf	HMW
Dibenzo[a,l]pyrene	191-30-0	302.376	DalP	HMW
Naphtho[2,3-k]fluoranthene	207-18-1	302.376	N2,3-kF	HMW
Naphtho[2,3-e]pyrene	193-09-9	302.376	N2,3-eP	HMW
Dibenzo[a,e]pyrene	192-65-4	302.367	DaeP	HMW
Coronene	191-07-1	300.36	COR	HMW
Dibenzo[a,i]pyrene	189-55-9	302.367	DaiP	HMW
Dibenzo[a,h]pyrene	189-64-0	302.367	DahP	HMW
1-nitronaphthalene	86-57-7	173.171	1NNap	NPAH
2-nitronaphthalene	581-89-5	173.171	2NNap	NPAH
2-nitrobiphenyl	86-00-0	199.209	2NBP	NPAH
3-nitrobiphenyl	2113-58-8	199.209	3NBP	NPAH
4-nitrobiphenyl	92-93-3	199.209	4NBP	NPAH
3-nitrodibenzofuran	5410-97-9	214.192	3NDBF	NPAH
5-nitroacenaphthene	602-87-9	199.209	5NAcn	NPAH
2-nitrofluorene	607-57-8	211.220	2NFlo	NPAH
9-nitroanthracene	602-60-8	223.231	9NAnt	NPAH
9-nitrophenanthrene	954-46-1	223.231	9NPhe	NPAH
2-nitrodibenzothiophene	6639-36-7	229.253	2NDBT	NPAH
3-nitrophenanthrene	17024-19-0	223.231	3NPhe	NPAH
2-nitrofluoranthene	13177-29-2	247.253	2NFln	NPAH
3-nitrofluoranthene	892-21-7	247.253	3NFln	NPAH
1-nitropyrene	5522-43-0	247.253	1NPyr	NPAH

2,8-dinitrodibenzothiophene	109041-38-5	274.25	28NDBT	NPAH
7-nitrobenz[a]anthracene	20268-51-3	273.291	7NBaA	NPAH
6-nitrochrysene	7496-02-8	273.291	6NCry	NPAH
3-nitrobenzanthrone	17117-34-9	275.263	3NBZN	NPAH
1,3-dinitropyrene	75321-20-9	292.25	13NPyr	NPAH
1,6-dinitropyrene	42397-64-8	292.25	16NPyr	NPAH
1,8-dinitropyrene	42397-65-9	292.25	18NPyr	NPAH
6-nitrobenzo(a)pyrene	63041-90-7	297.313	6NBaP	NPAH
p-benzoquinone	106-51-4	108.096	BZQ	OPAH
1,4-naphthoquinone	130-15-4	158.156	14NapQ	OPAH
1,2-naphthoquinone	524-42-5	158.156	12NapQ	OPAH
2,3-benzo-4-pyrone (chromone)	491-38-3	146.145	Chro	OPAH
9,10-anthraquinone	84-65-1	208.216	910AntQ	OPAH
1,4-phenanthrenedione	569-15-3	208.216	14PheONE	OPAH
9-fluorenone	486-25-9	180.206	9FIONE	OPAH
xanthone	90-47-1	196.19	XONE	OPAH
perinaphthenone	548-39-0	180.206	PNap	OPAH
1,4-anthraquinone	635-12-1	208.216	1,4AntQ	OPAH
Acenaphthalenquinone	82-86-0	182.178	AcnQ	OPAH
1,2-acenaphthalindione	82-86-0	182.175	1,2AcyONE	OPAH
4H-cyclopenta[def]phenanthrenone	5737-13-3	204.228	4HCdefP	OPAH
2-methyl-9,10-anthraquinone	84-54-8	222.239	2-ME-AntQ	OPAH
9,10-phenanthrenequinone	84-11-7	208.216	9,10-PheQ	OPAH
2-ethyl-9,10-anthraquinone	84-51-5	236.27	2ETANTQ	OPAH
benzo(a)fluorenone	116232-62-3	230.261	BAFONE	OPAH
Benzanthrone	82-05-3	230.266	BZN	OPAH
7,12-benz[a]anthracenequinone	2498-66-0	258.271	7,12-BaAQ	OPAH
benzo[c]phenanthrone	Unknown	245.295	BcPhONE	OPAH
5,12-naphthacenequinone	1090-13-7	258.271	5,12-NapQ	OPAH
6H-benzo(cd)pyren-6-one	3074-00-8	245.288	6HBPONE	OPAH
aceanthrenequinone	6373-11-1	232.23	AcyAntQ	OPAH
1,6-benzo(a)pyrendione	3067-13-8	282.298	16-BaPONE	OPAH
3,6-benzo(a)pyrendione	3067-14-9	282.298	36-BaPONE	OPAH
1-Hydroxynaphthalene	90-15-3	144.173	1-OHNap	OHPAH
2-Hydroxynaphthalene	135-19-3	144.173	2-OHNap	OHPAH
2,3-Dihydroxynaphthalene	92-44-4	160.172	2,3-OHNap	OHPAH
1,3-dihydroxynaphthalene	132-86-5	160.172	1,2-OHNap	OHPAH
1,5-dihydroxynaphthalene	83-56-7	160.172	1,5-OHNap	OHPAH
1,6-Dihydroxynaphthalene	575-44-0	160.172	1,6-OHNap	OHPAH
2,7-Dihydroxynaphthalene	582-17-2	160.172	2,7-OHNap	OHPAH
2,6-Dihydroxynaphthalene	581-43-1	160.172	2,6-OHNap	OHPAH
4-Hydroxyphenanthrene	7651-86-7	194.233	4-OHPhe	OHPAH
9-Hydroxyphenanthrene	484-17-3	194.233	9-OHPhe	OHPAH
3-Hydroxyphenanthrene	605-87-8	194.233	3-OHPhe	OHPAH
1-Hydroxyphenanthrene	2433-56-9	194.233	1-OHPhe	OHPAH
2-Hydroxyphenanthrene	605-55-0	194.233	2-OHPhe	OHPAH
2-Hydroxyanthraquinone	605-32-3	224.215	2-OHAntQ	OHPAH
3-Hydroxyfluoranthene	17798-09-3	218.255	3-OHFln	OHPAH
9-Hydroxyfluorene	1689-64-1	182.222	9-OHFlo	OHPAH
3-Hydroxyfluorene	6344-67-8	182.222	3-OHFlo	OHPAH
2-Hydroxyfluorene	2443-58-5	182.222	2-OHFlo	OHPAH
1-Hydroxy-9-fluorenone	6344-60-1	196.205	1-OH9Flone	OHPAH
2-Hydroxy-9-fluorenone	6949-73-1	196.205	2-OH9Flone	OHPAH

1-Hydroxypyrene	5315-79-7	218.255	1-OHPyp	OHPAH
3-Hydroxybenzo(a)anthracene	4834-35-9	244.293	3-OHBaA	OHPAH
3-Hydroxybenzo(c)phenanthrene	22717-95-9	244.293	3-OHBcP	OHPAH
10-Hydroxybenzo(a)pyrene	56892-31-0	268.315	10-OHBaP	OHPAH
12-Hydroxybenzo(a)pyrene	56892-33-2	268.315	12-OHBaP	OHPAH
7-Hydroxybenzo(a)pyrene	37994-82-4	268.315	7-OHBaP	OHPAH
9-Hydroxybenzo(a)pyrene	17573-21-6	268.315	9-OHBaP	OHPAH
3-Hydroxybenzo(e)pyrene	77508-02-2	268.315	3-OHBeP	OHPAH
3-Hydroxybenzo(a)pyrene	13345-21-6	268.315	3-OHBaP	OHPAH
1-Hydroxyindeno[1,2,3-c,d]pyrene	99520-65-7	292.337	1-OHlcdP	OHPAH
4-Hydroxychrysene	63019-40-9	244.293	4-OHCry	OHPAH
6-Hydroxychrysene	37515-51-8	244.293	6-OHCry	OHPAH
3-Hydroxychrysene	63019-39-6	244.293	3-OHCry	OHPAH
11-Hydroxybenzo(b)fluoranthene	Unknown	269.316	11-OHBbF	OHPAH
9-Hydroxybenzo(k)fluoranthene	Unknown	269.316	9-OHBkF	OHPAH
11-Hydroxybenzo(g)chrysene	Unknown	294.307	11-OHBgC	OHPAH
10-Hydroxybenzo(c)chrysene	Unknown	294.307	10-OHBcC	OHPAH
2-Methylbenzofuran	4265-25-2	132.162	2-Me-BZF	HPAH
Thianaphthene (benzothiophene)	95-15-8	134.196	TNAP	HPAH
Quinoline	91-22-5	129.162	QUIN	HPAH
Dibenzofuran	132-64-9	168.195	DBF	HPAH
Indole	120-72-9	117.151	IND	HPAH
8-Methylquinoline	611-32-5	143.189	8-Me-Qu	HPAH
Xanthene	92-83-1	182.222	XAN	HPAH
Acridine	260-94-6	179.222	ACR	HPAH
5,6-benzoquinoline	85-02-9	179.222	5,6-BQ	HPAH
Carbazole	86-74-8	167.211	CARB	HPAH
Dibenzothiophene	132-65-0	184.256	DBT	HPAH
Dibenzothiophene sulfone	1016-05-3	216.254	DBTS	HPAH

Figure A3.F1. DTT consumption assay reactions.



- Dithiothreitol (DTT) oxidized upon exposure to PM_{2.5} to create ROS which cause oxidative stress in human tissues.
- 5,5-dithio-bis-2-nitrobenzoic acid (DTNB) reacts with DTT to form 2-nitro-5-thiobenzoate (TNB).
- TNB absorbs light at a wavelength of 412 nm.
- Use DTT concentration calibration curve, calculate amount of DTT consumed by PM_{2.5} / sample.

Table A3.T2. Full results table, showing which PAH subclass each compound was classified as, molecular mass used in correlation analysis, the concentration (mM) of each compound required to use 50% of DTT (DTT₅₀), response factor (RF) in the DTT consumption assay, and calculated ΔG_{rxn} (eV) for the redox reaction of each compound with DTT. Ambient PM_{2.5} filter extract concentrations are listed in mM concentrations as quantified using GC/MS. Co-eluding compounds share a concentration measurement, for additive modeling, the measured concentration was attributed ½ to each compound. Priority Pollutant List (PPL) PAHs are **bolded**.

Compound	Class	Mass (AMU)	DTT ₅₀ (mM)	RF	ΔG_{rxn} (eV)	Filter A (mM)	Filter B (mM)	Filter C (mM)
Indole	HPAH	117.151	0.520	0.065	20.692	8.05E-04	1.28E-04	9.61E-04
Quinoline	HPAH	129.162	0.051	1.302	17.279	2.44E-04	4.15E-04	1.61E-04
2-methylbenzofuran	HPAH	132.162	0.207	0.121	20.225	< MDL	< MDL	< MDL
Thiannaphthalene	HPAH	134.196	1.219	0.012	19.454	7.21E-05	6.63E-04	2.15E-04
8-methylquinoline	HPAH	143.189	0.026	0.382	17.908	2.58E-04	3.85E-05	4.62E-05
Carbazole	HPAH	167.211	0.110	0.442	18.956	4.70E-03	3.89E-03	3.11E-03
Dibenzofuran	HPAH	168.195	0.114	0.376	18.477	3.19E-05	4.45E-05	5.77E-05
Acridine	HPAH	178.222	0.025	1.404	16.437	3.05E-04	7.38E-04	4.93E-04
5,6-benzoquinoline	HPAH	179.222	0.060	0.448	17.747	1.51E-02	1.33E-02	8.50E-03
Xanthene	HPAH	182.222	0.029	0.120	19.945	6.08E-04	8.47E-04	9.34E-05
Dibenzothiophene	HPAH	184.256	0.114	0.217	18.367	9.34E-06	3.29E-05	9.23E-06
Dibenzothiophene sulfone	HPAH	216.254	0.114	0.141	16.768	6.57E-06	1.27E-05	9.99E-06
Coronene	HMW	300.36	0.005	0.617		4.11E-05	1.51E-04	4.36E-05
Dibenzo(a)pyrene	HMW	302.376	0.021	0.001	16.609	< MDL	< MDL	< MDL
Dibenzo(ak)fluoranthene	HMW	302.376	0.050	0.001	15.724	< MDL	< MDL	< MDL
Dibenzo(jl)fluoranthene	HMW	302.376	0.051	0.001	15.805	7.29E-05	1.89E-04	7.50E-05
naphtho(1,2-b)fluoranthene	HMW	302.376	0.053	0.001	16.239	9.92E-05	2.70E-04	1.01E-04

naphtho(2,3-b)fluoranthene	HMW	302.376	0.062	0.001	16.306	< MDL	2.56E-04	< MDL
naphtho(2,3-j)fluoranthene	HMW	302.376	0.090	0.001	15.789			
Dibenzo(ah)pyrene	HMW	302.376	0.006	0.002	16.019	2.69E-04	6.40E-04	2.71E-04
Dibenz(bk)fluoranthene	HMW	302.376	0.023	0.002		< MDL	< MDL	< MDL
naphtho(1,2-k)fluoranthene	HMW	302.376	0.024	0.002	16.368			
naphtho(2,3-e)pyrene	HMW	302.376	0.036	0.002		2.25E-04	5.39E-04	2.27E-04
naphtho(2,3-k)fluoranthene	HMW	302.376	0.052	0.002	16.565	< MDL	2.25E-04	< MDL
Dibenzo(ae)pyrene	HMW	302.376	0.085	0.002	16.799	< MDL	< MDL	< MDL
Dibenzo(ai)pyrene	HMW	302.376	1.102	0.002	16.376	< MDL	2.24E-04	< MDL
dibenz(ae)fluoranthene	HMW	302.376	0.009	0.479		< MDL	< MDL	< MDL
1-nitronaphthalene	NPAH	173.171	0.158	0.259	15.887	1.53E-04	3.47E-04	1.55E-04
2-nitronaphthalene	NPAH	173.171	0.206	0.404	16.013	2.00E-04	4.55E-04	2.06E-04
2-nitrobiphenyl	NPAH	199.209	0.029	0.285	16.282	1.65E-04	3.72E-04	1.62E-04
3-nitrobiphenyl	NPAH	199.209	0.233	0.320	16.166	2.17E-04	4.91E-04	2.22E-04
4-nitrobiphenyl	NPAH	199.209	0.014	0.476	16.032	2.46E-04	7.20E-04	2.55E-04
5-nitroacenaphthalene	NPAH	199.209	0.010	1.211	15.131	2.69E-04	6.13E-04	2.69E-04
2-nitrofluorene	NPAH	211.22	0.160	0.453	16.08	< MDL	5.15E-04	2.26E-04
3-nitrodibenzofuran	NPAH	214.192	0.093	0.109		2.24E-04	< MDL	2.25E-06
2-nitroanthracene	NPAH	223.231	0.095	0.361	15.64			
9-nitrophenanthrene	NPAH	223.231	0.027	0.532	15.767	1.99E-04	4.53E-04	1.98E-04
9-nitroanthracene	NPAH	223.231	0.021	0.647	15.518	2.02E-04	4.98E-04	2.01E-04
3-nitrophenanthrene	NPAH	223.231	0.312	1.302	15.782	< MDL	< MDL	1.94E-04
2-nitrodibenzothiophene	NPAH	229.253	0.104	0.408	16.06	2.06E-04	4.70E-04	2.26E-04
1-Nitropyrene	NPAH	247.253	0.071	0.364	15.277	< MDL	4.43E-04	< MDL
3-nitrofluoranthene	NPAH	247.253	0.069	0.753	15.195			
2-nitrofluoranthene	NPAH	247.253	0.008	0.838	15.783	3.67E-04	8.60E-04	3.69E-04
7-nitrobenz(a)anthracene	NPAH	273.291	0.085	0.270	15.644	5.93E-06	1.03E-05	9.88E-06
6-nitrochrysene	NPAH	273.291	0.071	1.639	15.554	< MDL	< MDL	< MDL
2,8-dinitrodibenzothiophene	NPAH	274.25	0.050	0.254	15.906	2.55E-05	1.85E-05	1.87E-05
3-nitrobenzanthrone	NPAH	275.263	0.032	3.431	14.671	< MDL	< MDL	< MDL
1,8-dinitropyrene	NPAH	292.25	0.082	0.243	14.173	0.00E+00	3.61E-04	1.60E-04

1,3-dinitropyrene	NPAH	292.25	0.148	0.430	14.262	< MDL	< MDL	< MDL
1,6-dinitropyrene	NPAH	292.25	0.035	0.952	14.066	1.51E-04	3.45E-04	1.50E-04
6-nitrobenzo(a)pyrene	NPAH	297.313	0.127	0.458	15.518	3.70E-06	2.32E-05	1.80E-05
p-benzoquinone	OPAH	108.096	0.053	0.661	14.332	1.58E-03	3.63E-03	3.09E-03
chromone (2,3-benzo-4-pyrone)	OPAH	136.145	0.110	0.232		2.79E-04	4.59E-04	3.34E-04
1,4-naphthoquinone	OPAH	158.156	1.219	0.008	14.561	2.74E-03	1.17E-03	5.05E-03
1,2-naphthoquinone	OPAH	158.156	0.133	0.163	14.569	1.00E-04	2.01E-04	1.44E-04
Perinaphthenone	OPAH	180.206	0.109	0.224	15.415	2.47E-04	8.57E-04	2.30E-04
1,2-acenaphthylene-dione	OPAH	182.175	0.016	0.597	15.268			
acenaphthalenquinone	OPAH	182.178	0.069	0.475	15.337	4.57E-05	2.10E-03	2.16E-05
9,10-phenanthrone	OPAH	208.216	0.076	0.242	14.647	3.73E-04	4.68E-04	3.05E-04
1,4-anthraquinone	OPAH	208.216	0.108	0.256	14.615	6.04E-05	2.66E-03	1.25E-03
9,10-anthraquinone	OPAH	208.216	0.047	0.279	14.938	5.53E-04	8.23E-04	1.59E-04
Benzo(a)fluorenone	OPAH	230.261	0.097	0.543	15.507	2.08E-05	1.48E-04	1.14E-05
Benzanthrone	OPAH	230.266	0.025	3.939	15.644	1.91E-05	3.01E-04	8.09E-05
Pyren-4,5-dione	OPAH	232.096	0.005	0.312	14.619	< MDL	< MDL	< MDL
Aceanthraquinone	OPAH	232.23	0.103	0.174	16.741	4.21E-04	7.66E-04	3.36E-04
2-ethyl-9,10-anthraquinone	OPAH	236.27	0.089	0.060	14.988	7.79E-05	6.10E-05	4.65E-05
6H-benzo(cd)pyren-6-one	OPAH	245.288	0.248	0.367		5.94E-05	4.79E-04	8.97E-05
7,12-benzo(a)anthraquinone	OPAH	258.271	0.034	1.848	14.54	1.79E-04	1.14E-04	3.33E-06
9-fluorenone	OPAH	280.206	0.078	0.320	16.013	6.49E-05	1.86E-04	7.40E-05
1-hydroxynaphthalene	OHPAH	144.173	0.082	0.828	18.986	5.84E-05	3.07E-05	6.31E-04
2-hydroxynaphthalene	OHPAH	144.173	0.085	0.846		9.95E-04	1.13E-04	< MDL
1,3-dihydroxynaphthalene	OHPAH	162.172	0.094	0.090		1.90E-04	3.70E-04	2.34E-04
2,6-dihydroxynaphthalene	OHPAH	162.172	0.122	0.188	18.493	4.76E-05	1.08E-04	9.37E-06
1,2-dihydroxynaphthalene	OHPAH	162.172	0.049	0.203	18.975	< MDL	< MDL	< MDL
1,6-dihydroxynaphthalene	OHPAH	162.172	0.192	0.210	18.844	7.37E-06	9.11E-06	7.49E-06
1,5-dihydroxynaphthalene	OHPAH	162.172	0.131	0.268	19.599	1.05E-05	1.42E-05	7.62E-06
2,3-dihydroxynaphthalene	OHPAH	162.172	0.112	0.383	18.887	9.37E-06	9.40E-06	1.61E-03
2,7-dihydroxynaphthalene	OHPAH	162.172	0.199	0.468	18.695	1.76E-05	7.69E-06	6.31E-05
2-hydroxyfluorene	OHPAH	182.222	0.337	0.646	19.125	4.23E-05	2.83E-04	4.11E-04

9-hydroxyfluorene	OHPAH	182.222	0.042	0.648	18.335	3.23E-04	1.39E-03	5.63E-04
3-hydroxyfluorene	OHPAH	182.222	0.199	0.751	18.673	3.69E-05	2.40E-05	2.88E-04
4-hydroxyphenanthrene	OHPAH	194.233	0.110	0.219	18.377	4.47E-05	1.24E-04	1.27E-04
9-hydroxyphenanthrene	OHPAH	194.233	0.075	0.241	18.5	2.84E-05	8.89E-05	4.12E-05
2-hydroxyphenanthrene	OHPAH	194.233	0.128	0.439	18.223	2.38E-06	4.29E-05	3.23E-05
3-hydroxyphenanthrene	OHPAH	194.233	0.025	0.470		1.34E-05	2.26E-05	4.49E-05
1-hydroxyphenanthrene	OHPAH	194.233	0.101	0.492	17.984	5.61E-06	2.56E-05	3.03E-05
2-hydroxy-9-fluorenone	OHPAH	196.205	0.492	0.126	15.948	1.02E-05	5.14E-05	2.87E-05
1-hydroxy-9-fluorenone	OHPAH	196.205	0.198	0.373	16.112	1.13E-05	2.70E-05	1.72E-05
1,9-dihydroxyphenanthrene	OHPAH	211.306	0.081	0.153	18.609	< MDL	< MDL	< MDL
1-hydroxypyrene	OHPAH	218.255	0.022	0.122	17.246	2.57E-05	4.14E-05	2.44E-05
3-hydroxyfluoranthene	OHPAH	218.255	0.107	0.318	16.618	1.37E-05	8.78E-06	3.48E-05
2-hydroxyanthraquinone	OHPAH	224.215	0.139	0.281	14.947	8.68E-05	2.36E-04	< MDL
1-hydroxyanthraquinone	OHPAH	224.215	0.089	1.198	15.139	< MDL	< MDL	< MDL
2,6-dihydroxyanthraquinone	OHPAH	242.23	0.836	0.032	14.897	< MDL	< MDL	< MDL
1,4-dihydroxyanthraquinone	OHPAH	242.23	0.019	0.551	14.014	< MDL	< MDL	< MDL
1,8-dihydroxyanthraquinone	OHPAH	242.23	0.028	0.661	15.377	< MDL	< MDL	< MDL
1,2-dihydroxyanthraquinone	OHPAH	242.23	0.027	1.062	15.328	< MDL	< MDL	< MDL
3-hydroxybenz(a)anthracene	OHPAH	244.293	0.156	0.295		4.91E-06	1.75E-04	8.97E-05
3-hydroxybenzo(c)phenanthrene	OHPAH	244.293	0.098	0.510	17.725	4.83E-06	< MDL	3.77E-05
3-hydroxychrysene	OHPAH	244.293	0.129	0.549		6.22E-06	2.13E-05	2.03E-05
6-hydroxychrysene	OHPAH	244.293	0.123	1.097	17.943	1.29E-04	2.87E-04	1.37E-04
4-hydroxychrysene	OHPAH	244.293	0.031	1.405	17.872	7.45E-06	2.82E-04	1.29E-04
11-hydroxybenzo(g)chrysene	OHPAH	244.293	0.031	2.205		2.93E-05	7.89E-05	6.73E-06
3-hydroxybenzo(e)pyrene	OHPAH	268.315	0.030	0.416	17.619			
12-hydroxybenzo(a)pyrene	OHPAH	268.315	0.009	0.950	16.584	8.95E-06	1.57E-04	1.24E-04
3-hydroxybenzo(a)pyrene	OHPAH	268.315	0.015	1.146		4.76E-05	1.57E-04	< MDL
7-hydroxybenzo(a)pyrene	OHPAH	268.315	0.012	1.535	16.755	1.46E-05	3.46E-04	1.07E-04
9-hydroxybenzo(a)pyrene	OHPAH	268.315	0.008	3.075	16.819	1.10E-05	3.03E-05	1.74E-05
9-hydroxybenzo(k)fluoranthene	OHPAH	269.316	0.016	1.052	16.674	5.29E-06	2.79E-05	4.10E-06
11-hydroxybenzo(b)fluoranthene	OHPAH	269.316	0.083	1.851	16.647	2.44E-05	1.14E-04	7.16E-06

1-hydroxyindeno(1,2,3-c,d)pyrene	OHPAH	292.337	0.110	1.500	15.987	< MDL	< MDL	< MDL
10-hydroxybenzo(c)chrysene	OHPAH	294.307	0.078	0.466	17.132	0.00E+00	1.61E-04	8.70E-06
Naphthalene	UPAH	128.171	0.089	0.297	18.67	2.84E-04	5.02E-05	3.71E-04
acenaphthylene	UPAH	152.196	0.038	0.306	16.693	1.32E-04	6.77E-05	1.48E-04
Acenaphthene	UPAH	154.212	0.053	0.280	18.922	2.48E-05	7.10E-05	9.47E-06
Fluorene	UPAH	166.223	0.120	0.089	18.797	1.73E-05	6.36E-05	2.65E-06
Phenanthrene	UPAH	178.234	0.072	0.183	18.287	7.26E-05	2.78E-04	1.26E-05
Anthracene	UPAH	178.234	0.018	1.291	17.118	1.55E-05	6.14E-05	1.96E-05
Fluoranthene	UPAH	202.256	0.083	0.341	16.577	4.58E-05	3.13E-04	3.71E-05
Pyrene	UPAH	202.256	0.007	0.926	17.279	6.04E-05	3.15E-04	3.70E-05
benzo(c)fluorene	UPAH	216.283	0.129	1.170		8.51E-06	1.45E-05	9.25E-06
Benz(a)anthracene	UPAH	228.288	0.000	0.437	17.181	1.37E-05	1.55E-04	6.05E-06
Chrysene	UPAH	228.294	0.014	0.269	17.778			
Triphenylene	UPAH	228.294	0.031	1.124		3.66E-05	3.35E-04	1.65E-05
Retene	UPAH	234.336	0.133	0.283	18.177	7.91E-05	4.02E-04	1.37E-05
Benzo(k)fluoranthene	UPAH	252.309	0.225	0.281	16.486	9.12E-06	1.31E-04	3.69E-05
Benzo(j)fluoranthene	UPAH	252.309	0.103	0.495	16.168			
Benzo(b)fluoranthene	UPAH	252.309	0.019	1.246	16.548	7.51E-05	7.15E-04	7.07E-05
Benzo(a)pyrene	UPAH	252.316	0.025	0.699	16.657	7.93E-07	1.06E-04	3.81E-06
Benzo(e)pyrene	UPAH	252.316	0.036	1.278	17.306	2.57E-05	3.23E-04	9.20E-06
Indeno(1,2,3,cd)pyrene	UPAH	276.331	0.121	0.409	15.93	6.17E-05	3.33E-04	6.75E-05
Benzo(ghi)perylene	UPAH	276.338	0.066	1.786	16.642	5.03E-05	3.44E-04	5.21E-05
Dibenzo(ah)anthracene	UPAH	278.347	0.028	0.467	17.151			
Dibenzo(ac)anthracene	UPAH	278.347	0.208	0.519	17.096	< MDL	< MDL	< MDL
picene	UPAH	278.347	0.028	0.560		3.22E-04	3.38E-03	4.66E-04

Figure A3.F2 Structural components of PAHs considered for influence on reduction potential. The number of each component on each molecules were added up and the number of each component was then correlated with the DTT_{50} , the response factor in the assay, and the calculated ΔG .

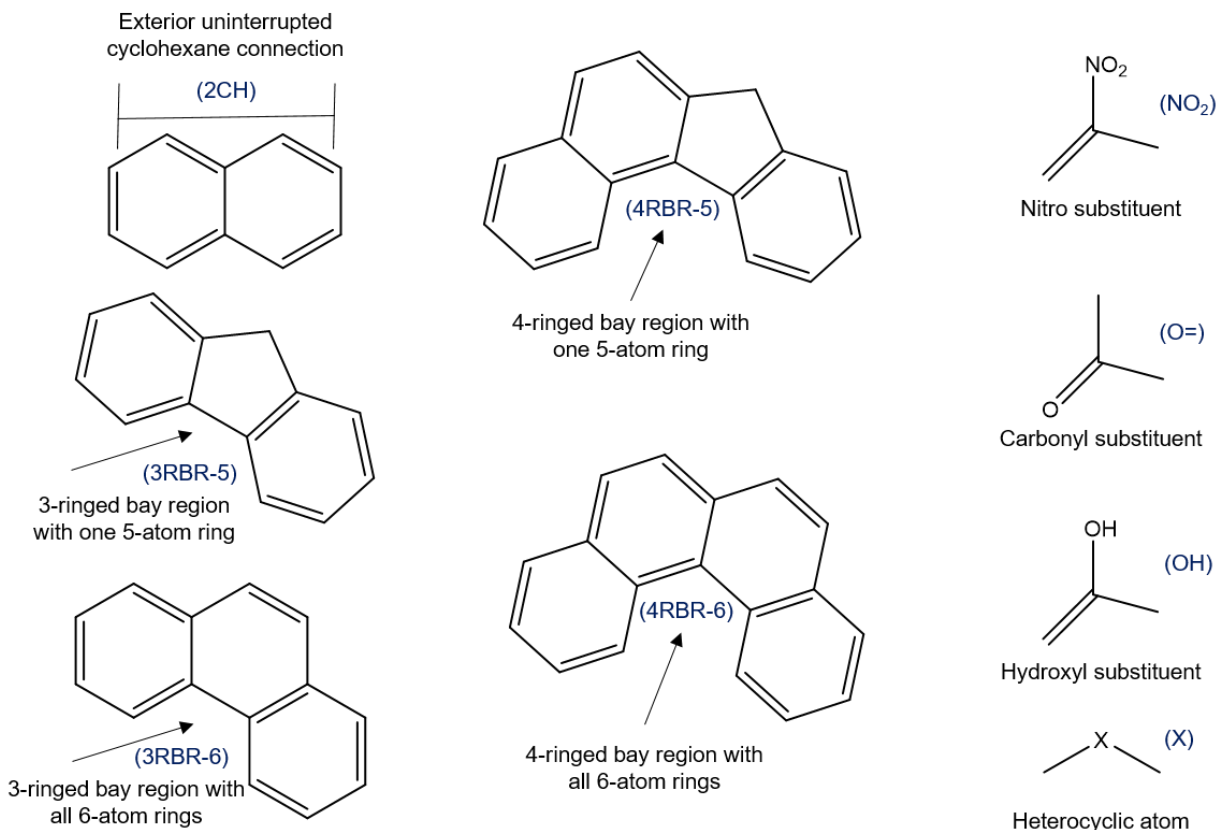


Table A3.T3. Average measured (± 1 SE), and calculated DTT consumed of mixtures of PAHs in DTT consumption assay. Extracts share a calculated prediction because whole mixtures were made to match the concentration of each PAH measured in the extracts of the ambient PM_{2.5} samples.

Sample	Filter A		Filter B		Filter C	
	Measured	Calculated	Measured	Calculated	Measured	Calculated
PPL	0.075 (± 0.004)	0.068	0.054 (± 0.003)	0.059	0.075 (± 0.004)	0.070
Whole	0.093 (± 0.002)	0.132	0.082 (± 0.003)	0.109	0.071 (± 0.003)	0.135
Extract	0.069 (± 0.001)		0.056 (± 0.004)		0.060 (± 0.003)	